1-1-2019

Mechanistic Insight into Tau Fibril Cross-Seeding Barriers: Structural Order and Disorder

Hilary Ann Weismiller
University of Denver

Mechanistic Insight into Tau Fibril Cross-Seeding Barriers: Structural Order and Disorder

Abstract

Filamentous deposition of microtubule-associated protein tau is a hallmark for a number of neurodegenerative diseases collectively termed tauopathies. While tau fibrils are directly linked to the etiology and pathogenesis of these diseases, fibril morphology and their phenotypic presentation can be quite disparate. Alternative splicing of tau results in two main isoform groups, four-repeat (4R) tau and three-repeat (3R), identified by their number of microtubule binding repeats. Some diseases show deposition of both 4R and 3R isoforms, while others show preferential deposition of only one type. The conformational templated growth scheme and trans-synaptic spreading of fibrils is influenced by fibril conformation. Therefore, conformationally distinct fibrils possessing different growth properties is one mechanistic explanation for disparate pathology; yet, molecular level insight on the core structure of these fibrils is lacking. Elucidating how distinct conformers arise, and how their structural features influence growth properties is critical to understanding fibril propagation.

The growth properties and the structural impact that physiologically relevant events including truncation, mutations, and oxidation have on 4R fibrils were investigated. The ability of full-length 4R fibrils to recruit both 4R and 3R tau is influenced by residues on its C-terminal end, as a 3R growth barrier was observed for fibrils formed from C-terminally truncated variants. A 3R growth barrier was also observed for fibrils with specific disease associated mutations. Structural investigations highlighted a region of structural disorder in these fibrils that exhibit 3R growth barriers, in contrast to full-length non-mutated fibrils. Fibrils formed from an oxidized version of 4R tau, with native cysteines intramolecularly disulfide bonded, are structurally distinct and exhibit different recruitment properties from their reduced counterparts. These findings provide mechanistic insight on how truncations, mutations, and oxidation can dictate fibril conformation and thus influence propagation.

Techniques for early diagnostic and therapeutic intervention of tauopathies are limited by their sensitivity of detection. Suppressing tau monomer self-nucleation is one factor critical to amplification assays used to detect low fibril concentrations. Increased suppression of self-nucleation was achieved using mutant tau and modifying assay parameters. These improvements bring this assay one step closer to detecting ultralow fibril concentrations.

Document Type

Dissertation

Degree Name

Ph.D.

Department

Chemistry and Biochemistry

First Advisor

Martin Margittai, Ph.D.

Second Advisor

David Patterson, Ph.D.

Mechanistic Insight into Tau Fibril Cross-seeding Barriers: Structural Order and Disorder

_____

A Dissertation

Presented to

the Faculty of Natural Sciences and Mathematics

University of Denver

_____

In Partial Fulfillment

of the Requirements for the Degree

Doctor of Philosophy

_____

by

Hilary A. Weismiller

March 2019

Advisor: Dr. Martin Margittai

Author: Hilary A. Weismiller
Title: Mechanistic Insight into Tau Fibril Cross-seeding Barriers: Structural Order and Disorder
Advisor: Dr. Martin Margittai
Degree Date: March 2019

ABSTRACT

Filamentous deposition of microtubule-associated protein tau is a hallmark for a number of neurodegenerative diseases collectively termed tauopathies. While tau fibrils are directly linked to the etiology and pathogenesis of these diseases, fibril morphology and their phenotypic presentation can be quite disparate. Alternative splicing of tau results in two main isoform groups, four-repeat (4R) tau and three-repeat (3R), identified by their number of microtubule binding repeats. Some diseases show deposition of both 4R and 3R isoforms, while others show preferential deposition of only one type. The conformational templated growth scheme and trans-synaptic spreading of fibrils is influenced by fibril conformation. Therefore, conformationally distinct fibrils possessing different growth properties is one mechanistic explanation for disparate pathology; yet, molecular level insight on the core structure of these fibrils is lacking. Elucidating how distinct conformers arise, and how their structural features influence growth properties is critical to understanding fibril propagation.

The growth properties and the structural impact that physiologically relevant events including truncation, mutations, and oxidation have on 4R fibrils were investigated. The ability of full-length 4R fibrils to recruit both 4R and 3R tau is influenced by residues on its C-terminal end, as a 3R growth barrier was observed for fibrils formed from C-terminally truncated variants. A 3R growth

barrier was also observed for fibrils with specific disease associated mutations. Structural investigations highlighted a region of structural disorder in these fibrils that exhibit 3R growth barriers, in contrast to full-length non-mutated fibrils. Fibrils formed from an oxidized version of 4R tau, with native cysteines intramolecularly disulfide bonded, are structurally distinct and exhibit different recruitment properties from their reduced counterparts. These findings provide mechanistic insight on how truncations, mutations, and oxidation can dictate fibril conformation and thus influence propagation.

Techniques for early diagnostic and therapeutic intervention of tauopathies are limited by their sensitivity of detection. Suppressing tau monomer self-nucleation is one factor critical to amplification assays used to detect low fibril concentrations. Increased suppression of self-nucleation was achieved using mutant tau and modifying assay parameters. These improvements bring this assay one step closer to detecting ultralow fibril concentrations.

ACKNOWLEDGEMENTS

I would like to thank Dr. Martin Margittai for allowing me the opportunity to join his lab and for his continued support over a number of years. The expertise and guidance he offered have been invaluable along with his unwavering example of scientific rigor and work ethic. I would also like to thank my committee members Dr. David Patterson, Dr. Kingshuk Ghosh, and Dr. Gareth R. Eaton for their continued advice and constructive criticism to enhance the quality of my research projects. I am also grateful to Drs. Sandra S. and Gareth R. Eaton for allowing me to do a research rotation in their lab, and for their collaborative efforts regarding EPR experiments. Financial support for the work discussed in this dissertation was through NIH grants awarded to Dr. Martin Margittai.

I would like to thank Dr. Virginia Meyer for her guidance and instruction when I first joined the lab, and other lab mates Emily Hager, Justin Shady, and Dr. Michael Holden without whom this experience would have been exceedingly more difficult. I also had the opportunity to work with some wonderful undergraduate students who really proved to me the saying “if you can’t explain it simply, you don’t understand it enough” is true. I am also grateful for the amazing friends I have made in the Biophysics program; especially Drs. Sarah Ryan and Carrie Moon.

Finally, I would like to thank my family who have been an incredible support system throughout my entire life. Special thanks to my parents for their endless encouragement and instilling in me a set of values that made completing this possible.

TABLE OF CONTENTS

LIST OF FIGURES

ABBREVIATIONS

3R	three repeat tau
4R	four repeat tau
AD	Alzheimer's Disease
AGD	Argyrophilic Grain Disease
BCA	bicinchoninic acid assay
BSA	bovine serum albumin
CBD	Corticobasal degeneration
CTE	Chronic Traumatic Encephalopathy
CW	continuous wave
GdnHCl	guanidine hydrochloride
DEER	double electron-electron resonance
DMSO	dimethylsulfoxide
DTT	dithiothreitol
EDTA	ethylenediaminetetraacetic acid
EPR	electron paramagnetic resonance
FTDP-17	Frontotemporal dementia and parkinsonism linked to chromosome-17
HEPES	4-(2-hydroxyethyl)-1-piperazineethanesulfonic acid
IDP	intrinsically disordered protein
IPTG	isopropyl β-D-1-thiogalactopyranoside
MAP	microtubule-associated protein
MT	microtubule

MTBR	microtubule binding repeat
MTSL	[1-oxyl-2,2,5,5-tetramethyl-Δ3-pyrroline-3-methyl]methanethiosulfonate
NDP	nucleation dependent polymerization
NFT	neurofibrillary tangle
Ox	Oxidized
PCR	polymerase chain reaction
PET	positron emission tomography
PHF	paired helical filament
PID	Pick's Disease
PIPES	piperazine-N,N'-bis(2-ethanesulfonic acid)
PK	Proteinase K
PSP	Progressive Supranuclear Palsy
PTM	Post-translational modification
Red	Reduced
ROS	reactive oxygen species
RPM	revolutions per minute
S.D.	standard deviation
SDS-PAGE	sodium dodecyl sulfate polyacrylamide gel electrophoresis
TCEP	tris(2-carboxyethyl) phosphine
TEM	transmission electron microscopy
ThT	thioflavin T
TRIS	tris(hydroxymethyl)aminomethane

CHAPTER ONE: INTRODUCTION

1.1 Tauopathies and their impact

Tauopathies are a collection of neurodegenerative diseases characterized by the filamentous deposition of the microtubule-associated protein tau. Some share common dementia and/or movement disorder symptoms, but the pathology of these diseases can be very disparate (1). Tauopathies are a subclassification of diseases called amyloidoses. Amyloidoses refer to pathology associated with the deposition of amyloid fibrils, and fall under the broad category of protein misfolding diseases (2). The most common and well characterized tauopathy is Alzheimer's disease (AD). Other diseases characterized by tau deposition include Chronic Traumatic Encephalopathy (CTE), Progressive Supranuclear Palsy (PSP), Corticobasal Degeneration (CBD), Pick's disease (PID) and Frontotemporal dementia and parkinsonism linked to chromosome-17 (FTDP-17) (3, 4). The problem that dementia imposes is immense, it is a burden not only to those who suffer from it but to caregivers and the economy as well. The cost of health care for people with AD or other dementias in just the United States was $277 billion in 2018 (5). If preventative measures are not developed it is projected that by 2050 the total number of people with AD dementia, in the United States alone, will be 13.8 million (6).

Therefore, it is critical that a deeper understanding of the underlying mechanism of these diseases, like tau fibril formation and propagation, be reached.

1.2 Microtubule associated protein tau

1.2.1 Native function and isoforms of tau

Tau is one protein in the microtubule-associated protein (MAP) family. Tau protein is primarily expressed in neurons (7) and its normal biological functions include stimulation of microtubule (MT) assembly and stabilization of MT structure (8, 9). Proper function of MTs to facilitate axonal transport is vital for neuronal health, therefore the loss of native tau function is one factor contributing to neurodegeneration (10). The other main factor is the gain of toxic function from tau aggregates, deposition of which have been linked to over 20 neurodegenerative diseases (4). In the most common tauopathy, AD, tau was identified to make up its associated paired helical filaments as early as the late 1980's (11, 12).

The gene for tau protein is found on chromosome 17 and contains 16 exons. Different isoforms arise due to the alternative splicing of exons 2, 3, and 10 (13). Exon 2 can appear with or without exon 3, but exon 3 never appears independently of exon 2. This results in a 0, 29, or 58 amino acid insert in the N-terminus (14). The splicing of exon 10 results in the absence of the second of four semiconserved microtubule binding repeats (MTBRs) in the C-terminal end of tau. These splicing options give rise to 6 isoforms ranging between 352 to 441

amino acids in length; three containing four MTBRs (4R) and three containing three MTBRs (3R) (Figure 1.1). During development these isoforms are differentially expressed, signifying that they have particular biological roles. The 3R isoforms provide less MT stabilization and are preferentially present during fetal stages when greater MT dynamics are needed for development. However, in the adult human brain all six isoforms are equally expressed (15).

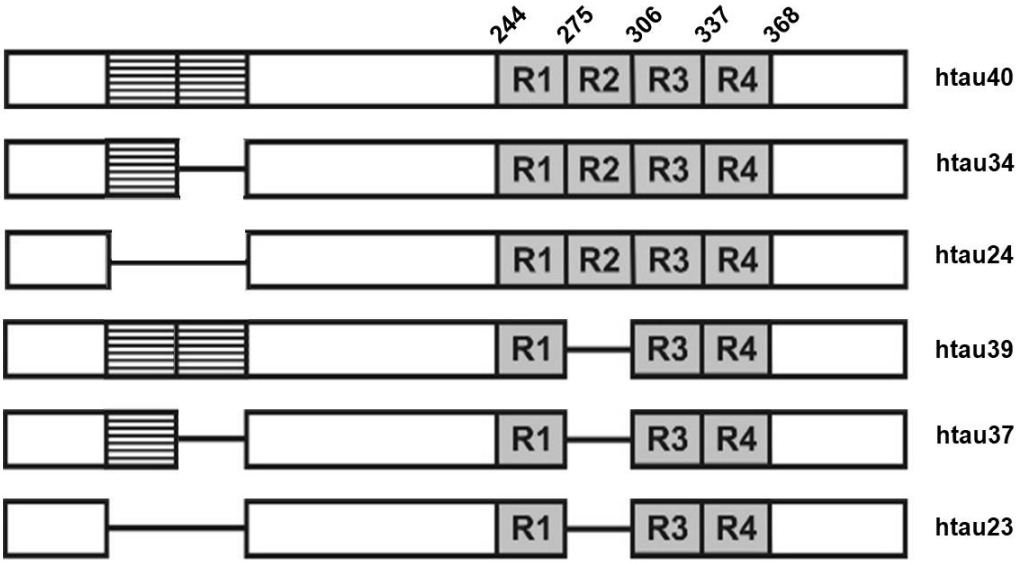

Figure 1.1. Tau isoforms. Six different isoforms of tau arise due to alternative splicing of exons 2, 3 and 10. Differential splicing of exons 2 and 3 results in the absence or presence of two N-terminal inserts (striped boxes). The splicing of exon 10 results in the absence of the second of four microtubule binding repeats (shaded boxes R1-R4).

The N-terminus, referred to as the projection domain, contains inserts that are acidic followed by a basic proline-rich region. This projection domain is responsible for interactions with cytoskeletal elements and the neural plasma membrane along with being involved in signal transduction pathways (16). The C-terminus contains the 4 or 3 semiconserved repeats. These repeats are

extremely important segments of the tau protein because together with the proline rich region they are responsible for binding to MTs (17). Additionally, *in vitro* studies show tau variants that have been truncated to only the repeats are sufficient to form fibrils (18). This is unsurprising given that proposed and published fibril structures show that these repeats largely make up the core of fibrils associated with different tauopathies (19–21). This implies that fibrils formed from variants containing residues outside the repeats have a large number of amino acids, particularly in the htau40 isoform, that are not contained in the structured core. These residues have been referred to as the fuzzy coat (22). But these residues can still have an impact on fibril growth properties due to N- or C- terminal regions backfolding to interact with residues in the core (23).

1.2.2 Post-translational modifications and mutations

Tau is prone to a host of post-translational modifications (PTMs) and has numerous mutations associated with it. Some of these, in combination or individually, change the growth properties of tau by shifting its aggregation propensity and/or recruitment properties (24). Some of the post-translational modifications of tau promote aggregation and include glycation, nitration, polyamination, sumoylation and ubiquitination (25). Other PTMs that will be discussed in more detail are the most common, phosphorylation, and the two that most impact the studies presented herein, truncation and oxidation.

1.2.2.1 Phosphorylation

Phosphorylation of tau is one mechanistic way its binding to MTs is regulated. Since stabilizing MTs along with regulating their assembly are the main functions of tau, some degree of phosphorylation is necessary (26). A normal phosphorylation state of tau involves approximately 2-3 moles of phosphate per mole of tau, but in disease this ratio is much higher, approximately 6-8 moles of phosphate per mole of tau in some AD patients (27). It is the hyperphosphorylation or mis-phosphorylation of tau monomers that leads to problems causing their dissociation from MTs and increased propensity to aggregate (28). Some groups believe the hyperphosphorylation of tau monomers to be the mechanism by which they dissociate from MTs, then other PTMs promote the formation of aggregates (25). Monomer refers to any non-aggregated tau variant, this includes full-length, truncated and mutant variants.

1.2.2.2 Truncation

Truncated variants of tau protein have been used for numerous *in vitro* studies, and their deposition has been associated with various tauopathies (29). The development of truncation-dependent conformational antibodies provided validation that truncated tau variants arise naturally in disease and are not just an artifact of protease treatment during sample analysis (30). Importantly, some of these antibodies are not dependent on the phosphorylation state of tau (31–33). One such antibody, DCII, shows strong immunoreactivity toward variants with

either N- or C- terminal truncations, or a combination of both. However, DCII shows no recognition for endogenous healthy tau or recombinant full-length tau (31). The first truncated variant to be identified in disease tissue absent of any protease digestion was a variant truncated at position 391 (numbering scheme with respect to htau40) (32). Since then, a variety of proteases have been identified to produce over 50 specific truncated tau fragments. These truncated variants have been shown to have differential effects in the context of neurodegenerative diseases (29). The caspase family of proteases has been shown to cleave tau at a number of different positions (34), and the resulting cleavage products are linked to different tauopathies such as AD and PSP (35, 36). Caspase activation happens early on in disease progression making it possible that truncated variants initiate fibril formation (37). Calpain-1 and -2 have been linked to a fragment associated with AD patients containing residues 243-441 (36), and have also been implicated in the creation of fragments that exclude the MTBRs, yet still have neurotoxic effects (36, 38). Asparagine endopeptidase has been shown to cleave tau at N255-V256 and N368-K369, and the resulting 1-368 and 256-368 fragments have exhibited increased aggregation propensity (39). Other proteases known to be associated with tau cleavage include cathepsins (40), puromycin-sensitive aminopeptidase (41), thrombin (42), and a disintegrin and metalloprotease 10 (43). The pathogenicity of some fragments remain unidentified, along with the origin of other fragments associated with disease (29). Truncated variants may play a role in initiating

aggregation. However, the mechanism by which they contribute to disease is not thoroughly known, and little has been identified about the impact truncations have on fibril core structure (44, 45).

1.2.2.3 Oxidation

A loss in redox homeostasis, and therefore increased oxidative stress, is known to be associated with numerous neurodegenerative diseases including tauopathies (46). The pathogenesis of diseases like AD are accelerated in many ways by the disruption of the oxidation-reduction balance. Many effects stem from this disruption, like the inhibition of proteasomes and/or the accumulation of reactive oxygen species (ROS), both impact protein aggregation (47). Considerable characterization has been done concerning the impact that oxidative processes have on AD with regard to amyloid beta (Aβ), which constitutes the senile plaques found in AD pathology, particularly oxidative stress via metal dyshomeostasis (48–50). Chelation of particular endogenous and exogenous metal ions have even been the subject of potential AD therapeutic strategies (51–53). While metal ion binding does effect tau aggregation, oxidation resulting in the formation of disulfide bonds between native cysteines in tau is also very important. Disulfide bonds in tau have the potential to greatly affect aggregation properties (54). As such, the aggregation potential of intramolecular and intermolecular disulfide bonded tau monomers has been the subject of numerous studies. The formation of intermolecular disulfide bonds, essentially

forming tau dimers or higher order species, has been shown to increase aggregation (55). However, the impact that intramolecular disulfide bonds (between the two native cysteines in one tau monomer) have on aggregation, has not been as well studied. There are inconsistencies in the studies that investigate tau with intramolecular disulfide bonds. For example, some studies suggest this species does not form fibrils (56), while other studies suggest it does (57). Also, the studies tend to highlight the nucleation properties of this species rather than its elongation properties (57–59).

1.2.2.4 Mutations

There are over 80 known mutations associated with tau deposited in various diseases, and many are in or near the MTBRs (60). The study of tau mutations began through characterization of tau from a number of individuals with familial FTDP-17 (61). In fact, the delineation that tau dysfunction is a cause of neurodegeneration, rather than tau dysfunction being a symptom of disease, was first made clear through the study of mutant tau (62). Mutations can have their primary effect at either the RNA level or the protein level, and some mutations have effects on both levels (24). Those mutations that have their primary effect at the RNA level result in overproduction of either 4R or 3R tau depending on the mutation, and thus alter the typically equimolar ratio of 4R/3R tau present in the brain (24). This altered ratio serves as an explanation for the preferential deposition of one isoform type over the other, yet not all mutations

cause altered splicing, so this is not a universal explanation. Specific mutations that take their primary effect at the protein level can do so in a number of ways. Some mutations are known to reduce the ability of mutated tau to interact with MTs. This increased pool of monomers not performing their native function increase the chance of aggregation (44). Mutations can also increase aggregation propensity by not only reducing tau's ability to interact with MTs, but also make β-sheet packing more favorable (63). Additionally, studies utilizing mutant tau for seeded growth reactions suggest that mutations also can impact fibril core conformation (64). Due to the conformational templating growth scheme of tau, which will be discussed in more detail in subsequent sections, the ability of a mutation to promote conformational differences in fibrils is one mechanism for some preferential deposition seen in diseases. This mutation effect is explored in the work presented here. The wide range of pathological features mutant tau is associated with speaks to the complexity of tau mutation effects (65). Teasing apart the mechanisms by which these mutations lead to preferential deposition seen in disease could help in understanding overarching propagation principles.

1.3 Amyloids

1.3.1 Amyloid structure

Protein aggregates can be classified in many ways. Amyloid fibrils are one type of classification, and tau fibrils are one subset of amyloid fibrils (66). The

association of amyloid fibrils with pathology in many diseases that have high morbidity and mortality rates is one reason why they are so heavily researched. A number of functional mammalian amyloid structures have been identified (67), but fibrils associated with disease states continue to be highly studied. Most proteins have the potential to form fibril-like structures under certain conditions. However, it is the similar response to biochemical analyses, ability to fragment and self-propagate, and common secondary structural characteristics that help delineate fibrils as being amyloid (68, 69). Structural characterization of amyloid fibrils began with the observation of their birefringence, suggesting a higher structural order (70). This proved to be true upon electron microscopy observations identifying dimensional features that allowed for morphological distinction of these fibrils from other fibrillar protein structures (71). Ultimately X-ray diffraction studies revealed that the core of amyloid fibrils share a common cross-β substructure. Parallel to the long fibril axis are β-sheets and perpendicular are β-strands, with consistent 4.8 Å spacing (72). A combination of side chain interactions between monomers and hydrogen bonds oriented parallel to the long axis stabilize this structure (73, 74). Additionally, tau fibrils have been identified to have a parallel in-register arrangement of their β-strands, a structural feature that is common to most amyloid fibrils (75). Figure 1.2 depicts a model of such structure. All amyloid fibrils possess this structural cross-β characteristic, but can differ in a more quaternary structural sense, for example how these fibrils associate and pack with one another (69). They can also differ in their molecular

level structure, such as the folding pattern of the monomers making up the fibril core. Different fibrils made up of the same protein monomer (or variant) can have different core conformations, sometimes referred to as strains (76). This concept of conformational variation will be discussed in more detail in subsequent sections and has a major influence on propagation patterns.

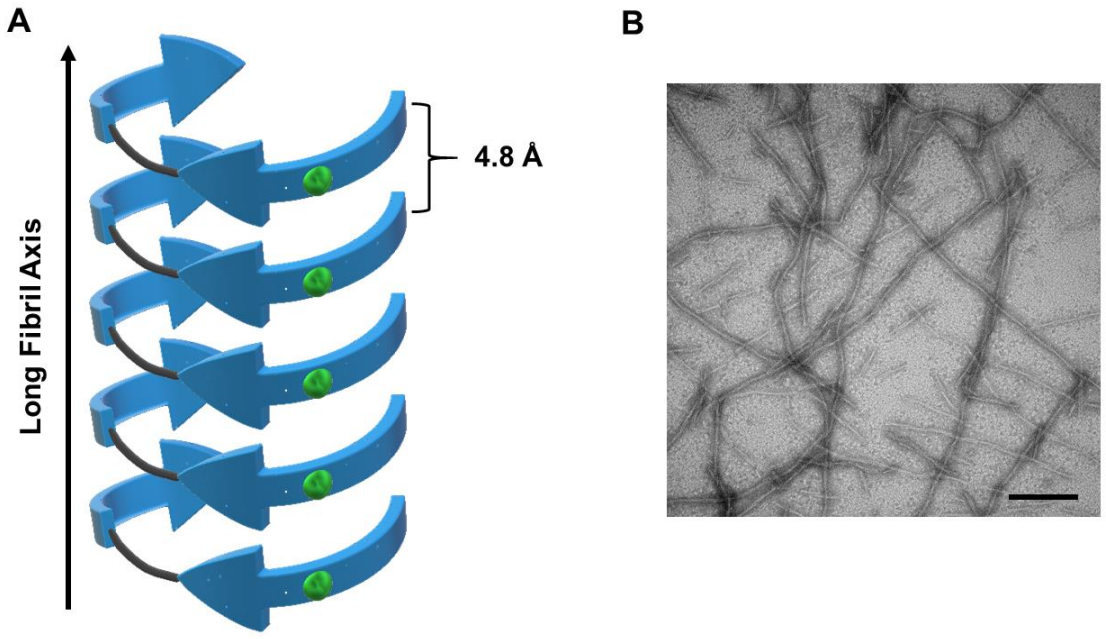

Figure 1.2 Basic tau fibril structure A, model showing β-sheets are parallel to the long fibril axis and β-strands are perpendicular with consistent 4.8 Å spacing. The arrangement of strands is parallel in-register so identical residues (green dots) of stacked monomers align with one another. B, electron microscopy image of tau aggregates highlights their fibrillar nature. Scale bar = 200 nm.

1.3.2 Amyloid growth scheme

Amyloid fibrils are composed of protein monomers with diverse amino acid sequences that are natively soluble, but upon association form fibrils which are insoluble (77). The accepted model of amyloid fibril assembly is nucleation dependent polymerization (NDP). NDP consists of an initial lag phase during

which nucleation processes occur, and a rapid growth phase (called elongation) (78). Fibril assembly is commonly depicted with a simple graph showing the fibrillar mass concentration, or aggregation, as a function of time (Figure 1.3). Analyzing the kinetics in these types of graphs has led to the understanding and ability to differentiate between different types of aggregation occurring, and establish equations that based on properties of the specific protein and solution can predict fibril growth *in vitro* (79). These plots differ greatly for different proteins and different reaction conditions of the same protein (80). Integrated rate laws are necessary to gain useful information from these types of plots due to the fact that after initial nucleation begins, all processes are occurring simultaneously (80). Also, these models can be more complex for the characterization of intrinsically disordered proteins (IDPs), like tau, due to the unstructured nature of their monomers (78).

Nucleus formation is typically the rate-limiting step. This is so because it is thermodynamically unfavorable due to the competition between enthalpic gain, from the formation of new contacts, and entropic loss, from the immobilization of monomers into a fibril (81). Another limitation to nucleation of amyloid fibrils is the inability to proceed without the existence of specific hydrophobic interactions, that only occur with a specific protein sequence (82). For some proteins that possess a native fold, exposure of the backbone groups allowing for hydrogen bonds between protein monomers creating the cross-β structure is achieved by a type of denaturation or misfolding event (83). Changes that thermodynamically

stabilize the transition from monomer to higher order species can include events such as a concentration increase promoting tighter packing, or changes to steric and hydrophobic interactions (84, 85). For *in vitro* tau aggregation studies, like those presented here, an external factor is needed to induce aggregation (nucleation and elongation) (86). Polyanionic cofactors are commonly used for this in tau aggregation studies. These cofactors work to lower the energy barrier of aggregation by charge compensation, with their negative charge compensating for tau's positive charge (81). While all the work presented here utilizes heparin for this purpose, other factors such as RNA or arachidonic acid have been used in other studies (86, 87).

The type of nucleation that initial fibril formation follows in the studies presented herein is known as primary nucleation, referring to formation of an oligomeric nucleus from only soluble protein monomers (81). Due to the fact that initial fibrils for the majority of growth studies presented here were formed under agitating conditions over multiple days, it is assumed that one type of secondary nucleation, fragmentation, along with elongation both contribute to overall fibril growth of initial fibrils once the formation of primary nuclei has occurred (81). Other types of secondary nucleation, lateral growth or branching, are less likely as no such characteristics were observed in the current study, nor in previous work that used a similar growth protocol (21, 76, 88, 89).

Once nuclei have formed, the growth phase, also referred to as elongation, can proceed by recruitment of monomer onto nuclei ends (80).

Aggregation via elongation is much faster than aggregation via nucleation due to the greatly decreased energetic barrier presented by monomer addition onto a preexisting template (78, 90, 91). If rate equations governing fibril formation are separated, the process for an elongation reaction, with no nucleation or fragmentation but only addition of monomer onto pre-existing aggregates, can be described with a maximal rate at the beginning of growth and decrease as the concentration of free monomers is depleted over time (80). Importantly, growth rate characterization has demonstrated that elongation occurs through monomer addition to ends of preexisting fibrils (92).

Aggregation of initial fibrils for the current study included all steps of the NDP growth scheme (Figure 1.3 A). However, once initial fibrils are formed they can be fragmented and used as seeds to initiate new fibril growth and circumvent the nucleation phase, this is commonly known as seeding (78) (Figure 1.3 B). Experimentally forcing aggregation to immediately enter the elongation phase by seeding is one way to study the growth properties of specific tau seed types (88). As seeds recruit new monomers onto their ends during elongation, these monomers assume the conformation of the seeds, thereby propagating the structure of the particular fibril (93). If the monomer offered to grow on a specific seed type is not compatible, or not able to assume that seed conformation, a growth barrier will be observed. This technique of conformational templating via seeded growth is employed in the majority of the studies presented here as a

way to assess structure and growth properties of seeds composed of different tau variants.

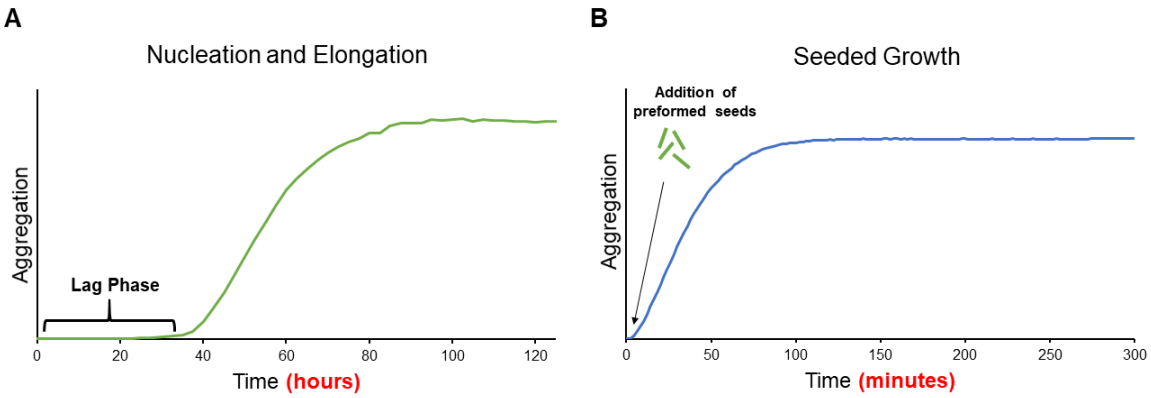

Figure 1.3 Kinetic distinction between nucleation vs seeded growth. A, representative trace highlighting the lag phase during nucleation before elongation occurs. B, representative trace of seeded fibril growth. Notice the difference in time scales for A and B.

1.4 Conformational variation of tau fibrils

1.4.1 Strain phenomenon

The study of mammalian and yeast prions led to the discovery that proteins themselves can be pathogenic through the transition from their native non-disease state, into fibrillar aggregates associated with various disease pathologies (94, 95). Studies on the propagation and transmissibility of these fibrils revealed that fibrils made up of the same protein, but are different conformations (strains), possess distinct pathological ramifications (96). This phenomenon is also referred to as structural polymorphism, and can be used to describe not only prions but amyloid fibrils such as tau (97). These conformational variants all retain the cross-β structural characteristic with parallel in-register β-sheet arrangement, but vary in the folding pattern of β-sheets and

result in different fibril core conformations. Evidence that different tau strains, or conformers corresponding to specific pathologies, was gained through studying the pathology that resulted from injecting mouse models with tau fibrils extracted from human brain material (98, 99). Specific pathology corresponding to tau fibrils from humans with various tauopathies including AD, PSP, and CBD was recapitulated upon injecting those fibrils into mouse models (100). This phenomenon was further corroborated by the cryo-EM structures of tau fibrils isolated from two different diseases, AD and PID. The structures revealed different folding patterns for these fibrils (19, 20).

1.4.2 Distinct pathology and isoform specific deposition

Tau fibril aggregation commonly follows NDP, yet the affected brain regions, morphology of the deposition, and even the types of isoforms present can vary greatly between different tauopathies. AD is the most studied tauopathy and therefore its progression and stereotypical spreading has been well characterized and is referred to in Braak stages (101). Tau deposition in AD patients presents as neurofibrillary tangles in the cell body and apical dendrites of neurons, neuropil threads in distal dendrites and/or abnormal neurites associated with some senile plaques, with affected brain regions including frontal, parietal, and temporal lobes (102, 103). The paired helical (PHF) and straight filaments making up these various deposits consist of a similar ratio of 4R to 3R isoforms, a distinguishing feature from other tauopathies (104). PID for

example is referred to as a 3R tauopathy as the tau isoforms making up its deposits are predominately 3R isoforms (105). PID is not only pathologically distinctive, but presents with its own characteristic histological features including cortical atrophy in the frontal and temporal lobes and severe neuronal loss, ballooned neurons, and spherical inclusions referred to as Pick bodies dominating the type of tau deposition (65), (106). There are also diseases that, unlike AD and PID, can be characterized by deposition of predominantly 4R tau isoforms. These include PSP, CBD, and Argyrophilic Grain Disease (AGD) (65). Much like AD and PID, these diseases can be distinguished from one another by distinct histological features, and their collective classification of 4R tauopathies arises from the shared feature of 4R isoforms making up their unique forms of deposition (65, 107–109). While the morphological and biochemical differences between the tau deposition in these diseases are well documented, the molecular mechanism of this preferential deposition still remains a question. Some preferential deposition can be explained by mutations that result in alternative splicing, therefore altering the ratio of 3R and 4R present in the brain; however, this is not a universal explanation. Other factors suggesting this preferential deposition have been identified, but it is still a pursued subject because unraveling the mechanisms by which certain conformers propagate would be universally beneficial to developing preventative therapeutics for tau propagation.

One mechanism aside from splicing to change 4R/3R ratios, arises from the strain phenomenon discussed in the previous section. Strains (or fibril conformers) that possess different physical properties, such as different growth rates or different fragilities, allow for differential selection and preferential propagation of certain strains over others. This was shown to be true for prions (96) and later on for tau fibrils as well (76). How these different strains arise is then a question of particular interest. Since fibrils spread from cell-to-cell, and once transferred grow via conformational templating, the exploration of different nucleating conditions that influence the structure of fibrils as they nucleate is one way to probe this question (93, 110). This includes not only environmental conditions such as pH and the presence of ROS influencing the extent of PTMs, but also how particular mutations and truncations influence fibril structure. In order to address questions concerning structural differences between fibrils, a host of various biophysical and biochemical techniques has been employed.

1.5 Tau fibril detection and analysis techniques

1.5.1 Fibril detection techniques

Experimental detection techniques to assess the presence of tau fibrils have existed for decades and are constantly being optimized to increase the sensitivity of detection. Many such as tau-binding dyes Congo red and Thioflavin (ThT), which were essential to initial tau discoveries, are still used today (111). Other common tau detection techniques such as immunofluorescence and

antibodies have been used since the 1980's (9, 112). Antibody detection has grown more sophisticated over the years to include conformer sensitive discontinuous epitope antibodies (113, 114). The use of positron emission tomography (PET) imaging with radiotracers is one method for early tau fibril detection (115). Specific tracers for this technique are currently being developed, and have shown promising results for targeting tau deposition *in vivo* (116). These techniques and others are critical to many of the *in vitro* and *in vivo* studies that have been performed and are currently taking place. There are also a number of techniques that are able to simply determine the absence or presence of fibrils by exploiting tau solubility. These include techniques like sedimentation assays utilizing high speed centrifugation (21) or the use of sarkosyl, a mild detergent that can distinguish soluble monomeric tau from insoluble fibrillar tau (117).

Limited tau concentrations can be detected through the use of specific antibodies. However, one of their limitations is in part due to the region of protein being detected, and they are not always successful in distinguishing between normal and pathological tau (113). Also, if fibrillar species are detected, the ability to study the structure of these fibrils is limited by their small quantity. To utilize structural analysis techniques that small population would need to be amplified. Development of an assay that could selectively amplify only fibrillar species by forcing a minute number of fibrils to elongate via conformational templating with a pool of fresh monomer addressed both of these goals. This was achieved

through adaptation of an assay from the prion field termed protein misfolding cyclic amplification (PMCA) assay, and involves cycles of sonication followed by incubation (118, 119). This same concept was then also applied to an assay utilizing cycles of shaking followed by incubation in conjunction with ThT fluorescence, termed real-time quaking-induced conversion or RT-QUIC assay (120). This assay was also originally developed for the detection of prions and was later applied to the detection of tau fibrils (121). These assays are successful at detecting low fibril concentrations, but the ability to detect ultralow concentrations is limited by the rate at which the monomer present begins to spontaneously nucleate. Spontaneous monomer nucleation negates the selective fibrillar detection aspect of the assay. Pushing the level of fibril detection to ultralow concentrations would be exceedingly useful in developing early diagnostic techniques that could detect tau fibrils from cerebrospinal fluid or blood samples.

1.5.2 Assessing tau fibril structure

Optimizing detection techniques is critical for antemortem diagnosis, and understanding the molecular level structure of the core of tau fibrils is also important. Structural data could reveal fundamental mechanisms of fibril propagation allowing for potential therapeutic design. A number of techniques are used to indirectly reveal fibril core characteristics. When used in conjunction with one another, these techniques have been successful in gaining insight into tau

fibril structure. Some of these techniques, many of which are utilized for the data presented herein, include seeded reactions (using various seed fibrils in combination with different types of monomer, where incompatibilities in the conformational templating results in growth barriers), visualizing proteolytic cleavage fragments, denaturation profiles, fibril images obtained via negative stain transmission electron microscopy (TEM), kinetics of fibril growth, or turbidity (21, 76, 122, 123). These techniques reveal overall structural properties and highlight structural differences, but alone they do not provide information with enough resolution to make molecular level conclusions on the core structure of tau fibrils. Some techniques that do gain molecular level insight into core structure include electron paramagnetic resonance (EPR) techniques such as site directed spin labeling (SDSL) in conjunction with continuous-wave (CW EPR) or double electron-electron resonance (DEER) spectroscopy (76, 89, 124, 125). Also, experiments assessing the effects of systematic point mutations and truncations can be highly suggestive of the structural significance of particular residues, and elucidate their role in core structure (21, 64). Förster resonance energy transfer experiments, while not utilized in these works, have also been successful in assessing fibril structure (126). High-resolution magic angle spinning NMR and solid state NMR experiments have also been successful at gaining structural insight into full-length and truncated tau fibrils, but have a number of limitations (127, 128). Finally, cryo-EM has provided atomic level resolution of fibrils extracted from human subjects (19, 20, 129). A host of

molecular modeling software is also available to be used in combination with any of these techniques, leading to enhanced structural insight (130, 131).

1.6 Scope of this research

The majority of my research presented in this current study involves investigating the mechanism of tau fibril growth barriers by identifying structural differences between fibrils that exhibit specific growth properties. The motivation for these studies came from the gap in knowledge surrounding how tauopathies present with such a wide range of pathological diversity (65), specifically the preferential deposition of certain isoforms in particular diseases (4). Previous works suggest conformational differences in fibrils to be one of the mechanistic ways this disparate pathology arises (97), yet little molecular level core structural data is known about the tau fibrils found in these diseases. Elucidating how structural differences relate to growth properties is vital to understating fibril propagation and finding a way to block it.

I began by optimizing growth conditions for full-length 4R tau (htau40) and observed its growth properties were different from those previously observed for truncated tau consisting only of the repeat regions, under otherwise similar conditions (88, 130, 131). In order to determine the regions responsible for this difference between truncated and full-length tau, I used 11 different truncated variants with varying N- and C- terminal truncations. These truncated variants were used to create seeds whose growth properties were tested. I also tested

growth properties for a number of mutant full-length tau variants to try and identify if mutations could be responsible for structural differences. CW EPR and DEER spectroscopy techniques were also used to probe the structure of particular truncated and mutant variants that exhibited 3R growth barriers.

To investigate whether or not manipulation of environmental conditions could promote the formation of distinct fibril conformers, I isolated intramolecularly disulfide bonded full-length 4R tau and tested its growth properties. To identify if these oxidized fibrils were structurally distinct from their full-length 4R tau counterpart lacking any disulfide bonds, I probed their susceptibility to denaturants, patterns of proteolytic cleavage, and sensitivity to fracture. I also investigated the structural significance of the disulfide bond in these oxidized fibrils.

The remaining part of the work presented here is part of an ongoing effort to improve the sensitivity of a minute fibril quantity detection assay, so that it can be applied to blood or cerebrospinal fluid samples for early diagnostic purposes. The goal was to develop a way to suppress spontaneous monomer nucleation without diminishing monomer elongation competency. These monomers could then be used to optimize amplification assay conditions for more sensitive detection. I made a series of mutants we postulated would suppress primary fibril nucleation due to their position in the hydrophobic core region of the protein. I tested the quiescent nucleation of these mutants in comparison to non-mutant full-length 4R tau. I also tested the elongation competency of these mutants

through sedimentation and ThT kinetics assays. Mutants that were identified to have an extended lag phase, and retained elongation competency, were investigated further in conjunction with our amplification assay developed previously in the lab (119). Optimization of this assay was pursued by measuring responses to assay parameter changes in the hope that single fibril detection will be possible.

CHAPTER TWO: METHODS

2.1 Tau constructs

The primary 4R and 3R tau constructs used for these studies were htau40, the longest 4R tau isoform containing 441 amino acids, and htau23 the shortest 3R tau isoform containing 352 amino acids. The sequence of these two isoforms along with their molecular weight, and the molecular weight of all variants used herein are shown in Appendix C: Tau variants. These constructs were previously cloned into pET-28 plasmids with Nco1/Xho1 restriction sites and two stop codons preceding the Xho1 cloning site to remove the C-terminal His6 tag (131). A number of truncated variants were also used, one variant commonly used in other tau studies, K18, is the only variant with this type of nomenclature. All other truncated variants are identified by the amino acids contained in each given variant with numbering scheme according to htau40. K18 was previously cloned in a similar manner to htau40 and htau23. All other truncated variants were ordered from Biomatic Corporation as lyophilized pET-28 plasmid containing the gene insert. Variants with no further identification include the native cysteines (positions 291 and 322) and no mutations. Two different versions of cysteine free or cysless (CL) constructs were also used, in these variants native cysteines were replaced by either serine or alanine. Unless explicitly stated as htau40 SS (indicating the serine replacement) or htau40 AA

(indicating the alanine replacement), experiments used serine replacement and is notated as htau40 CL. Point mutations are identified by the original amino acid, the residue number (with respect to htau40 sequence) and the new amino acid. For example, P301S refers to the proline at position 301 in the full-length 4R tau sequence being mutated into a serine, with native cysteines present.

2.2 Mutagenesis

Primers to make single point mutations were ordered from Integrated DNA Technologies as lyophilized DNA oligomers. These primers along with template DNA and QuikChange II Site-Directed Mutagenesis Kits (Agilent Technologies) were used to make point mutations. Specifically, by combining 5 µL 10x reaction buffer, 1 µL of DNA nucleotide bases (dNTP mix), 100-200 ng forward primer, 100-200 ng reverse primer, 20-30 ng stock DNA (DNA to be mutated), 29 µL PCR certified water (Teknova), and 1 µL Pfu Ultra DNA polymerase and subjecting that mixture to 17 cycles in a MJ Mini Personal Thermal Cycler (BIO RAD). Each cycle consisted of three classic denaturing, annealing, and extending stages at 95 °C for 1 min 15 seconds, 50-60 °C (5-7 °C lower than the melting temperature of the primers) for 1 min, and 70-72 °C for 11 min respectively. Following the completion of the cycles the reaction mixture was brought to 4 °C after which 1 µL of D*pn*1 restriction enzyme was added and let incubate at 37 °C for 1 hour to digest parental DNA.

2.3 Transformation

To obtain pure mutated DNA, digested PCR product was transformed into cells optimized for plasmid preparation, *E.coli* XL1-Blue supercompetent cells (Agilent Technologies). Transformation was carried out by combining 2 µL of Dpn1 treated DNA with 25 µL cells in a round-bottom polypropylene tube (Falcon) and set on ice for 30 min to allow plasmid to adhere to cell walls. Plasmid permeation into the cell walls was achieved with a heat pulse in 42 °C water for 45 seconds then placed back on ice for 2 min to prevent plasmid from exiting the cells. Following those 2 min on ice, 600 µL of preheated (37 °C) NZY mixture (10 g/L N-Z Amine (Sigma), 5 g/L Yeast (Difco), 5 g/L NaCl (J.T. Baker), 12.5 mM $MgSO_4$ (Fluka), 12.5 mM $MgCl_2$ (Sigma), 10 mM Glucose (Sigma)) was added, and cells were grown for 1-1.5 hours shaking at 200 rpm in a 37 °C incubator. Following growth, 200 µL of the NZY and cell mixture was plated onto a Kanamycin (50 mg/L) LB agar culture plate (100 mm x 15 mm sterile polystyrene, Fisher Scientific) and incubated at 37 °C for 15-20 hours. A single colony from a culture plate was used to inoculate a mixture of LB medium (Miller, BD) and Kanamycin (Gold Technology) that was placed in a 37 °C incubator shaking at 200 rpm for 15-17 hours. After growth, these cells were harvested by centrifugation at 6000 x g for 15 min and subjected to plasmid DNA purification using Qiagen Plasmid MIDI kit following the Qiagen protocol. Pure DNA was sent to Eton Bioscience for sequencing utilizing T7 promotor and T7 terminator primers. Samples with the desired sequence were then transformed into cells

optimized for expression, *E.coli* BL21 (DE3) cells (Agilent Technologies). Transformation was carried out as described above with two exceptions, starting with only 1 µl of pure DNA being combined with 25 µL cells, and only 50 µL of NZY cell mixture being plated onto Kanamycin culture plates. The increased transformation efficiency with pure DNA is the reason behind these changes, plating 200 µL results in overgrowth on the plates and increased difficulty in finding a single colony.

2.4 Expression and purification

Following transformation of pure DNA into *E.coli* BL21 cells, a single colony from a plate was used to inoculate liquid bacterial culture. The single colony was transferred to a mixture of LB medium (Miller, BD) with Kanamycin (Gold Biotechnology) and let shake at 200 rpm for 15-17 hours. That starter culture was then diluted 1:100 with sterile LB medium and Kanamycin (20 mg/L) and let shake at 200 rpm and 37 °C until optical density reached 0.7-1 at 600 nm. Protein expression was then induced by addition of 0.5 mM Isopropyl β-D-1-thiogalactopyranoside (IPTG; Gold Biotechnology). Bacteria were incubated shaking at 37 °C for another 3.5 hours before being pelleted at 3,000 x g and homogenized in resuspension buffer (500 mM NaCl, 20 mM piperazine-N,N'-bis(2-ethanesulfonic acid) (PIPES; Research Products International) pH 6.5, 1 mM ethylenediaminetetraacetic acid (EDTA; Fisher Scientific), and 50 mM β-mercaptoethanol (Fisher BioReagents). Cells were then lysed using heat and

sonication. Specifically, exposed to an 80 °C water bath for 20 min followed by tip sonication (Fisher Scientific sonifier model 40:0.15:4C at 50% power with a Branson 6-mm tip sonifer) for 1 min. The excessive heating from the 80 °C bath and continuous sonication do not negatively affect tau because it is intrinsically disordered. Once lysed, cell homogenate was centrifuged at 15,000 x g for 30 min to separate soluble protein from cellular debris. Soluble tau was then precipitated by gently shaking with 55-60% w/v ammonium sulfate (MP Biomedicals) for 3-20 hours at 25 °C. Precipitated tau pellets from a 15,000 x g spin were taken up in H_2O with 2 mM dithiothreitol (DTT; Gold Biotechnology), sonicated for 2 min (at 50% power on the same sonicator used previously), syringe filtered (GxF/GHP 0.45 µm) and loaded onto a cation exchange column (mono S 10/100 GL; GE Healthcare). Cation exchange can be used because tau carries a net positive charge, for example the isoelectric points for htau40 and htau23 are 8.4 and 9.4 respectively. Once loaded onto the MonoS column, proteins were eluted using a linear NaCl Gradient (50-1000 mM NaCl, 20 mM PIPES pH 6.5, 2 mM EDTA) and fractions were pooled based on SDS-PAGE with Coomassie stain assessment (representative chromatograph and gel shown in Appendix A). For further purification, pooled ion exchange fractions were loaded onto a Superdex 200 or Superdex 75 (GE Healthcare) gel filtration column and eluted with 100 mM NaCl, 20 mM Tris (Sigma), 1 mM EDTA and 2 mM DTT buffer pH 7.4 (representative chromatograph and gel shown in Appendix A). Fractions were again assessed using SDS-PAGE and those

containing pure tau were pooled. Tau from these pooled fractions was precipitated overnight at 4 °C using either a 1 volumetric equivalent of methanol or 3-fold volumetric excess of acetone depending on the length of the tau variant being purified, along with 5 mM DTT. Variants containing fewer than 200 amino acids were run over the Superdex 75 column and precipitated using acetone. Those larger than 200 amino acids were run over the Superdex 200 column and precipitated using methanol. Following precipitation, pellets were collected with a 15,000 x g spin for 10 min, transferred to 2 mL Eppendorf tubes, and centrifuged for 10 min at 13,500 x g. Supernatant was removed and pellets were spun again with 1 mL fresh methanol or acetone to completely exchange any buffer present. Pellets were then stored in methanol or acetone with 2 mM DTT at -80 °C until further use.

2.5 Monomerization

Precipitated protein pellets need to be solubilized into monomeric form, in an appropriate buffer, before use. Pellets being stored at -80 °C were taken from the freezer and all the methanol or acetone they were stored in was fully removed. Protein pellets were then dissolved in 200 µL of 8 M guanidine hydrochloride (GdnHCl; Thermo) for 2-5 hours. Once fully dissolved, denaturant was removed using a PD-10 desalting column (GE Healthcare). The total volume of dissolved protein solution was applied to one column followed by a volume of assembly buffer (100 mM NaCl, 10-40 mM 4-(2-hydroxyethyl)-1-

piperazineethanesulfonic acid (HEPES; J.T. Baker) and 0.1 mM NaN_3 (Fisher Scientific) at pH 7.4) that would make a total volume of 2 mL between dissolved protein and buffer. These 2 mL were allowed to fully enter the column. Protein was then eluted with 2 mL of assembly buffer. Before and after use, columns were cleaned by applying 200-300 µL of 6 M GdnHCl followed by 40-60 mL of assembly buffer to each column. Between runs columns were stored in assembly buffer, and discarded after approximately 20 uses. Concentration of eluted protein was determined using bicinchoninic acid assay (BCA assay; Thermo Fisher Scientific). The Pierce BCA Protein Assay Kit protocol was followed, and a standard curve with BSA was used each time. Extinction coefficients were not used for concentration determination because there are no tryptophans and only 5 tyrosines in even the longest 4R isoform. Once concentration was determined 0.5 mM tris(2-carboxyethyl)phosphine (TCEP; Gold Biotechnology) was added to cysteine containing variants to prevent disulfide bonding. Some experiments, where disulfide bond formation was desired, are exempt from this TCEP addition. Protein was then either flash frozen in aliquots appropriate for future experiments, or kept on ice at 4 °C for more immediate usage.

2.6 Initial fibril formation

Initial fibril formation (seed formation) was achieved by incubating a 500 µL mixture of 25 µM tau, 50 µM heparin (Celsus, average molecular weight 4400

kDa), 0.5 mM TCEP and assembly buffer stirring with a teflon-coated micro stir bar (5x2 mm) at 160 rpm for 7-8 days at 37 °C. Tubes with a flat bottom (MultiMax microcentrifuge tubes) were used so the stir bar could freely rotate. Heparin (or another polyanionic cofactor) is necessary for any aggregation, both initial fibril formation and seeded growth. Variants that did not contain any cysteines, or were oxidized, did not include TCEP during initial fibril formation. To ensure fibril formation, after 7-8 days 100 µL was taken from the mixture and centrifuged for 30 min at 128,000 x g (Beckman L7-55 ultracentrifuge). Any pellet was separated from supernatant and volumes were adjusted using SDS sample buffer (62.5 mM TRIS pH 6.5 (Sigma), 4% SDS (J.T. Baker), 10% sucrose (MP Biomedicals), 5% 2-Mercaptoethanol (βME; Fisher Scientific), 1.5 mM Bromophenol Blue (Sigma)) so equal sample amounts could be analyzed by SDS-PAGE with Coomassie staining. 12% or 15% gels were used depending on the length of the variant making up the fibrils. Seed fibrils that showed majority growth (quantified via Image J software as described below in Growth Analysis) and little to no degradation were used for seeded reactions.

2.7 Seeded sedimentation reactions

To create fibrils fragments, or seeds, fibrils grown as described above were subjected to 30 second sonication on ice at 20% power (4 ± 1 w(RMS)) with a Fisher Scientific sonifier (model 100 with a 2 mm tip). The 2 mm rather than 6 mm tip was used simply because the larger tip did not fit inside the seed tube.

Seeded reactions were carried out using these seeds (10% monomer molar equivalent) in combination with fresh 10 μM tau monomer, 20 μM heparin, 0.5 mM TCEP and assembly buffer, and let incubate quiescently at 37 °C for 20-24 hours. TCEP was not used in the majority of reactions containing oxidized tau, other deviations are noted in the text. After incubation, reactions were sedimented using a 30 min centrifugation at 128,000 x g. Sedimentation caused long fibrils to be pelleted, and monomers unable to be incorporated onto seeds, along with seeds that had no monomer grow on them to remain in the supernatant. Following centrifugation, pellet and supernatant were separated and both analyzed using SDS-PAGE with Coomassie staining as described in section 2.6.

2.8 Growth analysis

Image J software was used on scanned gels to assess the amount of fibril growth for a given reaction. This was done by dividing the pixel density of protein band in the pellet lane by the added density of both the pellet and supernatant lane. These values (multiplied by 100) are reported in all box-and-whisker or scatter plots as a percentage growth. 100% would represent a reaction where the entire protein density appeared in the pellet lane while 0% appeared in the supernatant lane. Data points for a given reaction condition represent results from reactions initiated from different seed batches (biological replicates), not multiple reactions initiated from the same seed batch (technical replicates). Plots

were created using GraphPad Prism 7 software where statistical significance between growth from different reactions is determined using a paired t-test. P-value summary for each comparison is shown as stars (**), and the p-value that corresponds to the specific number of starts is in the legend for each specific figure. Box-and-whisker plots utilize the Tukey method for displaying whiskers and outliers, and lines on scatter plots indicate mean with standard deviation.

2.9 Thioflavin T kinetics

Thioflavin T (ThT, Sigma) is a dye that fluoresces upon binding to amyloid fibril core structure (111) and was used to monomer fibril growth kinetics. These reactions contained 10 µM tau, 20 µM heparin, 5 µM ThT, 5% or 10% seed (overall 0.5 µM or 1 µM tau in sonicated fibril form) and assembly buffer. Unless oxidized variants were used, these reactions also contained 0.5 mM TCEP. The only time TCEP was used in conjunction with oxidized monomer/fibrils was as a treatment in the dissociation experiments, as noted in the text. Fibril growth was monitored in real time by thioflavin T fluorescence using a BGM Labtech FLUOstar Omega plate reader utilizing excitation/emission wavelengths at 440/480 nm and constant 37 °C. Readings were taken through the bottom of a Thermo Scientific 96 well optical Btm Plt PolymerBase plate. Some reactions, as indicated in figure legends, utilize a 2 second 100 rpm shake prior to the first reading to ensure reactions are mixed. Growth reactions were done in either triplicate or quadruplicate and the average values along with their standard

deviation (S.D.) are displayed for each reaction. Due to the different ways ThT can bind to different conformers resulting in different total fluorescence, intensity growth rates rather than end point intensity were used in some cases to compare different reactions. Growth rates were compared by the time it took ThT intensity to reach half its max value and are reported as T ½ values.

2.10 Transmission electron microscopy

Transmission electron microcopy was used to visualize aggregation from different reaction conditions. Formvar/ Carbon 200 mesh copper grids (Electron Microscopy Sciences) were exposed to a droplet containing approximately 2.5 µM fibrils for 1.5 min, blotted on filter paper to remove excess liquid, exposed to a droplet of 2% uranyl acetate (Electron Microscopy Sciences, 0.2 µm syringe filtered) for 1.5 min, and again blotted on filter paper then let air dry for approximately 5 min before being stored in holder until imaging. Fibril images were recorded at University of Colorado, Boulder with a FEI Tecnai T12 Biotwin Electron transmission microscope using a high tension of 100 KV and equipped with a Gatan CCD camera. The negative stain TEM images were taken by myself with the exception of those shown in Chapter 3 which were taken by Dr. Michael Holden. Quantification of seed length was done by analyzing micrographs of sonicated seeds using Image J software utilizing the scale bar on the image to calibrate the number of pixels to an accurate length. These lengths were then binned and plotted in GraphPad Prism 7.

2.11 MTSL labeling of tau

Electron paramagnetic resonance (EPR) experiments were performed to gain insight on side-chain stacking and structural rigidity of tau protein, and to determine distances between paramagnetic centers in a sample (124). The paramagnetic spin label used for all continuous wave (CW) EPR and double electron-electron resonance (DEER) spectroscopy experiments was [1-oxyl-2,2,5,5-tetramethyl-Δ3-pyrroline-3-methyl]methanethiosulfonate (MTSL; Toronto Research Chemicals). This label covalently binds to a cysteine residue as shown in Figure 2.1 (132). To ensure specific labeling, variants to be used for EPR experiments had native cysteines mutated into serines, and cysteines mutated in only the desired labeling position. Protein pellets being stored at -80 °C were taken from the freezer and all the methanol or acetone they were stored in was fully removed. Protein pellets were then dissolved in 200 µL of 8 M guanidine hydrochloride (GdnHCl; Thermo) for 2-5 hours. Once fully dissolved, MTSL (taken up from powder form in DMSO to 40 mg/ml) was added in approximately 10- fold molar excess. Labeling reaction took for place for at least 1 hour while sitting in the dark quiescently at 25 °C. Excess label was then removed, along with denaturant, when passed over PD-10 columns as described in Section 2.5. The non-paramagnetic analog of MTSL [1-acetyl-2,2,5,5-tetramethyl-Δ3-pyrroline-3-methyl]methanethiosulfonate (Toronto Research Chemicals) was attached in a similar manner and used for dilution of some CW EPR samples.

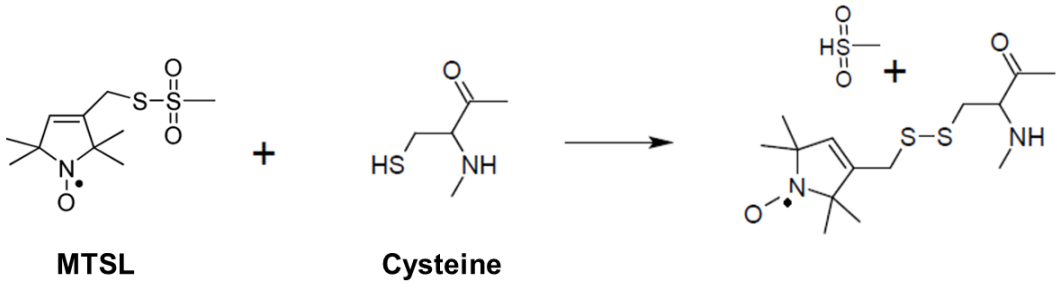

Figure 2.1 MTSL labeling of tau. MTSL spin label covalently links to a single cysteine residue.

2.12 CW EPR sample preparation

CW EPR spectra of monomers were taken to confirm MTSL had bound to monomer and was in a fairly mobile state. This is indicated by spectra with three sharp and narrow peaks with a 34 G outer peak separation (133). These spectra were collected at X-band (9.5 GHz) at 25 °C with 150 G sweep width, 12.05 mW power and 1 G modulation amplitude on a Bruker EMX Plus spectrometer fitted with an ER 4119HS resonator. Once monomer was confirmed labeled with MTSL, fibrils were formed by allowing a combination of 30 µM MTSL labeled monomer (either 100% paramagnetic MTSL labeled, or 20% paramagnetic MTSL labeled/ 80% non-paramagnetic MTSL labeled monomer), 15 µM heparin, 5% seed not labeled with MTSL (formed as described above in Section 2.6), and assembly buffer to quiescently incubate at 37 °C for 20-24 hours. Following incubation, fibrils were sedimented in a 128,000 x g 30 min spin after which supernatant was fully removed. Pelleted fibrils were gently mixed with 10 µL fresh assembly buffer in order to be loaded into round capillary tubes (Vitrotubes 0.6 ID x 0.84 OD).

2.13 CW EPR sample measurement and analysis

Tubes containing fibrils to be analyzed via CW EPR were inserted into the resonator such that the sample was centered vertically or filling the length of the resonator. Spectra are an average of 20 scans collected at room temperature with 150 G sweep width, 12.05 mW power, 3 G modulation amplitude, modulation frequency of 100 KHz, 5.02 x 10^3 receiver gain, 81.92 msec time constant, 20 msec conversion time, 1 harmonic, with 1024 x resolution on a Bruker EMX Plus spectrometer fitted with an ER 4119HS resonator operating at X-band. Spectra being compared were normalized to the same number of spins using double integration so amplitudes could be compared. These amplitudes are reported in histogram form for comparison between different monomer (differing by which residue was labeled) grown onto different seeds. Bars represent averages and error bars represent standard deviation from biological triplicate measurements for each reaction type.

2.14 DEER sample preparation

DEER samples were prepared by combining 48 µM non MTSL labeled tau (CL variants), 2 µM tau double MTSL labeled at positions 311 and 328, 10% seeds, 12.5 µM heparin and assembly buffer then incubating quiescently at 37 °C for 24 hours. Seeds were assembled as described in section 2.6, and fibrils indicated as mutant are 100% mutant meaning the tau used in the 48 µM non MTSL labeled, 2 µM MTSL labeled and seeds all contained the mutation of

interest. Following incubation, fibrils were sedimented for 30 min at 128,000 x g, supernatant was removed, and pellets were mixed with 10-15 µL of fresh assembly buffer for transfer into quartz Q-band tubes (VITROCOM SFS round cell 1.1 mm ID). Samples were then analyzed to ensure proper label incorporation using CW EPR (as described above) before being flash frozen and stored at -80 °C until DEER measurements could be performed.

2.15 DEER sample measurement and analysis

DEER measurements were collected at Q-band (34 GHz) using a four-pulse sequence depicted in Figure 2.2. A field-sweep spectrum was used to center the operating frequency (ν_1), and the pump frequency (ν_2) was adjusted to 37 MHz below ν_1. For each experiment the gate and τ_{-0} were optimized and ranged between 64-72 ns and 910-914 ns respectively, and the π/2 pulse at ν_1, the π pulse at ν_2, τ_1, τ_2 and τ_3 and τ_x remained constant at 16 ns, 32 ns, 200 ns, 3000 ns, 100 ns and 8 ns respectively. The shot repetition time was optimized for each sample to be 1.2 x T1 (spin-lattice relaxation time) and signal averaging took place for approximately 24 hours per sample with each scan containing 8 step phase cycling to remove unwanted echoes. Data was collected using a Bruker ELEXSYS E580 spectrometer with an ER 5107D2 dielectric resonator, a 580-400U ELDOR unit as the second microwave source and a 10 W amplifier. Temperature was kept at 80 K using an Oxford CF935 cryostat and liquid nitrogen. Data were analyzed with DEER Analysis 2018 (134) using Tikhonov

regularization, three-dimensional homogenous background fit, program-optimized selection utilizing validation tool for zero time, background time, regularization parameter, and phase, whereas cutoff time was kept constant for each sample at 2936 ns.

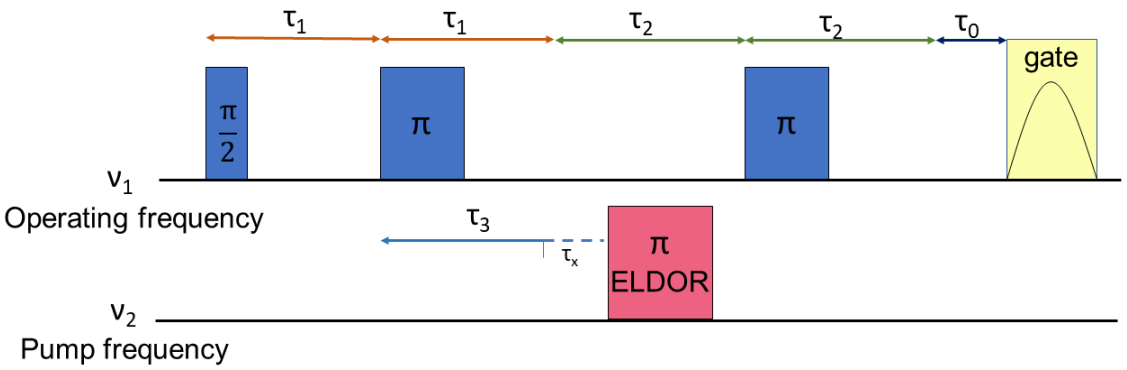

Figure 2.2 DEER pulse sequence. The echo formed after two pulses at ν_1 is refocused and decays with time after the third pulse. A separate part of the spectrum is excited by the fourth pulse at ν_2. If there is interaction between the two sets of spins at the frequencies ν_1 and ν_2 the strength of the interaction between the spins reveals information about the distance between them.

2.16 Oxidation of tau

The majority of experiments were done in the presence of reducing agent so disulfide bonds are not formed. However, some experiments wanted to explore the effect of intramolecularly disulfide bonded monomers. These monomers required further preparation following monomerization before experimental usage. Oxidation of htau40 was carried out by incubating 20 µM htau40 immediately following its monomerization with 5 mM H_2O_2 (Sigma-Aldrich 30% (w/w) in H_2O) at room temperature in the dark for 16-20 hours. To remove H_2O_2, and promote any oxidation that has not already occurred, the reaction was

then transferred into a dialysis tube (Spectra/Por flat width 10 mm, molecular weight cutoff 12-14 kDa) and let dialyze over 2-3 rounds of suspended agitation in 1 L 40 mM HEPES assembly buffer each for 1 hour at 5 °C. Following dialysis, the reaction was spin concentrated using Amicon Ultra centrifugal filter units (molecular weight cutoff 10 kDa) to a final volume 1.5-2 mL. This volume was desired given the capacity of the size exclusion column being used in the next step. Spin concentrated protein was run over a size exclusion column (GE Healthcare Superdex 200 10/300 GL) to separate higher order species from monomer, using 0.5 mL fraction size and 40 mM HEPES assembly. To identify fractions containing only monomeric intramolecularly disulfide bonded htau40 from those with some higher order intermolecularly bonded species, fractions were run on a regular SDS-PAGE gel. Importantly SDS sample buffer with no reducing agent was used because disulfide bonds needed to remain intact. Fractions containing only monomeric species with an intramolecular disulfide bond were pooled and a concentration was determined using BCA assay. To confirm the cysteines in this monomer are not free, this oxidized monomer was subjected to the protocol for MTSL labeling of tau (as described in Section 2.11). The lack of strong MTSL signal in a CW EPR spectrum following the labeling protocol confirms cysteines are not free. The reversibility of the disulfide bond was confirmed by the restoration of signal from oxidized monomer that was incubated with 20 mM DTT for 5 hours then had the DTT dialyzed out (in the

same manner as described above for dialysis), before being subjected to the protocol for MTSL labeling of tau.

2.17 Anaerobic sedimentation reactions

One set of sedimentation reactions, described in detail in Chapter 4, was carried out in the absence of oxygen. These experiments used Coy Lab Products anaerobic chamber and glove box. Oxygen content was kept between 10-20 parts per million using a Coy Anaerobic Monitor (CAM-12 detector) and compressed gas (nitrogen and hydrogen). Buffer to be used was purged with compressed nitrogen gas for 30 min prior to entering the chamber. After dissolving an htau40 precipitated pellet in ambient room conditions with GdnHCl, the dissolved protein was taken into the chamber where it was run through a PD10 column in the same manner as described in Section 2.5. Following elution off the column protein dilutions for BCA assay concentration determination were made and removed from the chamber for measurement. Once concentration was determined, the monomer (10 µM) was used for reaction setup inside the chamber with nitrogen purged buffer along with heparin (20 µM) and 10% seeds. Heparin and seeds were in tubes opened inside the chamber for 15 min prior to use. Once reaction components were combined the reaction tubes were placed in a digital dry bath set to 37 °C inside the chamber and let incubate for 20-24 hours. Following incubation, they were removed from the chamber and sedimented (30 min at 128,000 x g). Following sedimentation pellets separated

from supernatants and run on SDS-PAGE gels with Coomassie staining, then analyzed as previously described. This anaerobic experimental setup only applies to the data shown in Figure 4.6 B. The ambient oxygen content for all other experiments does not impact the results because reducing agent is present for experiments where no disulfide bond formation is desired, hydrogen peroxide was used to oxidize variants that did desire disulfide bond formation, and the slow oxidation (via dissolved oxygen content) of cysteine containing variants in reactions absent of reducing agent is part of the experimental question and is noted in the text in Chapter 4.

2.18 Guanidine melt of fibrils

Denaturation profiles were used to highlight structural differences between fibril types. Homotypic growth reactions utilizing 10% htau40 reduced or oxidized seeds were set up (as described in 2.7) and let incubate quiescently at 37 °C for 20-24 hours. Following incubation, a 100 µL aliquot of this growth was centrifuged and assessed using SDS-PAGE to confirm grown (presence of protein exclusively in the pellet) for each reaction mixture. Once growth was confirmed growth mixtures were aliquoted into seven tubes to which the same volume of solutions with various GdnHCl (Thermo) concentrations were added. The different final concentrations of GdnHCl in each aliquot were 0, 0.1, 0.25, 0.5, 0.75, 1, or 1.5 M GdnHCl. The contents of the tubes were mixed and let quiescently incubate at 25 °C for 1 hour. Following incubation, these mixtures

were centrifuged for 30 min at 128,000 x g, supernatant was discarded, pellets were taken up in 100 µL SDS sample buffer. These were then run on SDS-PAGE gels with Coomassie staining to assess the quantity of protein found in each pellet fraction. The amount of protein remaining fibrillar and present in the pellet fraction following this protocol was quantified using Image J software as described in Section 2.8. For each fibril type the average values corresponding to the remaining fibril content at each GdnHCl concentration, from biological triplicate measurements, are depicted in a scatter plot.

2.19 Limited proteolysis

Limited protease digestion was used to highlight differences in fibril structures by comparing their pattern of cleavage products on SDS-PAGE gels. Homotypic 10% seeded growth reactions for htau40 reduced and oxidized fibrils were assessed for growth as described in Section 2.18. Following growth confirmation, 80 µL aliquots of each fibril type were treated with 60 nM proteinase K (PK; Promega) or assembly buffer (in the same volume as PK in parallel reactions) at 25 °C for 30 min. Proteolysis was stopped with the addition of 4 mM phenylmethylsulfonyl fluoride (Sigma). SDS sample buffer was then added and samples were run on a 4-20% precast gradient gel (Bio-Rad Mini-PROTEAN TGX stain-free gels) and stained with Coomassie.

2.20 Limited sheering of fibrils

Differences in fibril fragility was used to highlight their structural differences. Homotypic 10% seeded growth reactions of htau40 reduced and oxidized fibrils were assessed for growth as described in Section 2.18. Following growth confirmation, 100 µL aliquots of growth mixture were subjected to 30 seconds of sonication in a Qsonica bath sonicator at 5% power (specifics on this sonicator are in section 2.24). Bath sonication rather than tip sonication was used because it produced the milder sheering needed for this experiment. Following sonication, aliquots were diluted with assembly buffer to approximately 2-2.5 µM and loaded onto Formvar/ Carbon 200 mesh copper grids for TEM imaging and analysis as described in Section 2.10.

2.21 Crosslinking htau40 monomer

Observing growth properties of htau40 monomer with something other than a disulfide bond linking the two native cysteines was desired. The bismaleimide crosslinker used to link native cysteines in htau40 monomer is shown in Figure 2.3. Methanol was removed from a pellet of precipitated htau40 before being dissolved in 2 mL of GndHCl. Once dissolved, an approximate 3-fold molar excess of bis(maleimido)ethane (BMOE; Thermo Scientific, taken up in DMSO to 20 mM) was added and let incubate at 25 °C in the dark quiescently for 1 hour. Following incubation, 500 mM DTT was added to quench any unbound label, then the dissolved protein containing crosslinker was run in ~500 µL aliquots

over PD10 desalting columns and eluted as described in Section 2.5. The protein containing elution fractions were spin concentrated to a final volume of 2 mL before being run over a size exclusion column (GE Healthcare Superdex 200 10/300 GL) utilizing 0.5 mL fraction size and 40 mM HEPES assembly buffer pH 7.4. To distinguish fractions containing monomeric crosslinked species from higher order species, fractions were run on SDS-PAGE gels. Fractions containing only monomeric species were pooled and a concentration was determined using BCA assay.

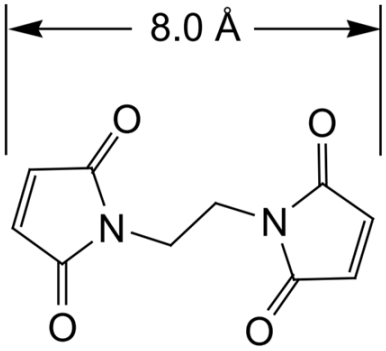

Figure 2.3 Bismaleimide crosslinker. Structure of bis(maleimidio)ethane, BMOE, which will crosslink two cysteine residues with an 8 Å spacer arm.

2.22 Dissociation of htau40 oxidized fibrils

The dissociation of oxidized fibrils was investigated by treating them with reducing agents. Growth of homotypic htau40 oxidized seeded reactions (setup described in section 2.7, with no TCEP present initially) were allowed to proceed for 5 hours at which time the reactions were removed from the 37 °C incubator and treated or sedimented. Treatments to each reaction were made with the same volume of different stock solutions to achieve different final reducing agent

concentrations. For control reactions the same volume of assembly buffer was added. The treated reactions were gently inverted once then returned to the 37 °C incubator to quiescently sit for 16-20 hours. Following incubation, the reactions were spun down in a high-speed spin (as described in Section 2.7) and 20 µL of the supernatant along with pellet fraction were assessed for percent growth by protein band quantification on SDS-PAGE gels. In some cases, the remainder of the supernatants, approximately 980 µL, were run over a size exclusion column (GE Healthcare Superdex 200 10/300 GL) to compare the elution peak patterns of the protein that supernatant. In a similar manner, 980 µL of 5 µM htau40 (with 0.5 mM TCEP present) was also run over this column as a control to confirm the elution volume of htau40 monomer peak. From each run, 6 µL of the 1 mL fractions from the elution volume were run on SDS-PAGE gels to observe and compare the banding patterns.

2.23 Monitoring quiescent nucleation

Hexapeptide mutants were investigated for their potential to suppress self-nucleation, a critical factor for use in our amplification assay. These mutants were made as described in Section 2.2. These mutants along with htau40 monomer were used in 200 µL reactions (25 µM monomer, 50 µM heparin, 5 µM ThT, and 1 mM TCEP with 40 mM HEPES assembly buffer) to quiescently monitor self-nucleation. These reactions were monitored in a 96-well clear bottom polymerbase plate (Thermo Scientific) and fibril content was monitored in

real time by ThT fluorescence using a BGM Labtech FLUOstar Omega plate reader utilizing excitation/emission wavelengths at 440/480 nm and constant temperature of 37 °C. Readings were taken in several hour increments over multiple days. Variation between runs included some plates being kept in a 37 °C incubator between readings, while some plates remained in the plate reader at 37 °C for the entirety of the experiment. ThT fluorescence readings were plotted in Excel as an average of three measurements.

2.24 Amplification assay

An amplification assay consisting of cycles of sonication and incubation was used to measure spontaneous monomer nucleation and/or growth from seeded reactions. Not all reaction component/parameter variations are shown in figure form, but some are listed in table format in Appendix B. However, specific reaction components for data shown in figures were 10 µM monomer, 40 µM heparin, 1 mM TCEP brought to a final volume of 200 µL with 40 mM HEPES assembly buffer. Seeded reactions additionally had htau40 seeds present; seed formation was done as described in Section 2.6 then diluted so the same final volume was added to each reaction for different final seed concentrations. Each seed dilution had heparin to a final concentration of 40 µM and TCEP to a final concentration of 0.5 mM. Reactions took place in nontreated black bottom 96 microwell plates (Thermo Scientific). Plates were sealed with certified DNase-RNase- free clear polyolefin sealing tape (Thermo Scientific) and floated in 700

mL of water in a microplate horn coupled to an ultrasonic processor (Qsonica) with a temperature control unit (Qsonica model 10-180-GI-PI-08S) to keep all experiments at a constant temperature of 37 °C. Individual parameters that varied between different experiments include the sonication time, incubation time, power amplitude of sonication, tau concentration and heparin concentration. Specific parameters for individual experiments can be found in Appendix B or in the text of Chapter 5. Following cycles of sonication and incubation, reactions were transferred to 1.5 mL Beckman Coulter centrifuge tubes and centrifuged at 128,000 x g for 30 min, pellets were separated from supernatants and analyzed by SDS-PAGE with Coomassie staining as described in Section 2.6.

CHAPTER THREE: TRUNCATIONS AND MUTATIONS AFFECT CORE CONFORMATION IN FOUR-REPEAT TAU FIBRILS

3.1 Formation of seed fibrils

Recruitment of tau monomers onto fibrils is a conformation-dependent phenomenon. This means if monomers are incompatible with a specific seed fibril conformer, they will not add on to elongate those fibrils. One potential mechanism causing the preferential deposition of 3R or 4R tau in some tauopathies is a conformation-based cross seeding barrier. This theory was investigated by testing the growth properties of different tau fibrils. Specifically, if truncated and mutated 4R tau variants could form different fibril conformers from full-length non-mutated 4R tau. In order to probe the elongation properties of specific fibrils, these fibrils had to first be formed. Initial fibrils were formed through the NDP growth scheme (nucleation and elongation) of specific monomeric tau variants, over several days through agitation at 37 °C in the presence of a polyanionic cofactor (heparin) and reducing agent (TCEP).

The first variant to be characterized was htau40. Initial growth of long unbranched fibrils was confirmed using negative stain transmission electron microscopy (TEM) (Figure 3.1 A). These fibrils were then sheared using a tip sonicator to create shorter fibril fragments referred to as seeds (Figure 3.1

B). The seeds were roughly the same length, as a distribution of their quantified lengths proved to be a fairly narrow distribution with an average of 39 nm (Figure 3.1 C). An indirect representation of this transition from long fibrils to short fibril fragments is the fraction they end up in following centrifugation at 128,000 x g, with visualization by SDS-PAGE and Coomassie staining. Identical centrifuge parameters cause long unbroken fibrils to experience a higher centrifugal force and transition into in a pellet, but the short seed fragments remain in the supernatant as the force they experience is not great enough to sediment them (Figure 3.1 D). The presence of the protein at the expected size for htau40 on SDS-PAGE suggests this sonication event is acting to disrupt the stacking of monomers within the long fibrils, not destroying the individual monomers. If the sonication event was acting to break apart monomer, protein would be observed as having a lower weight on SDS-PAGE, and it is not. Once the protocol was established for the creation of seeds, experiments to explore the recruitment properties of those seeds were pursued.

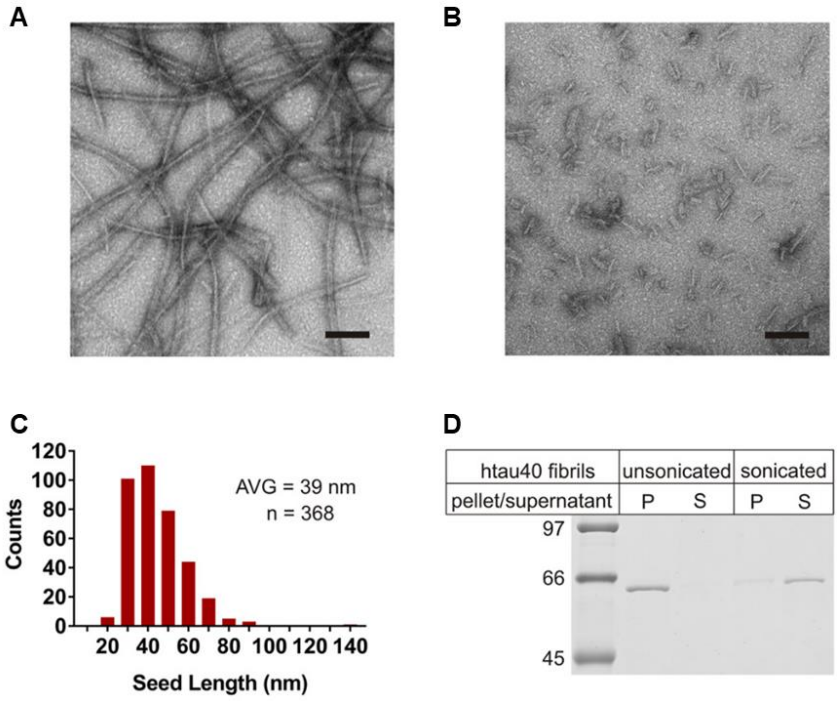

Figure 3.1 Characterization of htau40 fibrils. A and B, EM images of htau40 fibrils formed via nucleation and elongation before (A) and after (B) tip sonication. Scale bars = 100 nm. C, distribution showing quantified htau40 seed lengths. D, SDS-PAGE with Coomassie staining assessment of P = pellet and S = supernatant fractions of unsonicated and sonicated fibrils following centrifugation. This demonstrates that initial growth results in long fibrillar structures, which after tip sonication, show uniform fracture.

3.2 Growth of htau40 and htau23 monomer onto htau40 seeds

Growth properties of fibrils made up of the longest 4R isoform, htau40, were the first to be investigated. The ability of these htau40 seeds to recruit both 4R (htau40) and 3R (htau23) tau monomers was in question (Figure 1.1). Reactions contained 10% (molar monomer equivalence) of seeds combined with fresh htau40 or htau23 monomers (10 µM) along with reducing agent (0.5 mM TCEP) and heparin (20 µM). These reactions were allowed to quiescently incubate at 37 °C for 20-24 hours. Following the incubation period, reactions

were spun down and pellets were separated from supernatants before both were run on 12% SDS-PAGE gels. Growth assessment was done by comparing the percentage of protein in the pellet vs the supernatant for each given reaction, and results show that htau40 seeds fully recruit both 4R and 3R monomer (Figure 3.2 A). SDS-PAGE analysis shows the protein band from htau40 seed in the pellet for the reaction with htau23 monomers because the initial short seed fragments were elongated, and are part of the long fibrils being sedimented. This growth trend of htau40 recruiting both 4R and 3R monomers is highly reproducible as it was seen for >40 biological replicates (Figure 3.2 B). Biological replicates refer to reactions initiated from different seed batches. Thioflavin T (ThT) fluorescence can also be used to highlight the growth of these monomers onto htau40 seeds (Figure 3.2 C). The difference in end point fluorescence for each reaction can be attributed to the different ways in which ThT binds to the monomers making up the fibrils, however the significant point is the growth rates of these reactions are similar. This similar rate is shown by the comparable time it took each reaction to reach half maximum intensity (Figure 3.2 C), suggesting no preferential growth of 4R or 3R monomer. The lack of a lag phase and the absence of fluorescence increase for reactions incubated in the absence of seed, in agreement with previous observations (93), confirm that the aggregation seen in these seeded reactions is via elongation onto those seeds and not spontaneous monomer nucleation. Additional independent confirmation that the aggregation is fibrillar, not amorphous, was achieved by TEM (Figure 3.2 D).

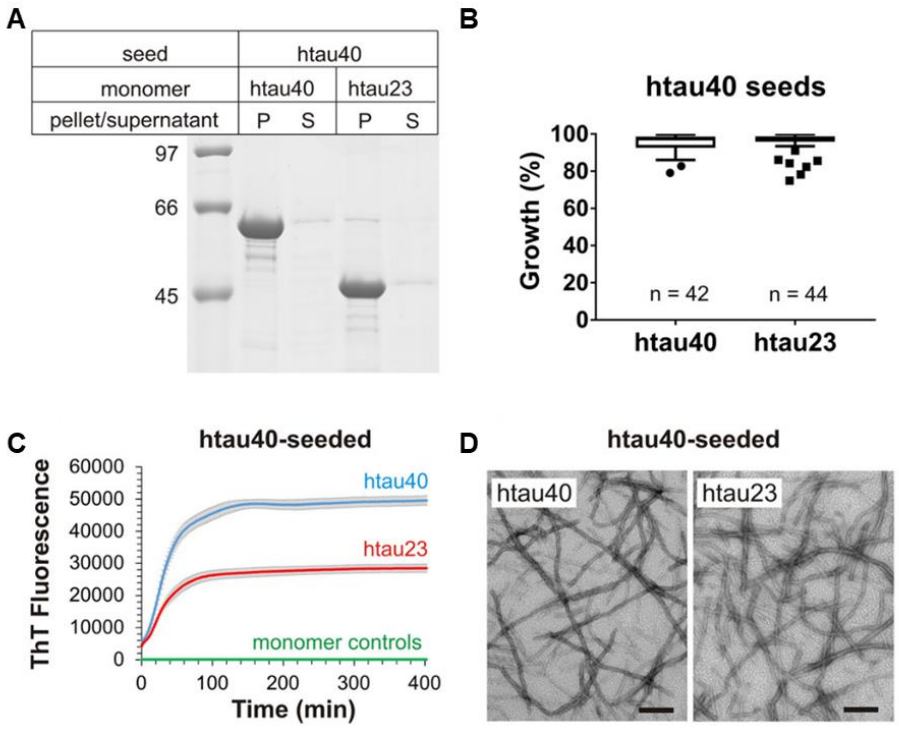

Figure 3.2 Seeding properties of htau40 fibrils. A, SDS-PAGE with Coomassie staining of 10% htau40 seeded reactions with htau40 monomer or htau23 monomer. P = pellet, S = supernatant. B, box-and-whisker plot displaying results from quantified growth from seeded reactions, n = number of biological replicates. C, average ThT fluorescence showing kinetics of htau40 (blue) and htau23 (red) monomer growth on htau40 seeds, and monomer controls (green) in the absence of seeds. Error bars represent standard deviation (S.D.) from triplicate measurements. D, negative stain TEM images of growth from htau40 seeded reactions with htau40 (left) and htau23 (right) monomers. Scale bars = 200 nm. These results demonstrate the full fibrillar growth of htau40 and htau23 monomer on htau40 seeds.

This lack of cross-seeding barrier on full-length 4R seeds showed a deviation from the trend observed in similar experiments using truncated 4R seeds (88, 131). To ensure experimental conditions that were changed from previous studies were not responsible for the difference in growth properties, these changes were applied to experiments with the full-length 4R seeds. The first difference was the temperature at which nucleation of monomeric htau40 took place, allowing initial seed fibrils to form at 25 °C rather than 37 °C. Once formed,

growth experiments were carried out in the same manner and no growth barrier was observed (Figure 3.3 A). Another difference was the mutation of the two native cysteines into serines for previous truncated experiments, so the same mutations were made to the full-length 4R to make it a cysteine free or cysless (htau40 CL) construct. Growth patterns for htau40 CL seeds also show no growth barrier (Figure 3.3 B). Finally, a combination of the two changes, nucleating the cysless construct at 25 °C, also resulted in fibrils with no growth barrier (Figure 3.3 C). Therefore, the additional residues present from the N- and C-terminal ends of the htau40 variant are likely responsible for this change in growth barrier.

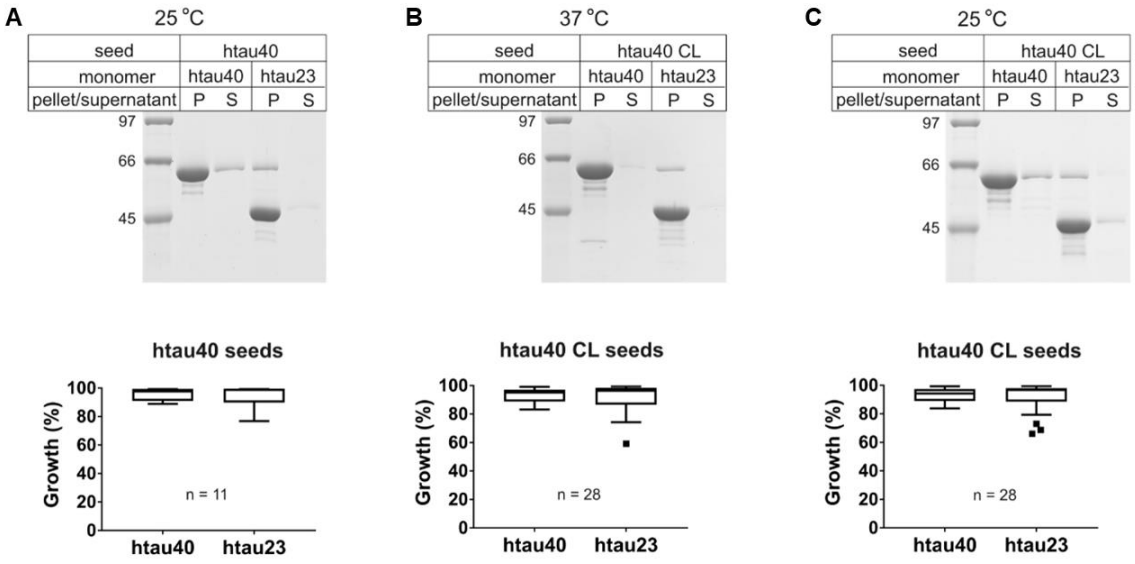

Figure 3.3 Growth properties of htau40 fibrils with various nucleation temperatures and/or native cysteine content. Representative gel and box-and-whisker plot showing quantification of fibril growth for reactions between htau40 seeds formed at 25 °C (A), htau40 CL (native cysteines replaced by serines) seeds formed at 37 °C (B), and htau40 CL seeds formed at 25 °C (C). P = pellet, S = supernatant, n = number of biological replicates. These findings show that changing the native cysteines in htau40 to serines and/or the nucleation temperature does not affect the ability of its seeds to recruit htau23 monomers.

3.3 Seeding properties of N- or C-terminally truncated tau

Growth properties of different truncated variants were used to investigate the impact regions of the N- and C- terminus have on the conformation fibrils assume during their nucleation. These variants differ by truncations made at either the N- or C- terminus, or both (Figure 3.4).

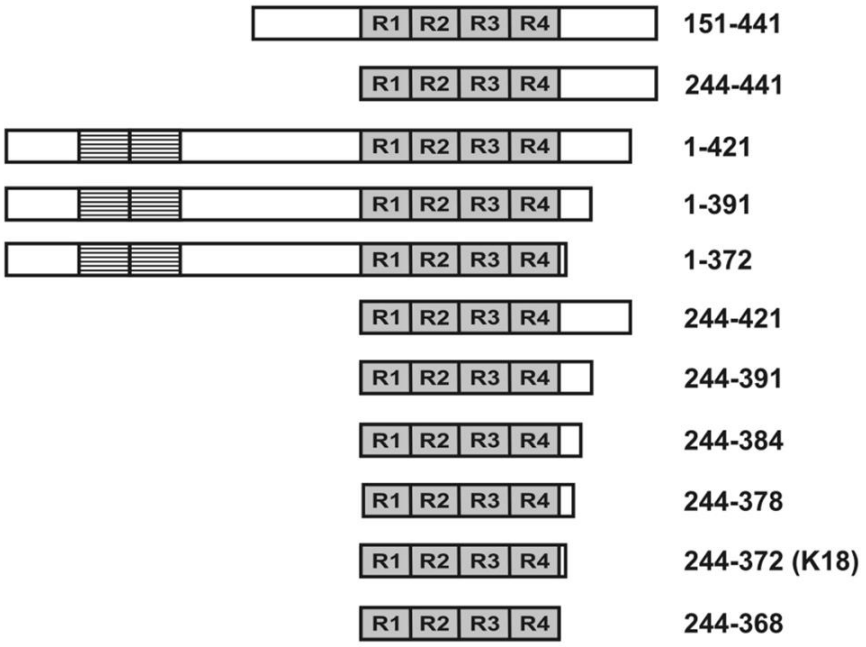

Figure 3.4 Schematic diagram of truncated variants used for growth studies. N-terminal inserts are striped, repeats are shaded. Numbers represent the amino acids contained in each variant, numbering with respect to htau40.

The first two variants to be investigated were those with truncations to only the N-terminal end, containing amino acids 151-441 or 244-441 (numbering scheme corresponding to htau40). When these variants were used as the monomeric species during nucleation, and the resulting fibrils were sonicated then offered full-length htau40 or htau23 monomers, no growth barriers were observed (Figure 3.5 A, B). Similarly, when C-terminally truncated variants, 1-421

and 1-391, were subjected to the same fibril formation, fragmentation, and seeded reaction conditions; they also showed no observable growth barriers (Figure 3.5 C, D). The 1-372 variant, while showing no barrier with htau40 monomers, did however show a significant growth barrier to full-length htau23 monomers (Figure 3.5 E). This suggests that the C-terminal end affects tau conformation and seeding competency.

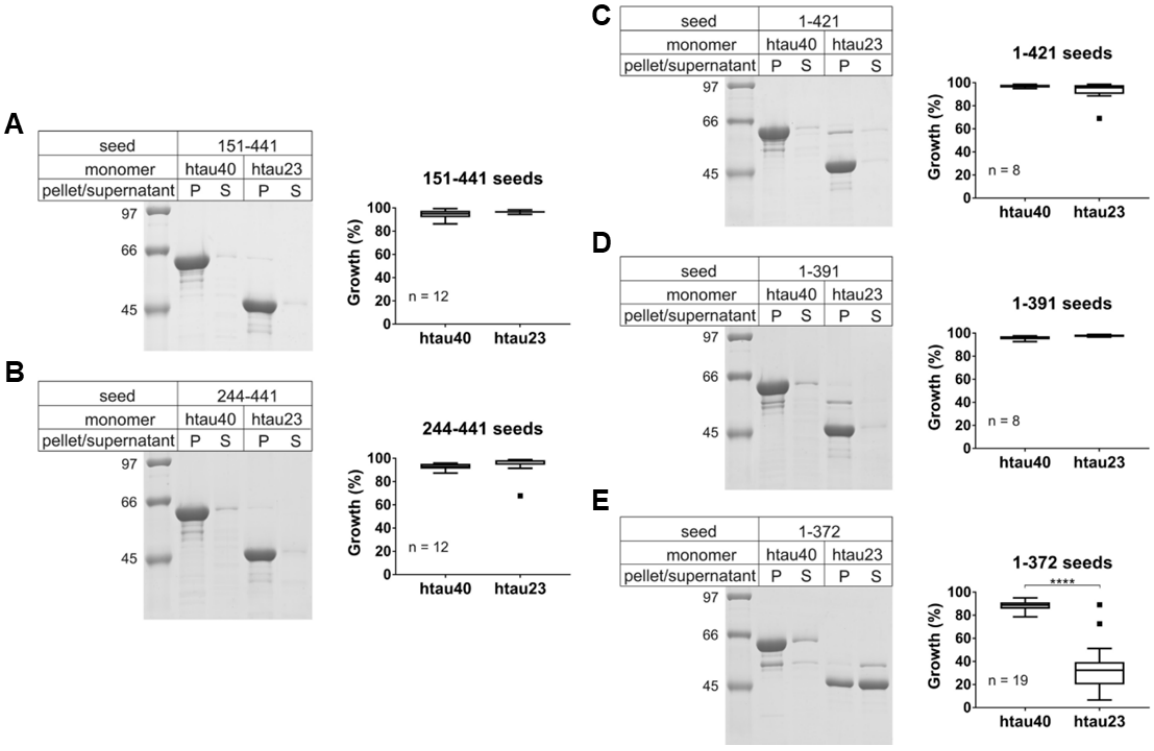

Figure 3.5 Seeding properties of fibrils composed of N- or C- terminally truncated variants. Fibrils used for seeding were formed from 5 different N- or C- terminally truncated htau40 variants, 10% of these seeds were offered to htau40 or htau23 monomers and let quiescently incubate for 20-24 hours at 37 °C. A-E, a representative gel with Coomassie staining of growth reactions with each seed type, along with a box-and-whisker plot depicting quantified results for multiple reactions. P = pellet, S = supernatant, n = number of biological replicates, statistical analysis was done using a paired t-test ****, p≤ 0.0001. Htau40 monomers were fully recruited to all seed types, and only the 1-372 variant produced fibrils with a partial htau23 growth barrier.

3.4 Seeding properties of N- and C-terminally truncated tau

To investigate the impact the C-terminus has on fibril conformation, and potential synergism between the N- and C-terminal regions, the growth properties of variants with truncations to both the N- and C-terminus were investigated. Variants all began at residue 244, the beginning of the first MTBR, and varied in the number of amino acids remaining on the C-terminal end extending to residue 421, 391, 384, 378, 372 or ending immediately at the end of the fourth repeat at residue 368 (Figure 3.4). The growth properties of seeds made up of these different variants was assessed in a manner similar to other growth reactions thus far, looking at their ability to recruit both htau40 and htau23 monomers. All seeds were able to recruit htau40 monomers, but the ability to recruit htau23 successfully diminished in correlation with systematic truncation to the C-terminal end (Figure 3.6 A-F). The mean percent of 3R growth on these variants started at 88% for the 244-421 variant dropping to 79%, 66%, 52%, 36%, and finally 26% for the 244-368 variant. These results suggest that the C-terminal residues of htau40 play a role in influencing the conformation of full-length 4R tau fibrils, and residues on the N-terminal end seem to play a synergistic role. The synergism of the N-terminal residues is suggested by results showing variants with only small C-terminal truncations were fully able to recruit htau23, but when that same C-terminal truncation was combined with a N-terminal truncation, partial growth barriers were observed (compare Figure 3.5 C, D to Figure 3.6 A, B).

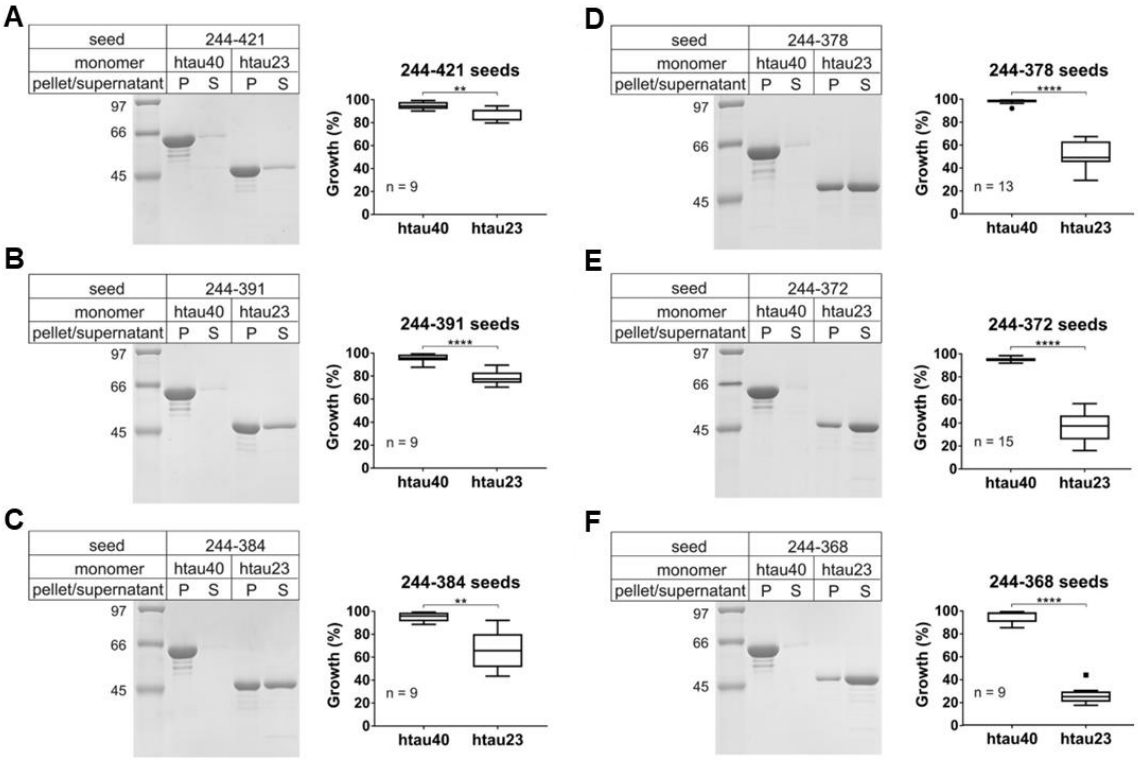

Figure 3.6 Seeding properties of fibrils composed of N- and C- terminally truncated variants. Fibrils used for seeding were formed from 6 different truncated htau40 variants that all have had residues N-terminal to the repeat regions removed and a systematically shorted C-terminus. 10% molar equivalent seeds were offered to htau40 or htau23 monomers and let quiescently incubate for 20-24 hours at 37 °C. A representative gel of these growth reactions with each seed type, along with a box-and-whisker plot depicting quantified results for multiple reactions are shown in A-F. P = pellet, S = supernatant, n = number of biological replicates, statistical analysis was done using a paired t-test ** , $p \leq 0.01$, **** , $p \leq 0.0001$. These results show that all variants are able to fully recruit htau40 monomers, and that the successive shortening of the C-terminus results in an increased growth barrier of htau23 monomers.

3.5 Seeding properties of P301S and P301L fibrils

In addition to truncations it was of particular interest to investigate the impact specific point mutations have on fibril growth properties, as number of familial mutations have been associated with 4R or 3R tauopathies (65). Some mutations cause an increase in splicing, resulting in the overexpression of either 4R or 3R variants. However, there are some mutations that have been shown to

not change the 4R/3R ratio, yet still present with preferential deposition of 4R or 3R in affected brain regions (24). The protocol exploring growth via conformational templating of monomer onto preformed seeds allows for investigation of whether fibril conformers formed from mutant tau exhibit growth properties that align with the pathology of the mutant *in vivo*. Mutations of the proline at position 301 to either a serine or a leucine, referred to as P301S or P301L, are associated with 4R tauopathies but have been documented to cause little to no change in the 4R/3R ratio (135). These mutations were introduced into the htau40 construct. Seeds formed from the respective mutant monomers were then subjected to the same growth analysis as previously described. Both P301S and P301L mutant seeds were able to recruit non-mutant htau40 monomers, but both showed a very robust seeding barrier for htau23 monomers (Figure 3.7 A, B left and middle panels). It is interesting to note that while mutant seeds did recruit htau40 monomers, this heterotypic recruitment was slower with T ½ = 60-68 min (Figure 3.7 A, B right panels), than the growth rate of homotypic htau40 monomers on htau40 seeds (T ½ = 25-27 min) (Figure 3.2 C). It is also significantly slower than the homotypic mutant monomers on mutant seed growth, displaying full recruitment with a T ½ = 5-9 min (Figure 3.7 C-F). This significantly slower heterotypic growth rate is in agreement with the previously observed preferential growth of mutant over non-mutant 4R tau (135). The aggregation seen here between mutant seeds and either htau40 monomers or mutant monomers is fibrillar in nature as evidenced by TEM images of this

growth. TEM additionally confirms the lack of fibril growth when htau23 monomers are offered to these same mutant seeds (Figure 3.8 A, B).

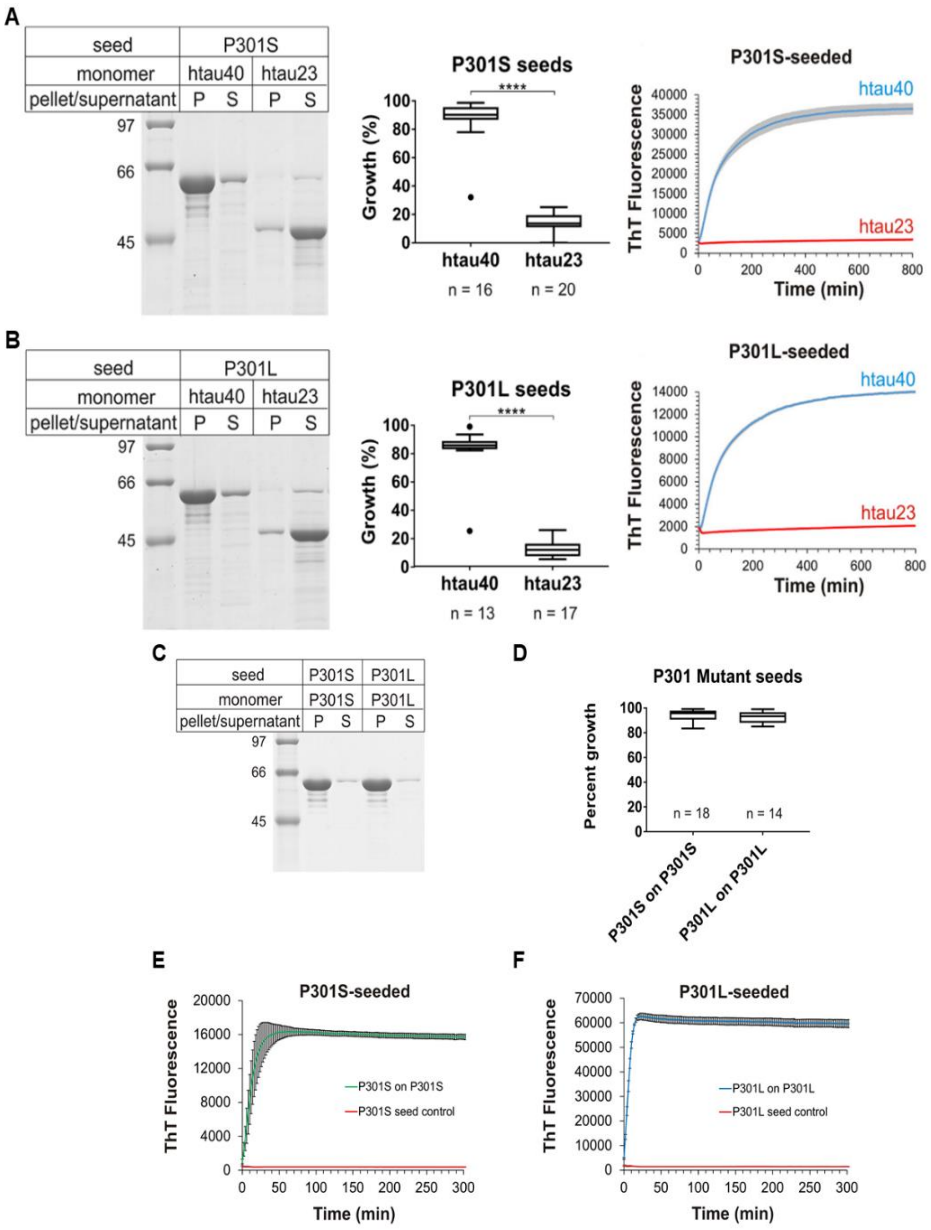

Figure 3.7 Seeding properties of P301S and P301L fibrils. A and B, representative gel, densitometric quantification represented as box-and-whisker plot, and ThT kinetics of heterotypic growth reactions between htau40 (blue traces) or htau23 monomers (red traces) with P301S and P301L mutant seeds respectively. C and D, representative gel and box-and-whisker plot depicting quantified results from homotypic P301 mutant seeding reactions. E and F, ThT kinetics of mutant homotypic growth reactions (green and blue traces), along with seed controls (red traces). P = pellet, S = supernatant, n = number of biological replicates, statistical analysis via paired t-test ****, $p \leq 0.0001$, error bars represent means ± S.D. from 4 measurements. These results indicate both P301S and P301L fibrils are able to recruit htau40 monomers and their respective mutant monomers, but are unable to efficiently recruit htau23 monomers.

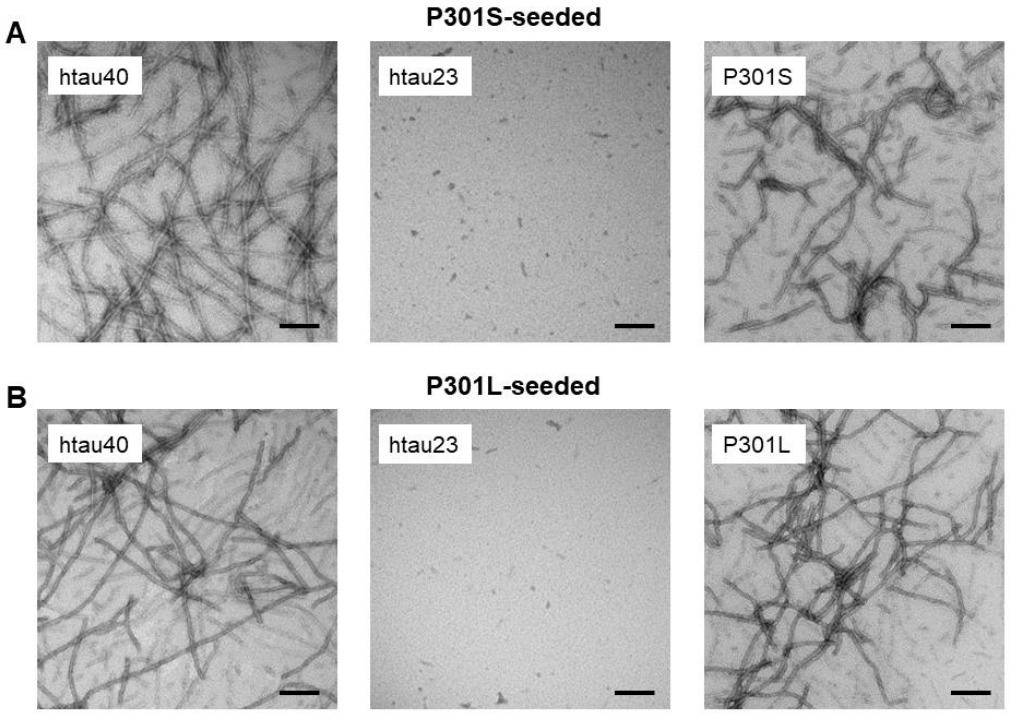

Figure 3.8 TEM analysis of P301S and P301L seeded reactions. Growth resulting from htau40 monomers (left panel), htau23 monomers (middle panel), or P301 mutant monomers (right panel) offered to mutant seeds. A, P301S seeded reactions. B, P301L seeded reactions. Scale bars on all images are 200 nm. These results indicate mutant P301 seeds with htau40 monomers or mutant monomers result in fibrillar growth, and confirms the inability of htau23 monomers to be recruited to either type of mutant seed.

3.6 Mutant fibrils without observable growth barriers

The significant seeding barrier of 3R tau monomers seen with P301 mutant fibrils led to question whether any variant with a point mutation in in this region would form fibrils with a 3R growth barrier, or if this growth phenomenon was particular to mutating this specific residue. In order to investigate this, six new mutant variants were created, again using htau40 as a template. These variants include three familial mutations, ΔN296, G303V, and S305N, also known to be

associated with 4R tauopathies (24). These mutants were subjected to the same fibril formation, fragmentation, and seeded reaction conditions as previously described. These mutant seeds were all able to fully recruit both htau40 and htau23 monomer, with the only exception being a slight htau23 barrier seen with ΔN296 seeds (Figure 3.9 A-C).

The three other mutant variants investigated were V306D, I308D and Y310D. These were chosen not because they were familial mutants, but because they reside in the PHF6 motif from residues 306-311. This motif has been identified as an important element for tau fibril aggregation (136). The anticipation was that a mutation to any of these natively hydrophobic amino acids into a negatively charged aspartic acid might cause a disruption of β-sheet packing and potentially alter fibril conformation. However, if the mutation did alter fibril conformation it was not in such a way as to cause preferential recruitment. Fibrils comprised of these mutants were able to nucleate under stirring conditions, and fully recruit both htau40 and htau23 monomers (Figure 3.9 D-F). Combined with the P301 mutant data, the lack of strong growth barriers for these six fibrils with mutations in close proximity to position 301 suggests the proline at position 301 plays a unique role in determining fibril structure.

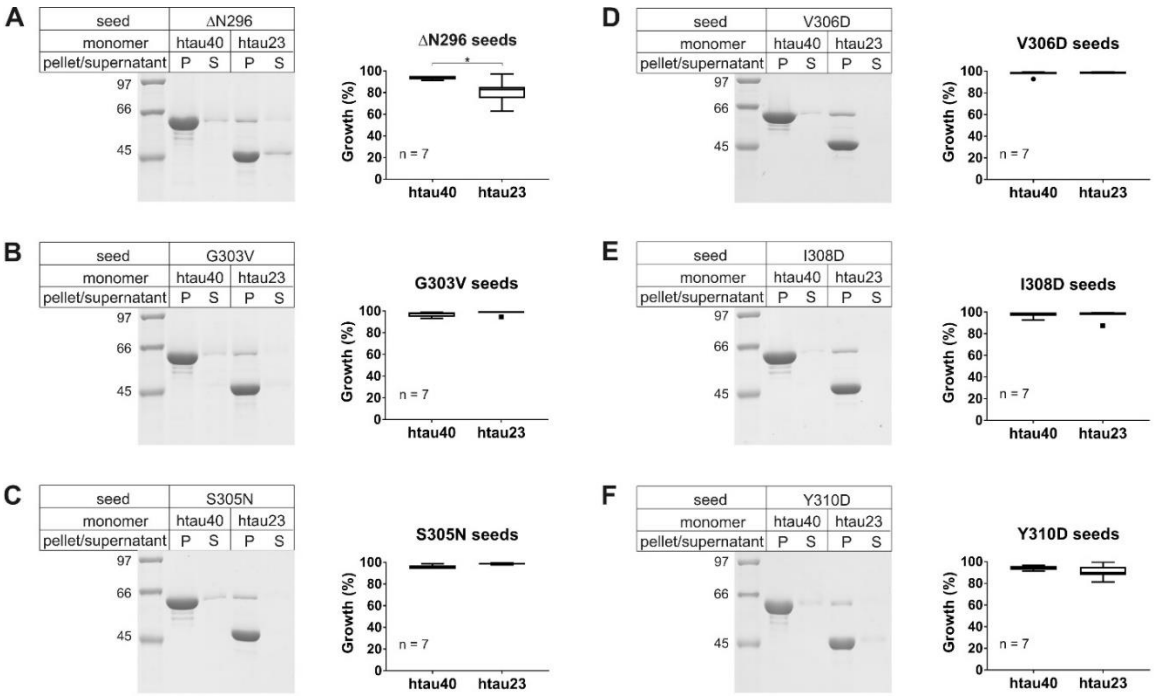

Figure 3.9 Seeding properties of fibrils with mutations flanking position 301. Representative gel and densitometric quantification represented as box-and-whisker plot for 10% seeded growth reactions between various mutant seeds with htau40 or htau23 monomers. A-C, results from reactions initiated from familial mutant composed seeds, ΔN296, G303V and S305N, respectively. D-F, results from reactions initiated from synthetic PHF6 motif mutant composed seeds, V306D, I308D, and Y310D respectively. P = pellet, S = supernatant, n = number of biological replicates, statistical analysis via paired t-test *, p≤ 0.05. These results identify no htau40 or htau23 growth barrier for any mutant seed type, with the exception of a minor htau23 growth barrier on ΔN296 seeds.

3.7 CW EPR of htau40, P301 mutant, and K18 seeded fibrils

The 3R growth barriers seen with some truncated and P301 fibrils, but not with htau40 fibrils, is likely due to structural differences in the core of these fibrils. To investigate whether or not certain residues reside in the core of different fibril types, site-directed spin labeling in conjunction with electron paramagnetic resonance (SDSL-EPR) experiments were performed. Continuous wave (CW) EPR was used due to its success gaining insight on side-chain stacking and

structural rigidity of tau protein in previous experiments (89, 125). Seven different reporter monomers were made to probe whether certain residues were part of the core of htau40, P301S, P301L, and K18 fibrils. These monomers had the native cysteines replaced with serines (shown to not affect growth barriers Figure 3.3), and a single cysteine introduced at one of the following residues, 342, 343, 345, 360, 369, 371 or 375. Mutants were made in the 4R construct because it was fully recruited onto all seed types. These mutant monomers were labeled with either paramagnetic nitroxide label MTSL or its nonparamagnetic analogue. Once attached, these paramagnetic and nonparamagnetic moieties are referred to as R1 and R1' respectively. The purity of these labeled monomers was confirmed before usage by SDS-PAGE with Coomassie staining (Figure 3.10 A). R1 proteins all diluted to 10 μM produced EPR spectra with similar signal intensity, suggesting a similar labeling efficiency. These spectra also exhibited three sharp lines with 34 G separation between outer peaks, as expected for a spin labeled intrinsically disordered protein (Figure 3.10 B) (133).

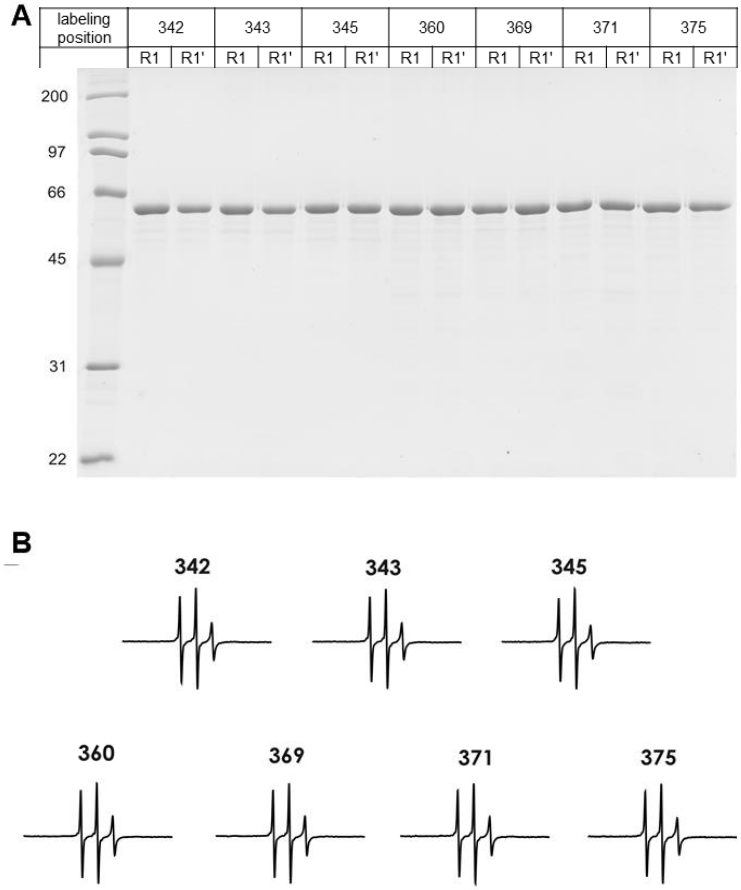

Figure 3.10 Site-directed spin labeling and CW EPR analysis of htau40 single cysteine mutant monomers. A, equivalent concentrations of seven single cysteine tau monomers with paramagnetic label (R1) or nonparamagnetic label (R1') visualized on SDS-PAGE with Coomassie staining. B, CW EPR spectra of 10 µM R1 monomer collected at X-band with 150 G sweep width, 1 G modulation amplitude, and 12 mW incident microwave power. Axes are the same for all spectra. This data confirms the purity and intrinsic disorder of these labeled monomers.

Once the quality of monomers was confirmed they were used in seeded reactions with htau40, P301S, P301L, or K18 (244-372) seeds. These seeds were chosen because we wanted to investigate regions of structure in htau40 fibrils in comparison to fibrils that exhibited a 3R growth barrier. Following incubation, the growth reactions were centrifuged at 128,000 x g for 30 min.

Pelleted fibrils were resuspended in 15 µL assembly buffer in order to transfer them into capillary tubes appropriate for EPR measurements. Fibril spectra with depressed amplitudes and single-line characteristic indicate a high amount of spin exchange is occurring. This increased spin exchange is due to the R1 moiety being in a region of high structural order, where they are stacked on top of one another. Alternatively, spectra exhibiting three sharp lines with increased amplitude suggests the labeled residue is in a region of more disorder (125). All seeded fibrils with label attached at positions 342, 343, and 345 produced spectra with single-line characteristics. This suggests that for all seed types, (htau40, P301S, P301L and K18) these residues likely reside in the structured fibril core comprised of parallel in-register β-strands (Figure 3.11 A). When monomer labeled at the remaining positions, 360, 369, 371 and 375 were grown onto htau40 seeds, the resulting fibrils also produced spectra with single-line characteristics. These spectra contain less than 2% contribution from mobile components as determined by spectral subtraction. Again, the lack of hyperfine structure in these spectra can be attributed to spin exchange between contacting labels since they are repeatedly stacked on top of one another along the fibril axis (75). However, when monomer labeled at positions 360, 369, 371 and 375 were grown onto fibrils that have a 3R tau growth barrier (P301S, P301L and K18), they revealed spectra dominated by three sharp lines. This spectral characteristic suggests these residues are in a less structured region, a striking difference from htau40 fibrils (Figure 3.11 A). The labeled monomer is still

incorporated into these fibrils, and as such does exhibit decreased mobility and some spin exchange component in comparison to labeled monomer that is not incorporated into a fibril. The label simply resides in a region of structural disorder rather than the ordered core region, and do not experience as much spin exchange as core labeled residues do. These spin exchange characteristics are consistent with spectra previously published where residues in the first and second repeat were labeled in the htau40 fibrils (125). Spectra to be compared were normalized to the same number of spins using double integration. Once normalized, spectral amplitude is one way to quantify and compare label mobility for different monomers grown on different seed types. A plot of these amplitudes for the spectra discussed above highlights the structural difference in htau40 fibrils which recruit both 4R and 3R, to those which do not recruit 3R (Figure 3.11 B).

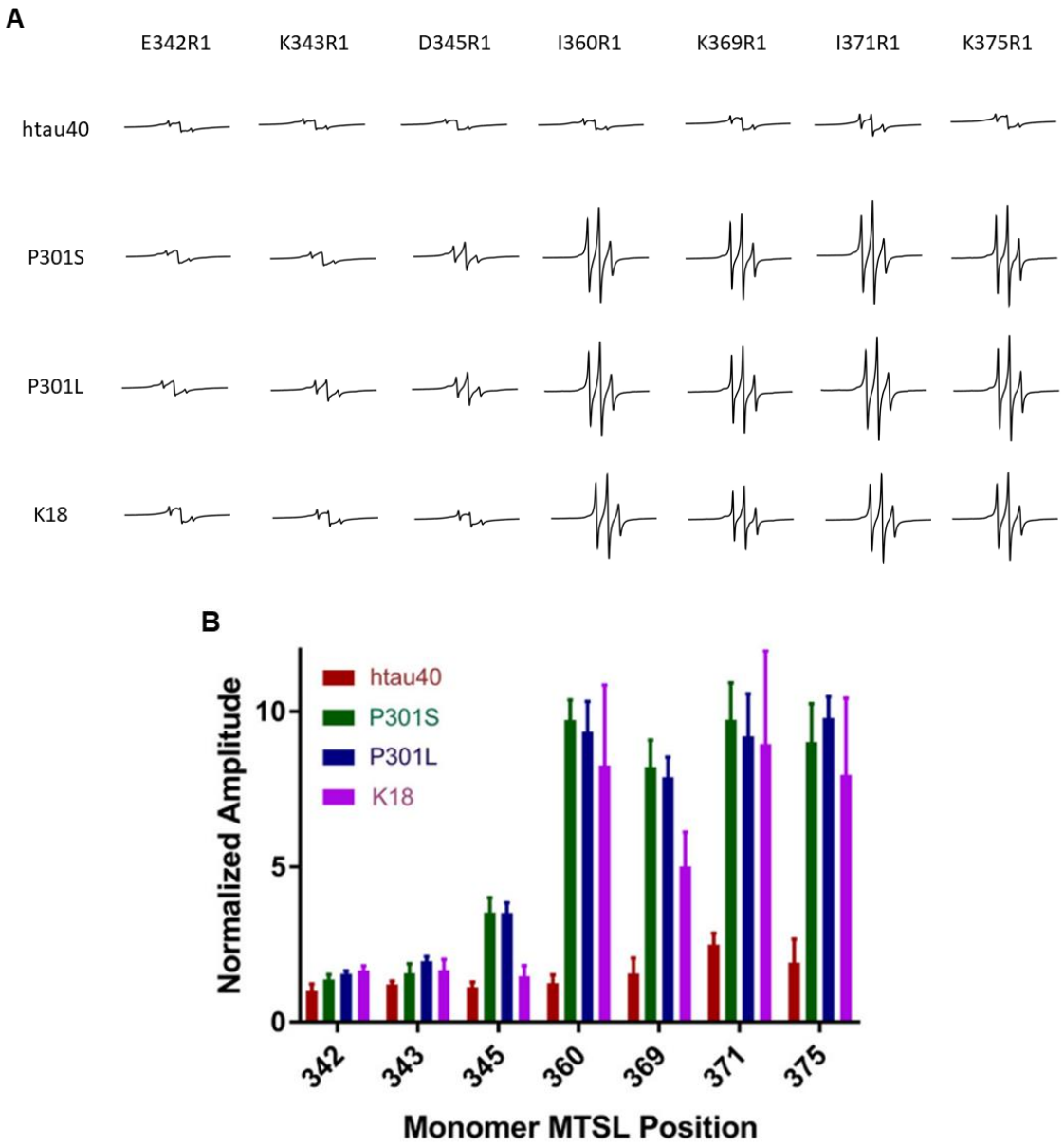

Figure 3.11 EPR analysis of MTSL labeled monomer grown onto htau40, P301S, P301L, and K18 seeds. Single cysteine mutant monomers labeled with paramagnetic spin label were offered to four different seed types, the resulting fibrils were pelleted and analyzed using CW EPR. A, spectra normalized to the same number of spins for all reaction combinations where the top horizontal row indicates the position of the R1 moiety in the monomer, and the leftmost vertical column indicates the type of seed used to initiate growth. Spectra were collected at X-band with 150 G scan width, 3 G modulation amplitude, and 12 mW incident power at room temperature. B, plot of signal amplitudes from biological triplicate measurements showing mean + S.D. This data highlights the difference in residues residing in the core of htau40 fibrils from those of P301S, P301L and K18 fibrils.

Many of the spectra for the growth reactions described above were dominated by spin exchange because 100% of the monomer used for the reactions was paramagnetically labeled. To gain information more specifically about label mobility, spectra absent of this complete spin exchange must be obtained. To do this, a dilution of the spins was done where reactions were set up with the same seed types, but used a 1:4 molar ratio of paramagnetic to nonparamagnetic labeled monomer respectively. The spectra from such growth reactions revealed the same overall spectral trend. All mutants grown onto htau40 seeds exhibited a broadened three-line spectrum with a 68 G outer peak separation, characteristic of immobilized spin labels (75). Monomer with labeled positions 342, 343, and 345 grown onto P301S, P301L and K18 seeds also shared this spectral characteristic (Figure 3.12 A). But on these three seed types, monomer labeled at the positions in the end of the fourth repeat or just outside the fourth repeat indicated higher side-chain mobility (75). These spectra have some immobile components, but are dominated by three sharp and narrow peaks with a 34 G outer peak separation. Again, a plot of signal amplitudes highlights the trend of different regions of structural order in the htau40 fibrils compared to P301S, P301L and K18 fibrils (Figure 3.12 B).

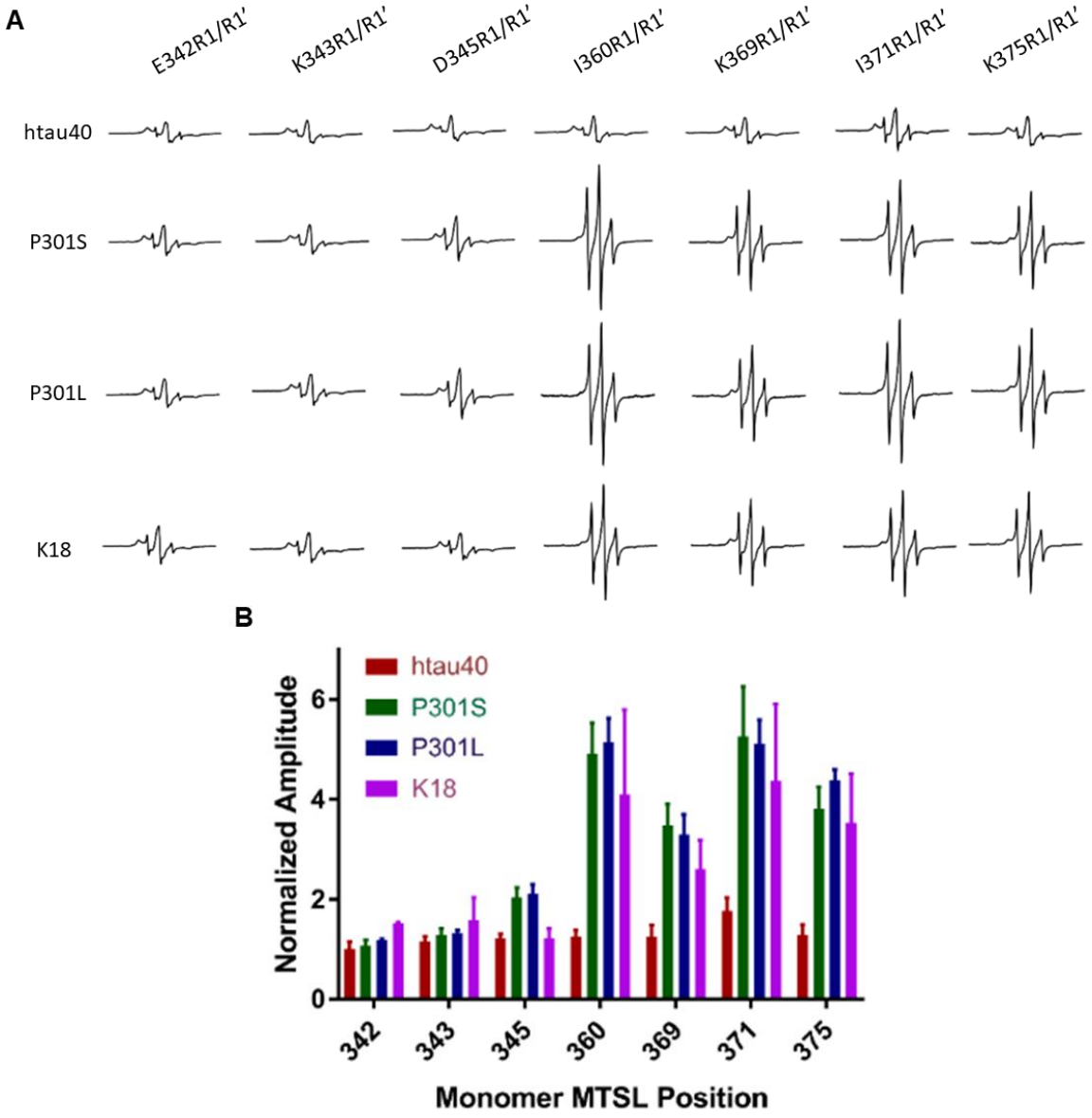

Figure 3.12 EPR analysis of fibrils containing a mixture of paramagnetically and nonparmagnetically labeled monomer. Four different seed types were offered single cysteine mutant monomers with paramagnetic and nonparamagnetic labels (R1 and R1') in a 1:4 molar ratio respectively, the resulting fibrils were pelleted and analyzed using CW EPR. A, spectra normalized to the same number of spins for all reaction combinations where the top horizontal row indicates the position of the R1 and R1' moiety in the monomer, and the leftmost vertical column indicates the type of seed used to initiate growth. Spectra were collected at room temperature at X-band with 150 G scan width, 3 G modulation amplitude, and 12 mW incident power. B, plot of signal amplitudes from biological triplicate measurements showing mean + S.D. This data highlights the difference in core structure of htau40 fibrils from P301S, P301L and K18 fibrils.

3.8 DEER analysis reveals distinct ensembles of fibril conformers

Experiments thus far have highlighted the different growth properties and different residues in the core of htau40 and P301 mutant fibrils. But identifying whether or not these growth reactions contain a mixture of fibril conformers or are defined by a single conformer remained a question. To address this question another type of EPR, DEER, was used. This technique allows for the measurement of distances between a pair of spin labels (137). Two spin labels were introduced within the same monomer type and a dilute percentage of this doubly spin labeled monomer was used in growth reactions. The distance distribution from a DEER measurement of all fibrils in a reaction mixture can identify whether or not multiple conformers exist. If only one conformer is present the distance between the labeled residues will be the same and only one peak will arise in the analysis. However, if multiple conformers exist within a single reaction, multiple peaks will be seen on spectral analysis as each different conformer will have a different distance between spin labels. This technique has been successfully used in previous studies to probe fibril structure and distinguish different fibril conformers (76).

The label positions used for these experiments were 311/328, as they were previously successful in structural studies of truncated tau protein (K18) (64). Three different monomeric versions, all in the htau40 template, of spin labeled monomer were used. Monomer to be grown on htau40 seeds had the native cysteines replaced by serines, and two cysteines introduced at the labeling

positions. Monomer to be grown on P301S or P301L seeds additionally had the mutation that their respective seed also contained. Successful MTSL labeling of these monomers was confirmed using CW EPR, where spectra showed three sharp lines as expected for label attached to a monomeric intrinsically disordered protein (133) (Figure 3.13 A-C top panels). Fibrils were grown by combining these labeled monomers with 25-fold molar excess of non-labeled monomer, 10% seed, and heparin then let incubate before being pelleted as previously described. Pelleted fibrils were resuspended in 15 µL assembly buffer and loaded into EPR tubes. The large dilution of labeled monomer was done to ensure that any detected distances were between spin labels on the same monomer, and not intermolecular distances between different monomers. CW EPR spectra of these fibrils were collected before being flash frozen and subjected to DEER measurements. Broadened three-line spectra with depressed amplitudes suggest label immobility indicating the paramagnetically labeled monomers have been incorporated into the fibril, and are not preferentially stacked on one another, but rather distributed along the long fibril axis (Figure 3.13 A-C bottom panels). If labeled monomers were preferentially stacked together, they would have experienced spin exchange, and the resulting spectra would have exhibited single line characteristics.

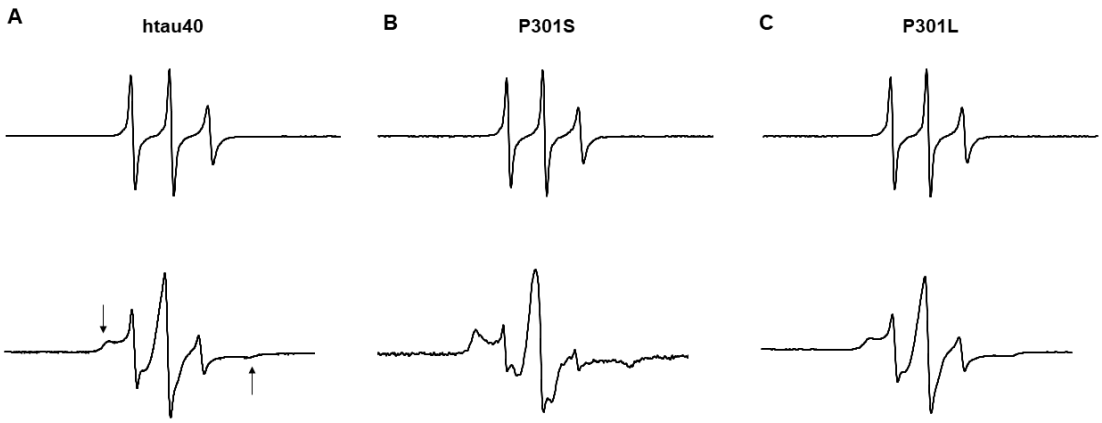

Figure 3.13 CW EPR analysis of spin labeled monomer and fibrils used for DEER measurements. CW EPR spectra collected at X-band with 150 G sweep width and 12 mW incident power. Spectra on the top and bottom row used 1 G or 3 G modulation amplitude respectively. A-C top row, representative CW spectra for the same concentration of htau40, P301S, P301L monomer doubly MTSL spin labeled at positions 311 and 328. Axes are the same and the similar sharp three-line spectra with 34 G peak separation indicate the similar labeling efficiency of the three monomer types. A-C bottom row, representative CW EPR spectra of fibrils to be further analyzed using DEER. Spectra collectively reveal that spin labeled monomers were incorporated into fibrils and distributed along the fibril axis as they show an immobile component (arrows indicating 68 G separated outer peaks), but are not dominated by spin exchange.

Triplicate DEER data was collected for each different seed type and a representative dipolar evolution curve with corresponding distance distributions after Tikhonov regularization are shown in (Figure 3.14 A, B). The steeper initial drop in the dipolar evolution curve from htau40 fibrils as compared to both P301S and P301L fibrils agrees with shorter distance peaks in their distributions (Figure 3.14 left vs middle and right panels). The lack of multiple strong dipolar oscillations in the evolution curves is consistent with bi-labeled molecules with broad distance distributions like those shown here (138). This data indicates that

all three types of fibrils are ensembles (clouds) of conformers, and that the ensemble of htau40 fibrils is different from that of P301S and P301L fibrils.

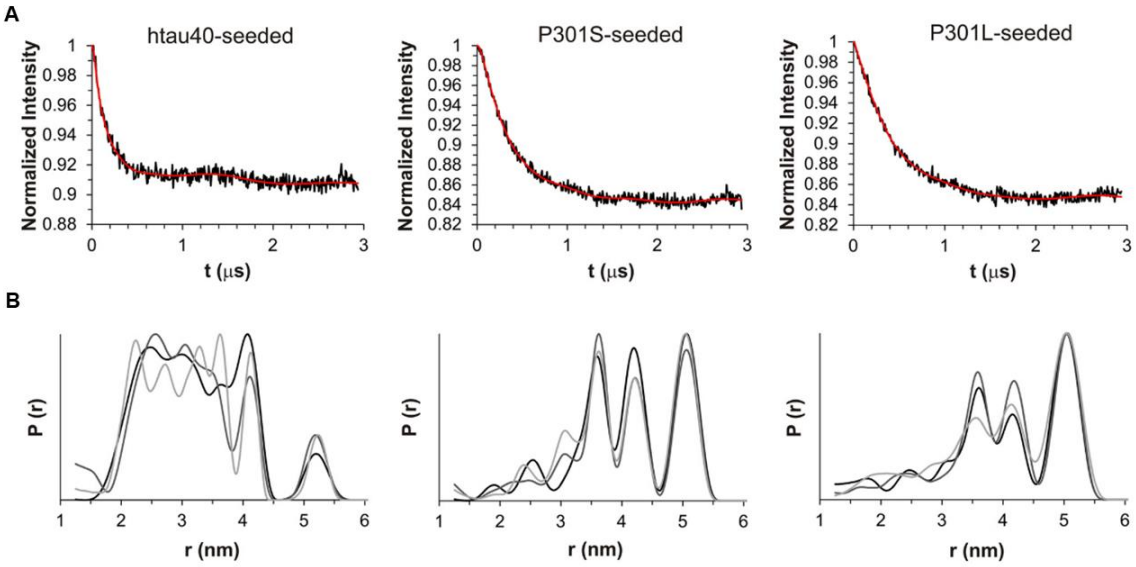

Figure 3.14 DEER analysis of fibrils seeded with htau40, P301S, or P301L. All data analyzed using Tikhonov regularization. Left panels, htau40-seeded fibrils. Middle panels, P301S-seeded fibrils. Right panels, P301L-seeded fibrils. A, representative background corrected dipolar evolution curves in the time domain shown as black traces with best fits in red. B, distance distributions, different shaded traces represent biological triplicates for each different fibril type. The data shows that all fibrils are ensembles of conformers, and that the htau40 fibril ensemble is distinct from those of P301S and P301L fibrils.

CHAPTER FOUR: OXIDATION OF FOUR-REPEAT TAU RESULTS IN UNIQUE FIBRIL PROPERTIES

4.1 Implications of htau40 oxidation on fibril structure

Identification that truncations and specific point mutations promote the formation of distinct fibril conformers raised the question whether changes in reaction conditions could have a similar result. Oxidation of tau protein is a condition of interest because brain tissue is particularly vulnerable to oxidative stress given its high oxygen consumption and high metabolic rate (47). Additionally, neurodegenerative disease pathology correlates to increased exposure to oxidative conditions (139). Increased oxidative damage has also been identified in early disease stages meaning its effects have the potential to influence initial fibril formation (140). Due to the presence of two native cysteines in htau40 at positions 291 and 322, under oxidizing conditions, the formation of a disulfide bond between these residues is possible. This disulfide bond could affect the preferred monomer fold, thus impacting fibril core structure and growth properties. Previous studies have highlighted how intermolecular disulfide bonds form species which readily promote aggregation (56). This is consistent with the NDP growth model for tau fibril formation, as the bringing together of monomers with a disulfide bond would decrease the energetic barrier of nucleation, which is

typically the rate limiting step in fibril formation (90). These intermolecular species however are not the subject of the experiments herein. My interest lies in the growth properties of intramolecularly disulfide bonded htau40 monomers. It has been proposed that monomers with an intramolecular disulfide bond can influence fibril structure (57), but a thorough characterization of these fibrils and their growth properties is lacking.

4.2 Isolation of intramolecularly disulfide bonded htau40 monomer

In order to study the growth properties of fibrils comprised of monomers that possess an intramolecular disulfide bond, these monomers first need to be isolated from species that possess intermolecular disulfide bonds. Oxidation reactions took place by combining freshly monomerized htau40 with hydrogen peroxide. After allowing this reaction to incubate at 25 °C for 16-20 hours the hydrogen peroxide was dialyzed out and the reaction was spin concentrated down to 1.5-2 mL. In order to separate any higher order species (dimers, trimers, etc) from monomers, a 0.5 mL fraction size was utilized on a superdex 200 10/300 GL size exclusion column. The higher order species begin to elute off the column at approximately 10 mL and are represented by the small peak seen as a left shoulder of the large absorption peak (Figure 4.1 A, C). In order to correctly pool fractions containing only monomer, the fractions containing elution volume 9-16 mL were run on SDS-PAGE gels using SDS sample buffer that did not contain any reducing agent. Reducing agent is present in typical sample buffer

so with the combination of the SDS in the gel and the reducing agent in the buffer, all proteins running on the gel will be denatured and no disulfide bonds will be present. However, since the only way the monomers in question can be differentiated from higher order species are disulfide bonds, it is critical that they not be broken. Using this method, fractions containing only monomer were able to be differentiated from those with some higher order species, and these fractions (elution volume 13-14.5 mL) were then pooled for experimental use (Figure 4.1 B). The formation of more intramolecular disulfide bonds rather than intermolecular bonds in the sample was promoted by optimizing the concentration of monomer to be 20 µM htau40 with 5 mM H_2O_2 in the initial oxidation reaction. When a higher monomer concentration (100 µM htau40) is used an increased percentage of higher order species can be seen (Figure 4.1 C, D) and therefore less monomer can be recovered for further experimental use.

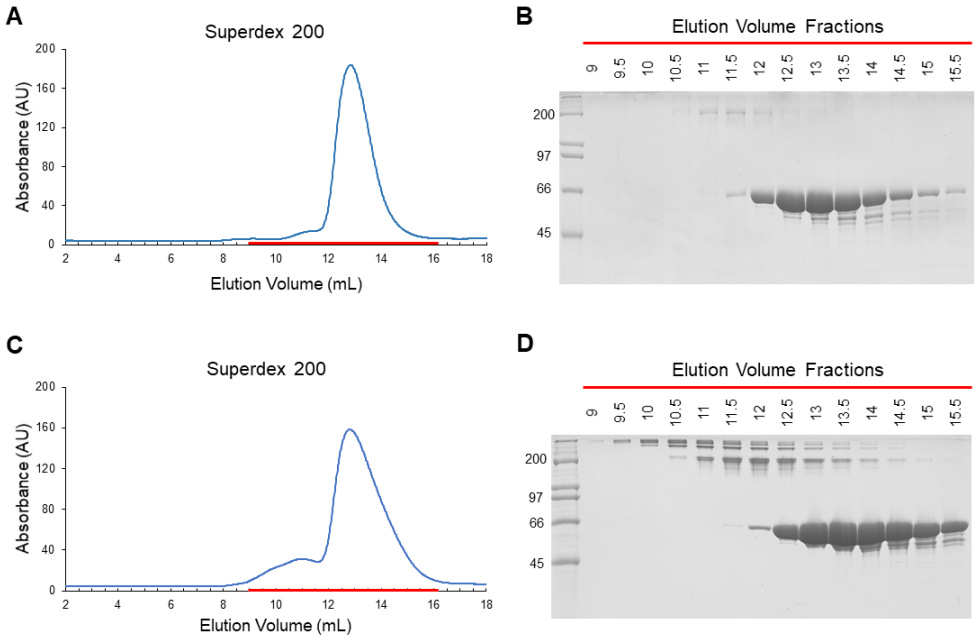

Figure 4.1 Isolation of intramolecularly disulfide bonded htau40 monomer. Following oxidation of htau40 monomer with hydrogen peroxide, reactions were sent over a superdex 200 gel filtration column. Fractions (0.5 mL) were collected and those corresponding to the absorbance peak were analyzed using SDS-PAGE with no reducing agent present in the SDS sample buffer. A and B, show the absorbance peak profile and corresponding gel from an oxidation reaction with 20 µM htau40 and 5 mM hydrogen peroxide. C and D, show the absorbance peak profile and corresponding gel from an oxidation reaction with 100 µM htau40 and 5 mM hydrogen peroxide. Different total reaction volumes were used. These data highlight that optimization of htau40 to hydrogen peroxide concentration allows for the promotion of intra over intermolecular disulfide bond formation, and the ability to isolate this intramolecular disulfide bonded monomer.

Verification that oxidation had in fact occurred, and the monomeric species recovered from gel filtration did possess an intramolecular disulfide bond, was done using CW EPR. Due to the fact that the spin label MTSL attaches to a cysteine residue, in monomers that possess a disulfide bond between its two cysteine residues no label should be able to attach. This would be represented by a lack of signal in their spectrum following an MTSL labeling protocol. A control utilizing htau40 monomer that has not been oxidized (free

cysteines) is shown in Figure 4.2 A. The three sharp lines in this spectrum are indicative of high spin label mobility, as expected when attached to intrinsically disordered proteins like monomeric tau (133, 141). In comparison, htau40 oxidized monomer (collected from the protocol discussed above) that was subjected to the same labeling protocol shows negligible signal (Figure 4.2 B), indicating that the cysteines are not free. If the bond blocking these cysteines from being MTSL labeled is a disulfide it should be reversible in nature. To test this, monomer collected from gel filtration following the oxidation protocol was treated with DTT, dialyzed to remove the reducing agent, then subjected to the MTSL labeling protocol. The spectrum from this monomer now does show MTSL signal (Figure 4.2 C). Collectively these data suggest that monomeric intramolecularly disulfide bonded htau40 has been isolated, and I will refer to it as htau40 oxidized.

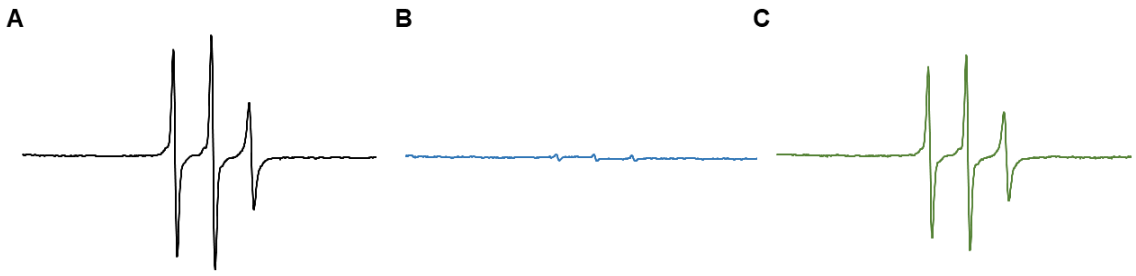

Figure 4.2 Verification of disulfide bond in monomeric species. Three different types of monomer were subjected to MTSL labeling protocol followed by CW EPR to assess labeling efficiency. All samples were 5 µM. A, htau40 freshly monomerized not subjected to oxidation reaction. B, htau40 oxidized monomer following oxidation protocol. C, htau40 oxidized monomer following oxidation protocol then treated with reducing agent. Spectra were collected at room temperature at X-band with 150 G scan width, 1 G modulation amplitude, and 12 mW incident power. Same axes used for all plots. These results suggest that the monomer collected following the oxidation protocol is intramolecularly disulfide bonded.

4.3 Htau40 oxidized monomer forms fibrils competent to seed homotypic growth

It was necessary to first form oxidized fibrils before their growth barriers could be assessed. This was done in a similar manner as described in the previous chapter, by combining htau40 oxidized monomer with heparin and allowing it to aggregate following the nucleation and elongation scheme for 7-8 days at 37 °C under agitating conditions. Due to some discrepancies in the field whether intramolecularly disulfide bonded monomer form fibrils (57, 142) or not (56), the fibrillar nature of this initial growth was confirmed using TEM (Figure 4.3 A). Once fibrillar nature was confirmed it was of interest to also show these fibrils, when subjected to a harsh sonication, fragment in such a way that it is practical to use them as seeds to initiate fibril growth as shown in the previous chapter. Under harsh sonication conditions these oxidized fibrils do fracture in a fairly uniform manner into shorter fibril fragments with an average length of 42 nm (Figure 4.3 B, C). The seeding competency of these fibrils was first tested in homotypic growth reactions utilizing 10% molar monomer equivalent seed. These reactions result in protein exclusively being found in the pellet fraction (Figure 4.3 D). This growth trend is reproducible as it was observed for >15 biological replicates (Figure 4.3 E). Seeded growth of oxidized monomers was also demonstrated using ThT fluorescence (Figure 4.3 F). Importantly the experiments suggest that this aggregation is not spontaneous monomer nucleation. This is evidenced by the lack of a lag phase and lack of signal

intensity increase from monomer controls in the absence of seeds. TEM was again used to highlight that the assembled structures from these seeded reactions are fibrillar (Figure 4.3 G). Collectively, these results suggest that fibrils form from intramolecularly disulfide bonded htau40 monomers, and that those fibrils are competent to recruit other htau40 oxidized monomers.

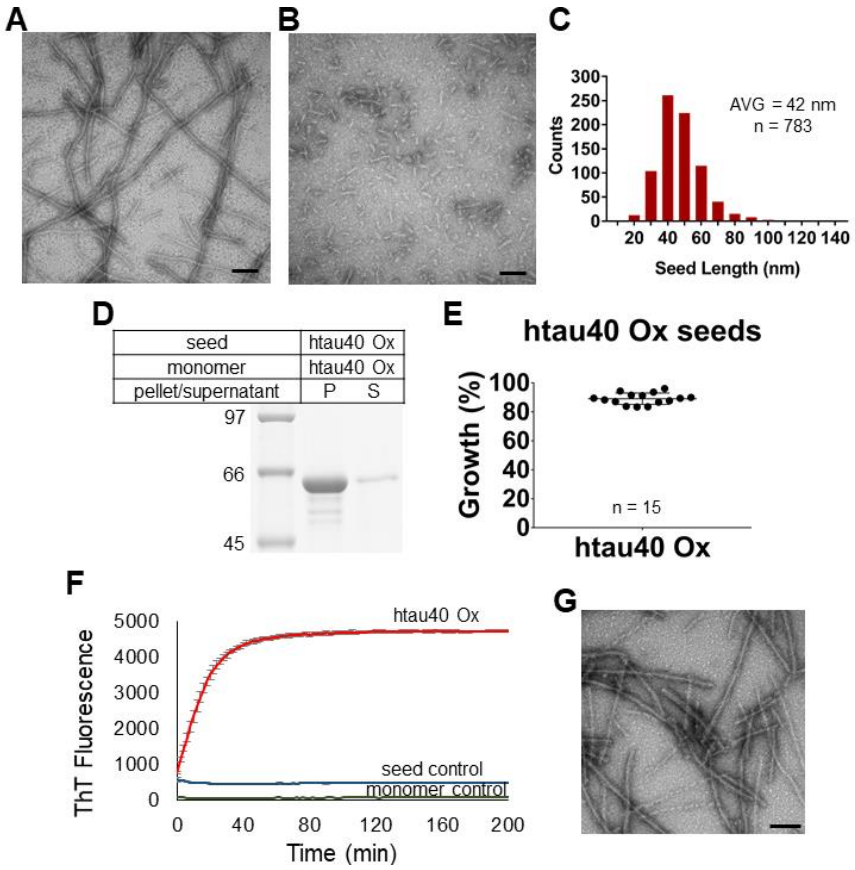

Figure 4.3 Fibril formation of htau40 oxidized monomers and homotypic growth. A and B, TEM image of fibrils formed from htau40 oxidized monomer before (A) and after (B) sonication. Scale bars = 100 nm. C, distribution of htau40 oxidized seed lengths. D and E, representative gel and scatter plot displaying results from quantified 10% seeded homotypic htau40 oxidized (Ox) growth reactions. P = pellet, S = supernatant, n = number of biological replicates. F, ThT fluorescence showing kinetics of a homotypic htau40 Ox seeded reaction (red trace), seed control in the absence of monomer (blue trace), and monomer control in the absence of seed (green trace). Error bars represent ± S.D. from triplicate measurements. G, TEM image of fibrils resulting from a homotypic htau40 Ox seeded reaction. Scale bar = 100 nm. The results demonstrate the ability of htau40 oxidized monomers to form fibrils that can seed homotypic fibrillar growth.

4.4 Specific recruitment properties of oxidized fibrils

It was observed that oxidized monomers grew on htau40 oxidized seeds in homotypic reactions. Next, the recruitment of other monomeric species in heterotypic reactions was examined. The monomers chosen to probe this question were two different variants of htau40 cysless, where the native cysteines have been replaced with serines (htau40 SS) or alanines (htau40 AA), and htau23 containing only one native cysteine at position 322. The lack of an increase in ThT fluorescence when these monomers are offered to htau40 oxidized seeds indicates the inability of these monomer types to elongate oxidized seeds (Figure 4.4 A). This seed type is not simply incompetent for all seeding reactions, just with these particular monomers. As highlighted in the previous section (Figure 4.3 D-G), and by the control trace showing oxidized monomer on oxidized seed growth (Figure 4.4 A red trace). Sedimentation reactions offering 10% oxidized seed to cysless and htau23 monomers also show a significant growth barrier as the protein is seen entirely in the supernatant following a 20-24 hour incubation period, high speed centrifugation, and SDS-PAGE assessment (Figure 4.4 B). This growth barrier is reproducible, as different biological replicates showed an average of 12%, 6% and 5% growth for all three monomer types, htau40 SS, htau40 AA, and htau23 respectively (Figure 4.4 C). This growth barrier is in contrast to the growth observed when htau40 SS, htau40 AA, or htau23 monomers are offered to htau40 reduced seeds. For purposes of comparison I will refer to htau40 fibrils formed in the presence of reducing agent,

like those discussed in the previous chapter, as htau40 reduced fibrils. These htau40 reduced fibrils show no growth barrier or diminished recruitment properties towards htau40 SS, htau40 AA, or htau23 monomer. This is shown by ThT fluorescence kinetics where all three monomer types, along with htau40 reduced monomer as a control, show an increase in fluorescence intensity (Figure 4.4 D). Growth efficiency was also determined by sedimentation reactions using the 10% (molar equivalent) seeded protocol. Protein is seen entirely in the pellet fractions when using reduced seeds rather than oxidized seeds (Figure 4.4 E). This trend is reproducibly seen for multiple biological replicates, displaying 95%, 95% and 98% growth of all monomer types (htau40 SS, htau40 AA, htau23 respectively) (Figure 4.4 F).

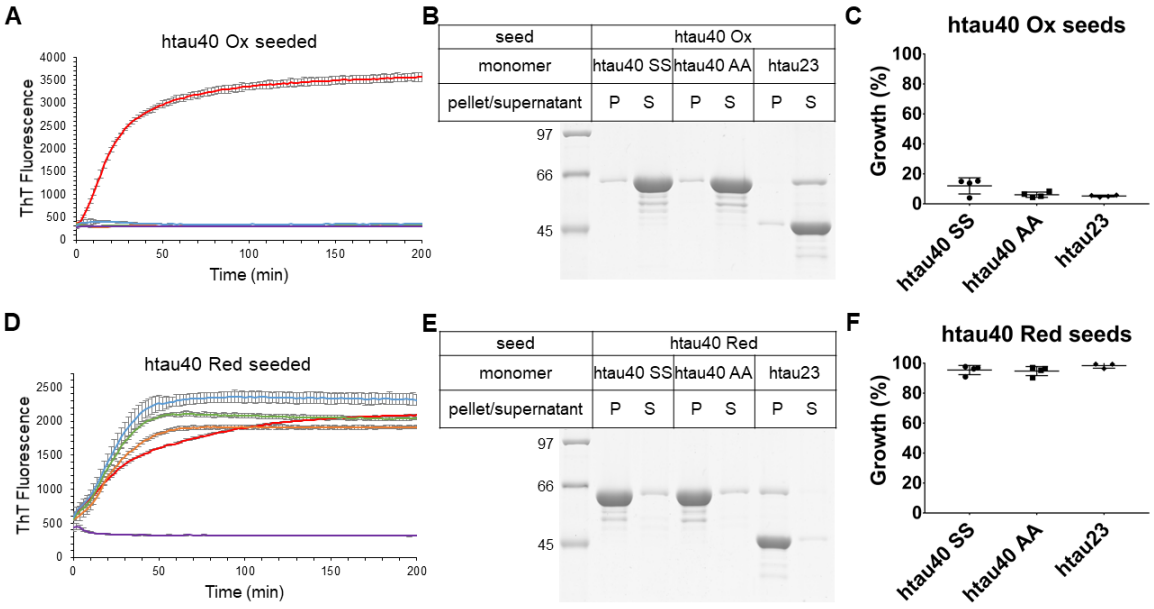

Figure 4.4 Growth barrier of htau40 SS, htau40 AA, and htau23 on htau40 oxidized seeds. A-C, results from growth reactions utilizing htau40 oxidized (Ox) seeds. D-F, results from growth reactions utilizing htau40 reduced (Red) seeds. A and D, homotypic growth reactions on either Ox or Red seeds show full growth (red traces), while reactions with htau40 SS, htau40 AA, and htau23 monomer (orange, green and blue traces respectively) show no growth on htau40 Ox seeds (A) and full growth on htau40 Red seeds (D). Seed control for Ox and Red seeds shown in purple. Error bars represent mean ± S.D. from triplicate measurements. B and C, representative gel and scatter plot depicting quantified results from heterotypic seeding reactions on htau40 Ox seeds, or (E and F) htau40 Red seeds. P = pellet, S = supernatant. The results highlight the inability of monomers without intramolecular disulfide bonds to be recruited onto htau40 oxidized seeds. Recruitment of these monomers only occurs on reduced seeds. This suggests a structural difference between oxidized and reduced fibrils.

To investigate if a minor population of oxidized seed conformers exists that could recruit cysless tau, experiments were performed where htau40 SS monomers were offered to 50% (molar monomer equivalent) htau40 oxidized seeds. These results showed negligible htau40 SS recruitment (average 8%) onto oxidized seeds (Figure 4.5 A). Additionally, it is interesting to note that a crosslinked version of htau40 monomer, with a bismaleimide crosslinker

possessing an 8 Å spacer arm connecting the two cysteines, also showed minimal growth on htau40 oxidized seeds (average 4%) (Figure 4.5 B). Collectively, the results presented thus far suggest that monomer recruitment onto oxidized seeds is dependent on the presence of an intramolecular disulfide bond in the monomer, and that the compact spacing of the disulfide bond is potentially important to fibril growth.

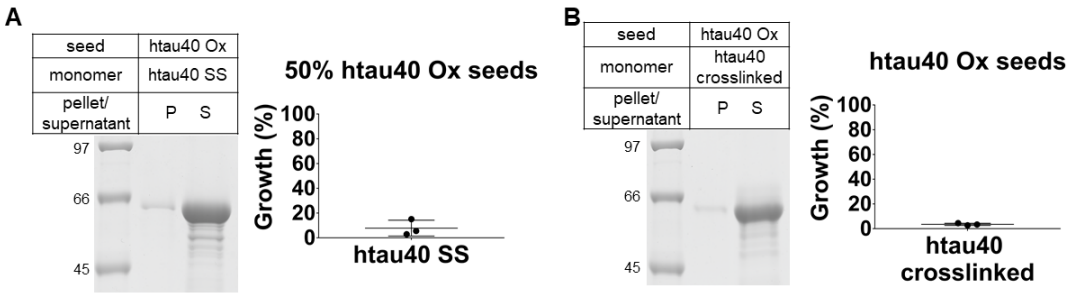

Figure 4.5 Increased seed percentage and htau40 crosslinked growth reactions. Representative gel and scatter plot depicting quantified results from htau40 SS monomer with 50% (rather than typical 10%) htau40 oxidized (Ox) seeds (A), and crosslinked monomer with 10% htau40 Ox seeds (B). The lack of growth in these reactions is additional evidence supporting the importance of the disulfide bond within monomer for growth on htau40 oxidized seeds.

To further investigate the necessity of an intramolecular disulfide bonded monomer to elongate oxidized seed fibrils, htau40 monomer that had not been subjected to reducing agent or an oxidizing agent was used for seeding reactions. Cysteine containing htau40 monomer combined with 10% oxidized seed and heparin was allowed to incubate in at 37 °C for 20-24 hours. The growth resulting from these reactions was highly variable for different batches of monomer offered to different batches of seeds on different days (data not shown). One factor which could contribute greatly to this variability is the amount

of oxidation the monomer has undergone. Without a reducing agent present it is likely that oxidation can occur to the monomer because of the presence of dissolved oxygen (55). To test this, two parameters were explored, allowing or not allowing monomer oxidation during reaction incubation. No TCEP was included for these reactions. To allow for more oxidation the temperature of incubation was decreased from 37 °C to 25 °C (ambient room conditions) for reactions between freshly monomerized htau40 and oxidized seeds. These reactions were covered with a filter instead of in a closed tube to allow oxygen exchange, but prevent any particulate matter from entering. Quantifying the amount of protein in the pellet fractions from such reactions revealed that the average percentage of growth for these reactions was 40% (Figure 4.6 A). The opposite regime, where htau40 monomer has no chance to oxidize, was explored using an anaerobic chamber. Again, no TCEP was used for these reactions. Inside the chamber htau40 was monomerized, reactions were set up, and incubation (at 37 °C) took place, ensuring the monomer being used has no chance to oxidize and form disulfide bonds. Quantified results from these reactions show a significant growth barrier, average of only 8% growth, from biological triplicate seeds (Figure 4.6 B). Parallel experiments for both the 25 °C open tube and anaerobic conditions utilizing the same setup and monomer, but offered 10% htau40 reduced seeds, both yielded an average of 93% growth (Figure 4.6 A, B). Collectively, these results suggest that in order for monomer to be recruited onto oxidized seeds it needs to be able to form an intramolecular

disulfide bond. This highlights the structural significance of the intramolecular disulfide bond to these htau40 oxidized fibrils.

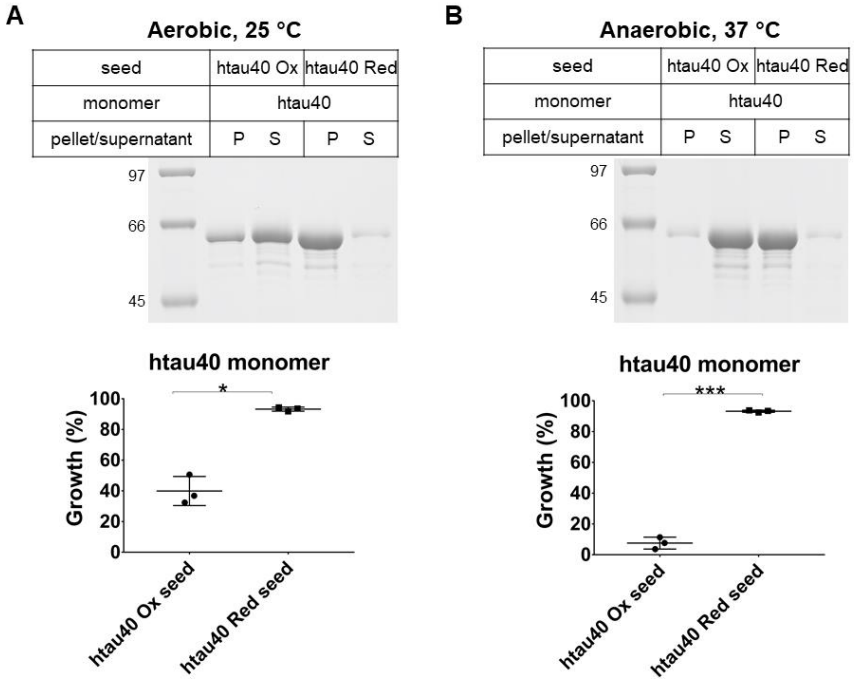

Figure 4.6 The oxidation of htau40 monomer determines its recruitment onto htau40 oxidized seeds. Reactions on htau40 oxidized (Ox) seeds or htau40 reduced (Red) seeds all utilizing freshly monomerized htau40 monomer that had no reducing agent or oxidizing agent present. A, representative gel and scatter plot depicting quantified results from reactions incubated at 25 °C in the presence of ambient room oxygen. B, representative gel and scatter plot depicting quantified results from reactions where the htau40 monomer was prepared in an anaerobic chamber, and reactions were also set up then incubated at 37 °C in an anaerobic chamber. P = pellet, S = supernatant. Paired t-test for statistical comparison *, $p < 0.013$, ***, $p < 0.0006$. Control reactions on htau40 reduced seeds for both scenarios reveal the monomer being used is growth competent. The difference in growth under variant conditions on htau40 oxidized seeds suggests that the recruitment of htau40 monomer onto oxidized seeds is dependent on its ability to form an intramolecular disulfide bond.

4.5 Oxidized and reduced fibrils are structurally distinct

Different growth barriers seen for oxidized and reduced fibrils suggest they are structurally distinct from one another, yet further evidence of these differences was desired. Due to the inability of cysteine free monomer to grow on

oxidized seeds, structural analysis through EPR experiments was not possible. However, other biochemical assays were employed to highlight the structural differences between oxidized and reduced fibrils. One technique used to evaluate conformational stability of fibrils is a guanidine melt. Fibrils are exposed to a specific concentration of denaturant and the amount of fibrils that remain can be quantified. When done over a series of concentrations a denaturation profile for a fibril type can be determined (143). A fibril's susceptibility to denaturation is dependent on what regions of the protein are exposed (144), therefore structurally distinct fibrils made up of the same monomer type could display different denaturation profiles. Homotypic growth reactions were set up for htau40 reduced and oxidized fibrils. Following incubation, the resulting fibrils were aliquoted and guanidine hydrochloride (GndHCl) was added such that total volumes were identical, but final GdnHCl concentration varied from 0-1.5 M. These mixtures were then incubated quiescently at 25 °C for one hour before being subjected to high speed centrifugation. Following sedimentation, pellet fractions were analyzed by SDS-PAGE with Coomassie staining to assess the amount of protein which remained fibrillar after GdnHCl treatment (Figure 4.7 A). Oxidized fibrils appear to be more susceptible to denaturation, showing an average of 36% of original fibrillar content remaining after a 0.25 M GdnHCl treatment. In comparison, reduced fibrils retain 80% of their fibrillar content upon 0.25 M GdnHCl treatment for the same time frame. The different denaturation

profiles for reduced and wild type fibrils suggest a difference in their conformational stability (Figure 4.7 B).

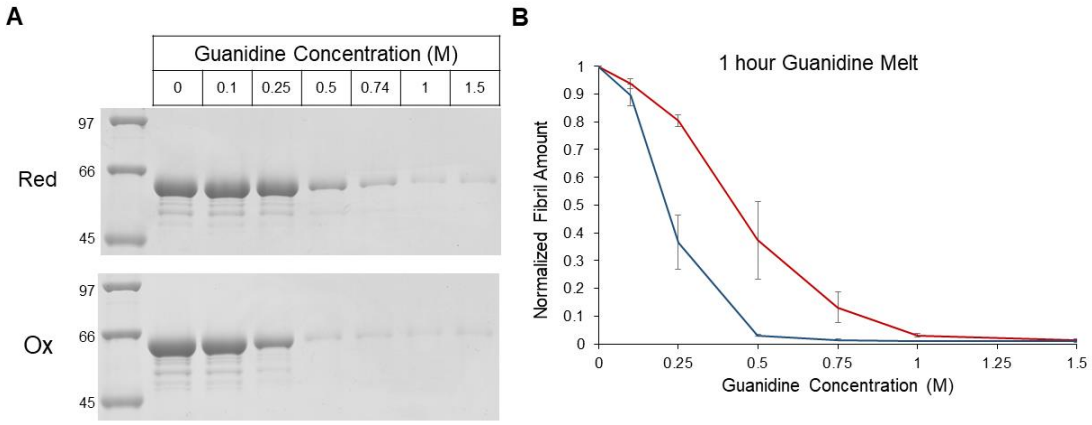

Figure 4.7 Structural analysis of reduced and oxidized fibrils using Guanidine denaturation. Following homotypic growth for htau40 reduced and oxidized fibrils, reactions were aliquoted and treated with varying concentrations of GdnHCl for 1 hour before being sedimented and pellets analyzed. A, representative SDS-PAGE assessment of pellets for reduced (Red, top gel segment) compared to oxidized (Ox, bottom gel segment) reactions when exposed to the same treatment conditions. B, densitometric quantification of results from biological triplicates of reduced fibrils (red trace) and oxidized fibrils (blue trace) indicating the normalized amount of pelleted protein after each GdnHCl concentration treatment. Error bars ± S.D. from triplicate measurements. The different denaturation profiles for reduced and oxidized fibrils suggest a difference in their conformational stability.

One distinguishing feature of amyloids is their protease resistant core (77). Limited protease digestion has been employed as a technique to highlight how fibrils composed of the same type of monomer can be structurally distinct (76). This is possible because proteases have preferential cleavage sites, and if the conformation or packing of the monomer making up the core of two fibrils is different, different cleavage sites will be exposed resulting in different cleavage products. The protease used for these experiments was proteinase K (PK), a broad-spectrum serine protease that preferentially cleaves after hydrophobic

amino acids (145). Reduced and oxidized fibrils were grown in homotypic seeding reactions and then subjected to a final concentration of 60 nM PK and let incubate at 25 °C for 30 min. Following incubation, they were treated with a protease inhibitor and mixed with SDS sample buffer before being run on SDS-PAGE with Coomassie staining to visualize cleavage products. Controls were also performed where assembly buffer rather than PK was used. Representative control fibrils treated with only buffer show no degradation. Importantly, there are subtle differences in the cleavage products of PK treated reduced and oxidized fibrils (Figure 4.8). These differences are reproducible as they are observed for fibrils initiated from biological triplicate seed batches. The data suggest that reduced and oxidized fibrils are structurally distinct from one another.

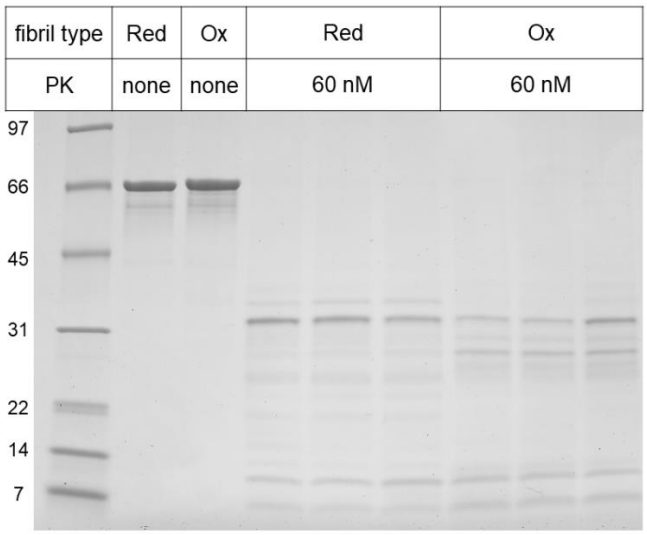

Figure 4.8 Limited protease digestion of reduced and oxidized fibrils. Following reduced (Red) and oxidized (Ox) homotypic growth reactions fibrils were proteolyzed for 30 min at 25 °C with equal amounts of proteinase K (PK) before being analyzed by SDS-PAGE and Coomassie staining. Representative control growth for each fibril type with no PK treatment (none for Red and Ox lanes), and biological triplicates of Red and Ox fibrils all treated with 60 nM PK. The different banding pattern of reduced vs oxidized fibrils reveals different proteolytic sensitivities of the two fibrils, suggesting they are structurally distinct from one another.

One final characteristic that was explored to show reduced and oxidized fibrils are structurally distinct was their fragility. If fibrils are structurally identical, they should fracture to a similar extent when exposed to the same sonication stress. The tip sonication, described for the fracture of initial nucleated fibrils to create seeds, is quite harsh as evidenced by the small, fairly uniform fragment products (Figure 3.1 B, C and Figure 4.3 B, C). This is too extreme of a breakage event to expect detection of any fragility differences, instead a milder sonication event was necessary. Following homotypic seeding reactions, 100 µL of reduced or oxidized fibrils were subjected to a 30 second sonication event in a bath sonicator utilizing only 5% power. The sonicated fibrils were then diluted to be approximately 2 µM and loaded onto EM grids to observe their extent of fracture. Nonsonicated reduced and oxidized fibrils appear similar (Figure 4.9 Left panels of A, B). However, after being subjected to the same sonication event, oxidized fibrils fragment to a greater and more uniform extent than reduced fibrils (Figure 4.9 Middle panels of A, B). Quantifying the lengths of these fibril fragments revealed that oxidized fibrils fracture to an average length of 209 nm, and reduced fibrils fracture to an average length of 531 nm (Figure 4.9 Right panels of A, B). The higher number of measured oxidized fibrils was due to their shorter nature. To make sure no bias was introduced measuring the reduced fibril lengths, quantifications shown in the bar graph are an average from biological triplicates imaged on 9 different grids from >30 images.

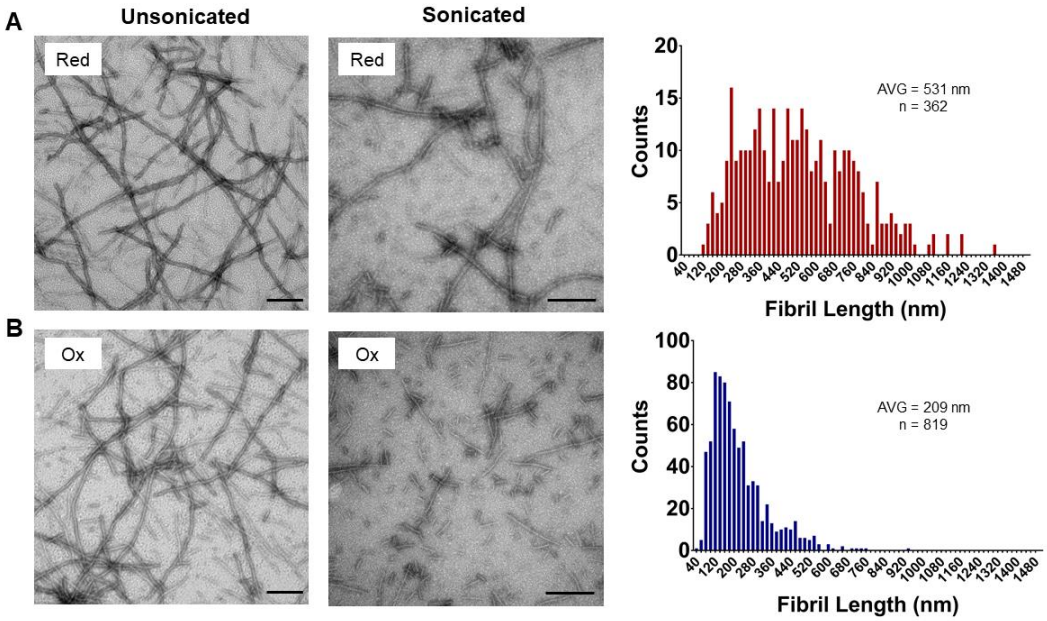

Figure 4.9 Fragility of reduced and oxidized fibrils assessed using EM. Following homotypic growth reactions reduced (Red) (A) and oxidized (Ox) (B) fibrils were analyzed by EM before (left panels) and after (middle panels) 30 second bath sonication. Unsonicated images 49,000 x direct magnification. Sonicated images 98,000 x direct magnification. All scale bars = 200 nm. A and B right panels, length distributions for sonicated Red and Ox fibrils, showing the average lengths when subjected to the same sonication event are 531 nm and 209 nm respectively. This indicates that oxidized fibrils are more fragile than reduced fibrils.

4.6 Partial dissociation of oxidized fibrils

Seeded reactions with htau40 oxidized seeds identified the intramolecular disulfide bond in oxidized fibrils is an important factor dictating their growth properties. This factor made it of interest to investigate whether or not the persistence of these bonds was critical to the fibrils after they were formed. Identical homotypic oxidized seeded reactions were set up to be monitored via ThT fluorescence. No reducing agent was present in initial reaction setup. Once traces leveled off (suggesting the excess pool of monomer had been depleted and equilibrium had been reached) the run was paused and reactions were

treated with buffer as a control, or TCEP to a final concentration of 3 mM, then incubation continued for 17.5 hours. Following treatment, the diminished intensity in the ThT trace of those reactions treated with reducing agent (red trace), as compared to the control reaction's intensity (green trace), suggests some dissociation of the oxidized fibrils (Figure 4.10 A). Quantification of the dissociation event was done using a similar reaction setup without the presence of ThT. Triplicate homotypic oxidized seeding reactions were set up and let incubate. After 5 hours of growth one reaction was sedimented, one was treated with assembly buffer, and the final reaction was treated with TCEP to a final concentration of 3 mM. The two reactions that received treatments were incubated quiescently at 37 °C for another 16-20 hours before being sedimented. Fibril content for all three reactions was visualized on SDS-PAGE as described previously (Figure 4.10 B). Protein being exclusively in the pellet fraction for reactions spun down at the 5-hour time point suggests the observed effect is not a stalling of growth at the time of treatment. The protein in the pellet for the reaction treated with buffer indicates the dissociation is not a consequence of the treatment protocol. The dissociation seen with a 3 mM TCEP treatment is due to the effect of the reducing agent acting on the disulfide bonds within oxidized fibrils. Biological replicates show the reproducibility of this trend, with an average of 53% protein remaining in the pellet following 3 mM TCEP treatment (Figure 4.10 C).

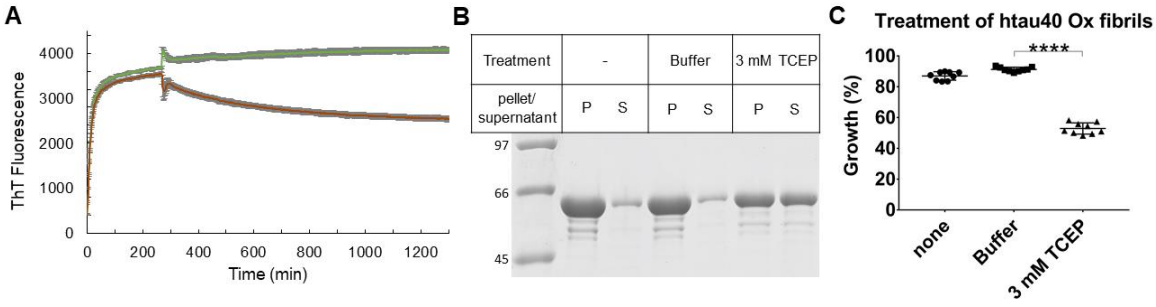

Figure 4.10 Dissociation of oxidized fibrils. Fibrils from identical homotypic htau40 oxidized seeded reactions were let form before being treated with buffer or reducing agent, followed by continued incubation. A, reactions monitored by ThT fluorescence, after 4.5 hours of growth monitoring was paused so buffer (green trace) or 3 mM TCEP (red trace) could be added to reactions, after treatment monitoring was resumed for another 17.5 hours. B and C, representative gel and scatter plot depicting quantified results from reactions that were either spun down after 5 hours of incubation, or treated with buffer or 3 mM TCEP after 5 hours of incubation, then allowed to incubate for another 16-20 hours before being sedimented to be analyzed by SDS-PAGE. P = pellet, S = supernatant, paired t-test for statistical comparison ****, $p < 0.0001$. The results indicate that the addition of reducing agent causes an approximate 50% dissociation of oxidized fibrils.

Fibril dissociation could be an important physiological event; so, the species present as a result of diminished long fibril content was characterized. As described in chapter 3 and shown in Figure 3.1 D, short fibril fragments, like those used for seeding reactions, remain in the supernatant when spun at 128,000 x g. Therefore, in order to determine what species is dissociating from these oxidized fibrils, whether it be small seeding competent fibril fragments or monomers that are in the supernatant following reducing agent treatment and sedimentation, another technique must be used. Following sedimentation, supernatants from these treated reactions were subjected to size exclusion chromatography. The elution profile for the supernatant of buffer and TCEP treated oxidized fibrils, along with a monomer control can be seen in Figure 4.11

A. When supernatant from buffer treated oxidized fibrils was run over a superdex 200 10/300 GL size exclusion column the resulting elution profile showed one fairly prominent peak with an average elution volume of 8 mL and a significantly smaller peak between 12-13 mL. The supernatant from TCEP treated oxidized fibrils revealed a peak overlapping the 8 mL retention peak seen in supernatant of the buffer control, along with a major peak eluting between 11-13 mL. The elution profile of reduced htau40 monomer reveals the species eluting off between 11-13 mL to be the monomeric species. SDS-PAGE on elution volume 6-17 mL, with 1 mL fractions corresponding to different lanes, was done for each run (Figure 4.11 B-D). The intensity of protein bands corresponding to the pre-monomer peak do not match the expectation given the area under their peak when measuring absorbance at 280 nm. This exaggerated peak intensity can most likely be attributed to a scattering effect of this higher order species. Densitometric quantification of protein bands on gels from the supernatant of TCEP treated fibrils, from 10 different samples, reveals that an average of 88% of the total protein is monomeric despite the intensity of the peak at 8 mL elution volume. To explore the elongation competency of the dissociated monomeric species, following centrifugation the supernatant fraction from treated fibrils was offered to htau40 reduced seeds. The reactions resulted in full growth (data not shown), and indicate the competency of the dissociated species to be recruited onto new htau40 reduced seeds.

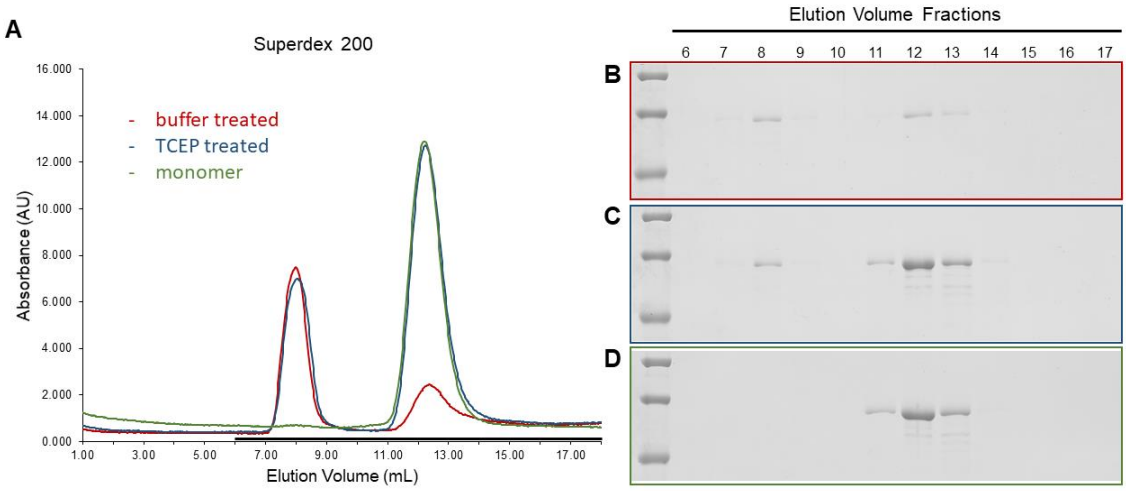

Figure 4.11 Monomeric htau40 accounts for the dissociation of oxidized fibrils. Supernatants from htau40 oxidized treated fibrils following growth, treatment, incubation, and sedimentation, (along with a monomer control) were run on gel filtration. Resulting elution fractions were analyzed using SDS-PAGE with Coomassie staining. A, elution profiles from the supernatant of fibrils treated with buffer (red trace) or with 3 mM TCEP (blue trace), and htau40 monomer control (green trace). Elution volumes 6-17 mL (in 1 mL fractions) were analyzed on SDS-PAGE for buffer treated fibrils (B), 3 mM TCEP treated fibrils (C), and htau40 monomer (D) gel filtration runs. This data reveals that the majority of species accounting for the 50% reduction in oxidized fibril content is monomeric.

Notice that in the presence of reducing agent, fibrils did not fully dissociate (Figure 4.10). Additional experiments were performed to test whether this was due to insufficient amount of reducing agent, or whether the ensemble of fibrils contains conformers that are differentially affected by reducing agent. To probe the maximum extent of dissociation, oxidized fibrils were again grown in homotypic seeding reactions and treated, this time with a different reducing agent. DTT rather than TCEP was used to investigate if a different reducing agent produced the same effect. The DTT concentrations used to probe the maximum extent of oxidized fibril dissociation were 20 mM, 50 mM, and 100 mM. Reactions were carried out as described with TCEP treatment, where seeded

reactions were grown for 5 hours, treated, then let incubate for another 16-20 hours before being sedimented and fibrillar content assessed using SDS-PAGE with Coomassie staining. The 20 mM, 50 mM, and 100 mM DTT treatments resulted in an average of 46%, 50%, and 45% of protein remaining in the pellet, respectively. This trend was reproducible for multiple biological replicates (Figure 4.12 A and B). The results suggest that the oxidized fibril growth reactions, like reduced fibrils, contain a heterogeneous ensemble of conformers with a subpopulation resistant to dissociation.

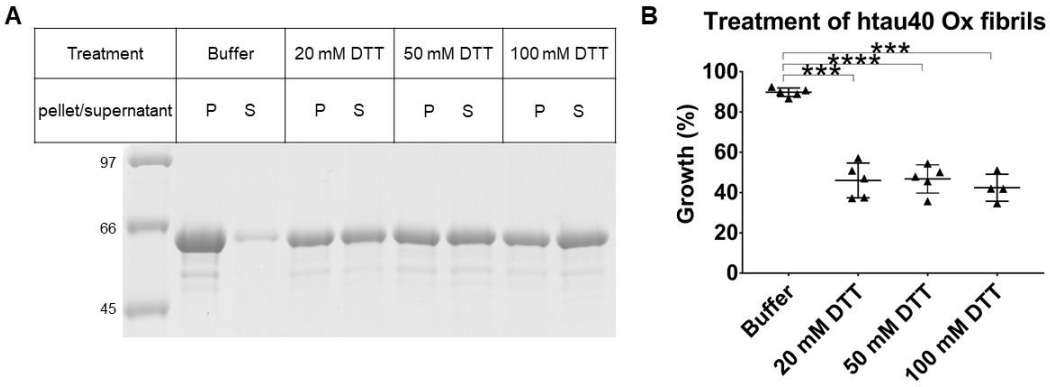

Figure 4.12 Maximum extent of oxidized fibril dissociation. Identical homotypic htau40 oxidized seeded reactions were grown for 5 hours before being treated with various concentrations of DTT, followed by a 16-20 hour incubation, then sedimented for analysis via SDS-PAGE with Coomassie staining. A, representative gel for reactions treated with buffer or 20 mM, 50 mM, or 100 mM DTT. P = pellet, S = supernatant. B, scatter plot depicting densitometric quantification of results from biological replicates. Paired t-test for statistical comparison ****, $p < 0.0001$, ***, $p \leq 0.0005$. These results highlight an approximate 50% as the maximum extent these htau40 oxidized fibrils can be dissociated, suggesting htau40 oxidized fibrils are an ensemble of conformers.

4.7 Oxidation of htau40 by copper (II)

Dyshomeostasis of metal ions has been associated with neurodegenerative diseases and been suggested to even alter the pathology of

some diseases, like AD (146). Previous studies have used Cu^{2+} ions as an oxidizing agent (142). This raised the question whether fibrils nucleated in the presence of copper would exhibit properties more like the oxidized or reduced fibrils discussed here. To investigate this, Copper (II) chloride ($CuCl_2$) was included during initial fibril formation and the growth properties of the resulting fibrils were then probed. Fibril nucleation took place over several days agitating at 37 °C, using freshly monomerized htau40 that had not been treated with reducing agent or hydrogen peroxide, 5 µM $CuCl_2$, and the usual cofactor heparin. These fibrils were not formed in anaerobic conditions. Fibrils nucleated using these conditions exhibit the same growth characteristics as fibrils formed from fully oxidized monomer. The seeds exhibit an average growth of 91% with oxidized monomer, partial growth with htau40 freshly monomerized without reducing agent (average 56%), and a significant growth barrier for monomers unable to form an intramolecular disulfide bond (average growth for htau40 SS 5%, htau40 AA 3%, and htau23 1%). Reproducibility of these growth trends was confirmed with biological triplicate measurements (Figure 4.13 A and B). ThT kinetics also suggest the oxidized nature of these seeds by their rapid fluorescence increase with oxidized monomers (red trace), slower fluorescence increase with htau40 monomers in the absence of reducing agent (blue trace), and lack of fluorescence increase for htau40 SS, htau40 AA or htau23 monomers (Figure 4.13 C). The slow htau40 growth (blue trace) is ascribed to the slow oxidation of those htau40 monomers, which are then able to be incorporated. It is

also interesting to note, a control experiment utilizing htau40 SS nucleated in the presence of $CuCl_2$ does not exhibit a growth barrier with htau23 monomer. This highlights the nature of copper's action with htau40 is directly related to the cysteines. These *in vitro* findings suggest that a physiological increase of Cu^{2+} ions could impact not only tau nucleation kinetics, but the fibril growth properties through oxidation of the native cysteines.

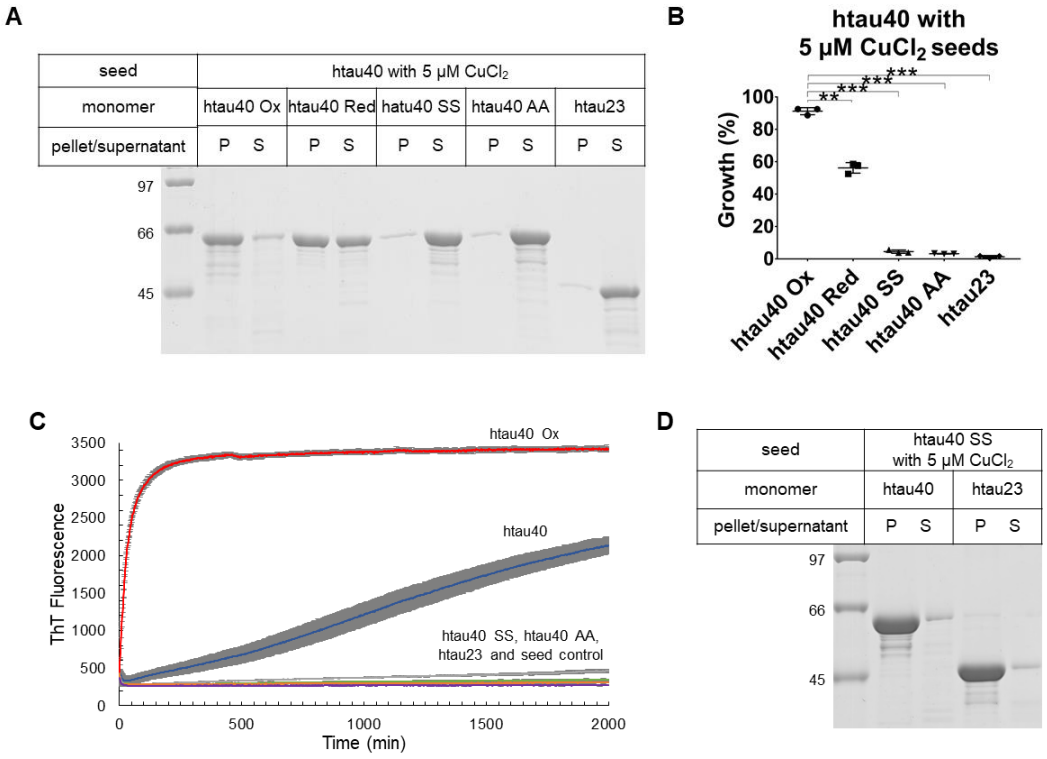

Figure 4.13 Copper can act to oxidize htau40 during nucleation. A and B, representative gel and scatter plot showing densiometric quantification of reactions carried out using seeds that had 5 µM $CuCl_2$ added to provide Cu^{2+} ions during initial fibril formation with htau40 monomer. Paired t-test for statistical comparison **, p = 0.0066, ***, p ≤ 0.0004. C, ThT kinetics showing the results of htau40 oxidized (Ox) (red trace), htau40 (no reducing agent) (blue trace), htau40 SS (grey trace), htau40 AA (green trace), or htau23 (orange trace) monomer offered to the htau40 with 5 µM $CuCl_2$ seeds, and a seed control absent of any monomer (purple trace). D, representative gel showing full recruitment of htau40 and htau23 monomer onto htau40 SS seeds formed in the presence of 5 µM $CuCl_2$. The results suggest that the Cu^{2+} ions are capable of oxidizing htau40 monomer if present during nucleation of the fibrils, resulting in oxidized fibril conformers.

CHAPTER FIVE: SUPRESSING SELF-NULCEATION OF MONOMERS FOR FIBRIL AMPLIFIATION ASSAY

5.1 Principles behind fibril amplification assay

Detection of minute fibril concentrations is one method for advancement of early disease detection and therapeutic intervention of tauopathies. One way to detect small fibril concentrations is to use an assay to amplify the initial small fibril concentration into an easily observed fibril concentration. The Margittai lab has previously shown observable growth in quiescent seeded reactions to be dependent on the initial seed concentration used (119). For quiescent reactions the lower limit of seed concentration that could be used and still result in substantial detectable growth was 0.1% molar equivalent of the monomer in the reaction. However, successful adaptation of an amplification assay, rather than quiescent growth, was able to extend this limit to an approximate 4 orders of magnitude lower seed concentration resulting in growth (119). This assay, originally developed for prion amplification, termed protein misfolding cyclic amplification (PMCA) assay, involves a pool of protein monomer and a minute number of seeds undergoing cycles of sonication followed by periods of incubation (118). The principles of the amyloid NDP growth scheme govern the success of this assay by exploiting the fact that energetically the least hindered type of growth is monomer addition onto fibril ends (90). By successive cycles of

sonication (to break fibrils), followed by incubation (to allow new growth), the number of new ends exposed is increased and overall growth is increased. A schematic representation of this assay is shown in Figure 5.1. This assay has been successfully used to detect fibrils from AD patient brain extract (119), but increasing this assay's limit of detection is desired for further applications. A previous study from our lab, using 0.00001% molar monomer equivalent seeds, showed amplified growth that is statistically significant from monomer controls absent of any seed (119). That same study also identified factors critical to the success of this assay including multiple cycles of sonication, the inclusion of cofactor (heparin), and setting specific sonication time/power low enough that spontaneous monomer nucleation does not occur (119). Spontaneous monomer nucleation is not wanted because the purpose of the assay is only to amplify fibrils from seeds. Therefore, it is vital that the monomer in the reaction be competent to participate in elongation, but not be prone to self-nucleate. To increase the sensitivity of this assay I explored ways to suppress the nucleation of monomers through point mutations and modification of assay parameters.

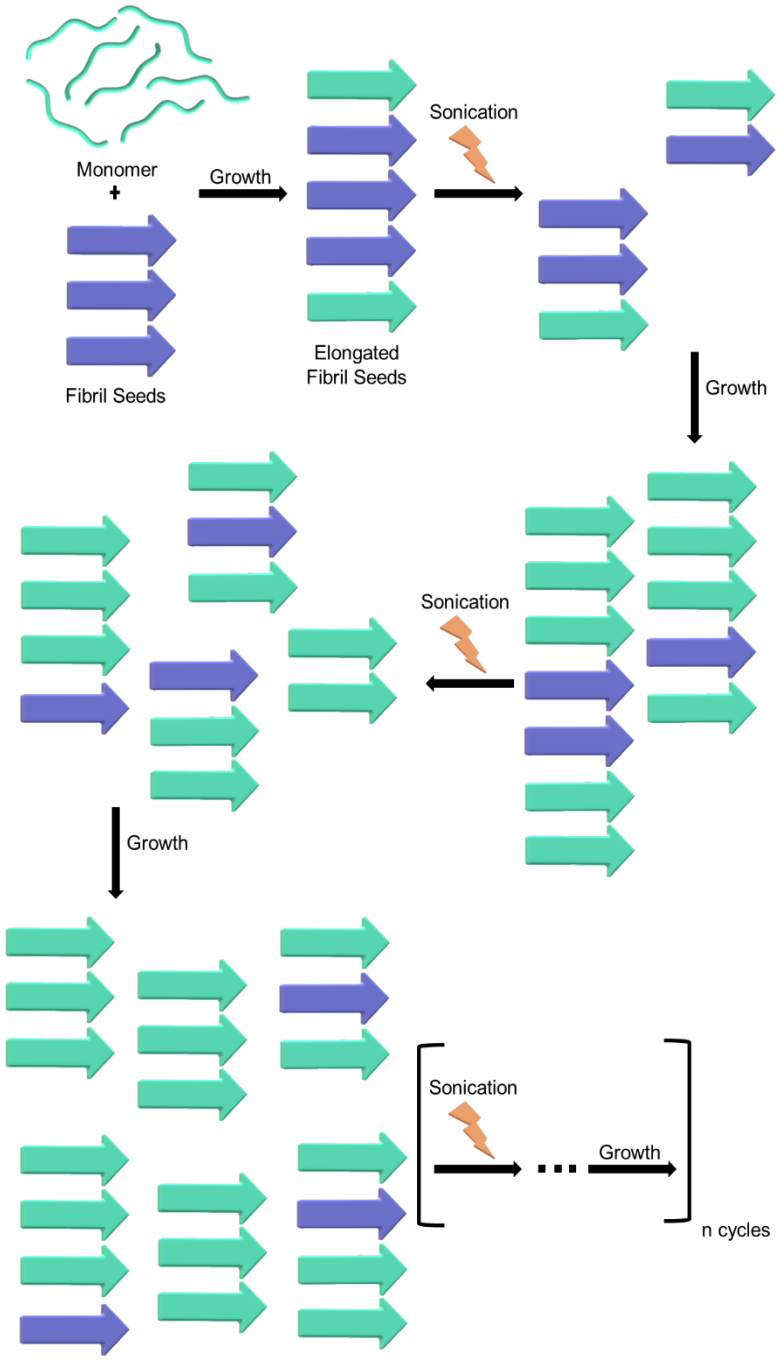

Figure 5.1 Schematic of cyclic amplification. Fibril seeds (blue arrows) are offered to a pool of tau monomers (green lines). During a growth phase, monomers get incorporated onto the fibril ends (green arrows). Elongated fibrils are then fractured by sonication exposing new ends for additional monomers to add onto during another growth phase. This cycle of fracture followed by incubation is repeated multiple times resulting in a large amount of fibrils from what was initially a minute quantity of seeds.

5.2 Suppression of monomer self-nucleation

Suppression of primary nucleation is a key factor in the success of this cyclic amplification assay. Htau40 monomer was previously being used for this assay, but exploring the use of mutant monomer was of interest. We hypothesized that specific point mutations could differentially affect a monomers nucleation and elongation capacity. Specifically, that they could suppress nucleation without hindering the monomer's ability to participate in elongation. Mutations were made in the hexapeptide motif in the third repeat because this motif has been identified to play a central role in fibril nucleation (136). The residues of interest were β-branched hydrophobic valine at positions 306 and 309, and isoleucine at position 308. These residues were mutated into a smaller unbranched alanine, a polar serine, or a positively charged lysine. Additional mutations made only at position 308 include negatively charged aspartic acid and glutamic acid. Two double mutants were also made, I308K/V309K and I308K/V308S. Figure 5.2 highlights where the substitutions reside with respect to the repeat region and shows the purity of all 13 mutants.

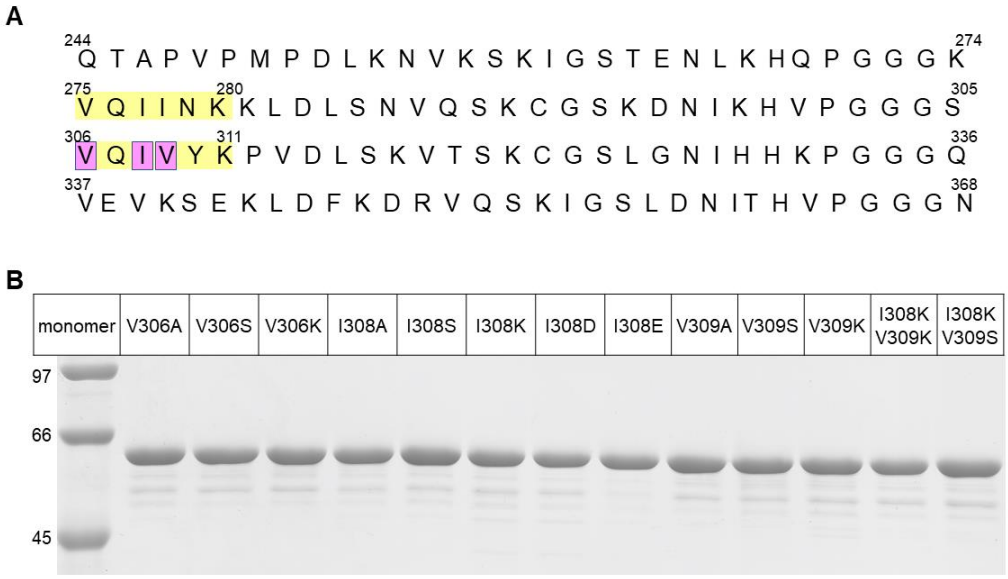

Figure 5.2 Self-nucleation suppressing mutants. A, shows the amino acid sequence of the four repeats of htau40 with the two hexapeptide motifs highlighted in yellow, and the three positions where mutations were made highlighted in pink. B, SDS-PAGE with Coomassie staining showing the purity of all 13 mutants.

Preliminary screening was done to investigate the nucleation lag phase and the elongation competency of these mutants prior to using them in the amplification assay. During the amplification assay, growth is not monitored in real time, but rather assessed at the end of a given number of cycles. An alternative approach to gain initial insight into the lag phase of mutants, with respect to htau40, is to use ThT fluorescence monitoring growth in real time. Mutant or htau40 monomers and heparin in a 1:2 molar ratio were quiescently incubated at 37 °C periodically measuring the ThT fluorescence to indicate the extent of fibril formation. The goal of these experiments was to identify mutants that show an extended lag phase with respect to htau40, because they will most likely also show suppressed self-nucleation in the amplification assay. The

mutants tested showed a wide range of lag phases. Monomer with mutations to V306 all showed a decreased lag phase with respect to htau40. Compare the earlier time the red traces start to rise compared to the black trace in Figure 5.3 A. The decreased lag phases of these mutants make them poor candidates for use in the amplification assay. The higher end point ThT fluorescence of V306 mutants could be attributed to them forming different structures with differential dye incorporation, as seen previously with other mutants (21). Monomer with mutations to only V309 were also poor candidates for use in the amplification assay due to their very similar lag phases compared to htau40. This is evidenced by the similar time the blue and black traces start to rise in Figure 5.3 B. Monomer with mutations to I308, and those with double mutations to I308 and V309, show extended lag phases compared to htau40 monomer. Notice the delay before ThT fluorescence increase for monomer represented by green or orange traces in Figure 5.3 C and D, compared to the black htau40 monomer trace. Some of these I308 and I308/V309 mutants show little to no fibril nucleation in the time frame measured (approximately 7 days). This characteristic made these mutant monomers good candidates to do additional screening on, and potentially use in the amplification assay.

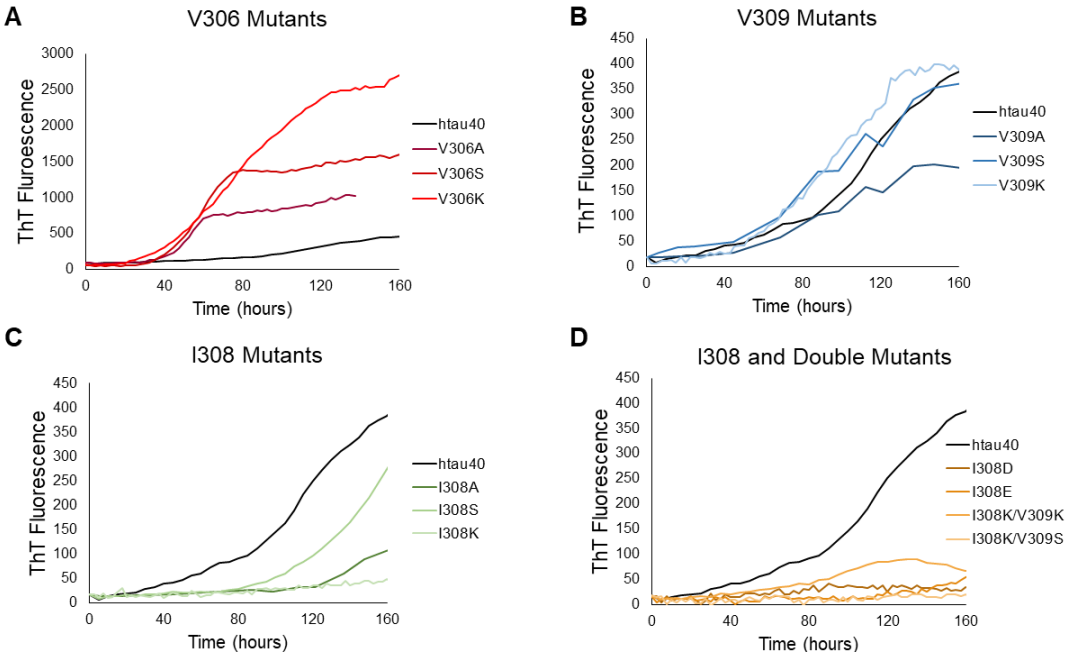

Figure 5.3 Characterizing lag phases of monomers with mutations in the hexapeptide motif. ThT fluorescence was used to monitor quiescent aggregation of htau40 and mutant monomers over several days. ThT traces for V306 mutants (A, red traces), V309 mutants (B, blue traces), I308 mutants (C, green traces), and additional I308 and double I308/V309 mutants (D, orange traces) all with respect to htau40 (black trace, all panels). Traces represent the average from triplicate measurements. The scale of the Y axis in panel A is changed due to the higher ThT fluorescence intensity of V306 mutants. These results show that, with respect to htau40, V306 mutants have shortened lag phases, V309 mutants have similar lag phases, and I308 along with I308/V309 mutants have extended lag phases. This makes I308 mutants and I308/V309 mutants the most promising candidates for use in our amplification assay.

5.3 Elongation competency of nucleation suppressing mutant monomers

The elongation competency of these hexapeptide mutant monomers was the next parameter to be screened before use in the amplification assay. Despite some having suppressed self-nucleation, if these monomers are unable to participate in elongation reactions, they would not be useful in the amplification assay. Using quiescent sedimentation reactions with 10% molar monomer equivalent seed, all mutants were able to elongate onto htau40 seeds. The

results for mutants that showed the most extended lag phase during nucleation experiments (single I308 mutants and double I308/V309 mutants grown on htau40 seeds) are shown in Figure 5.4. Protein being seen in the pellet following incubation, sedimentation, and SDS-PAGE with Coomassie staining highlights the growth of those I308 and double I308/V309 mutants on htau40 seeds (Figure 5.4 A). Growth rates for these particular mutants onto htau40 seeds were compared using ThT fluorescence. This was done to identify if particular mutants showed a significantly diminished growth rate. If a mutant exhibited a slow growth rate that would exclude them from use in the amplification assay. However, the similarity in the time to reach half max ThT fluorescence suggests that none of these mutants had a major kinetic effect on htau40 seeded growth (Figure 5.4 B).

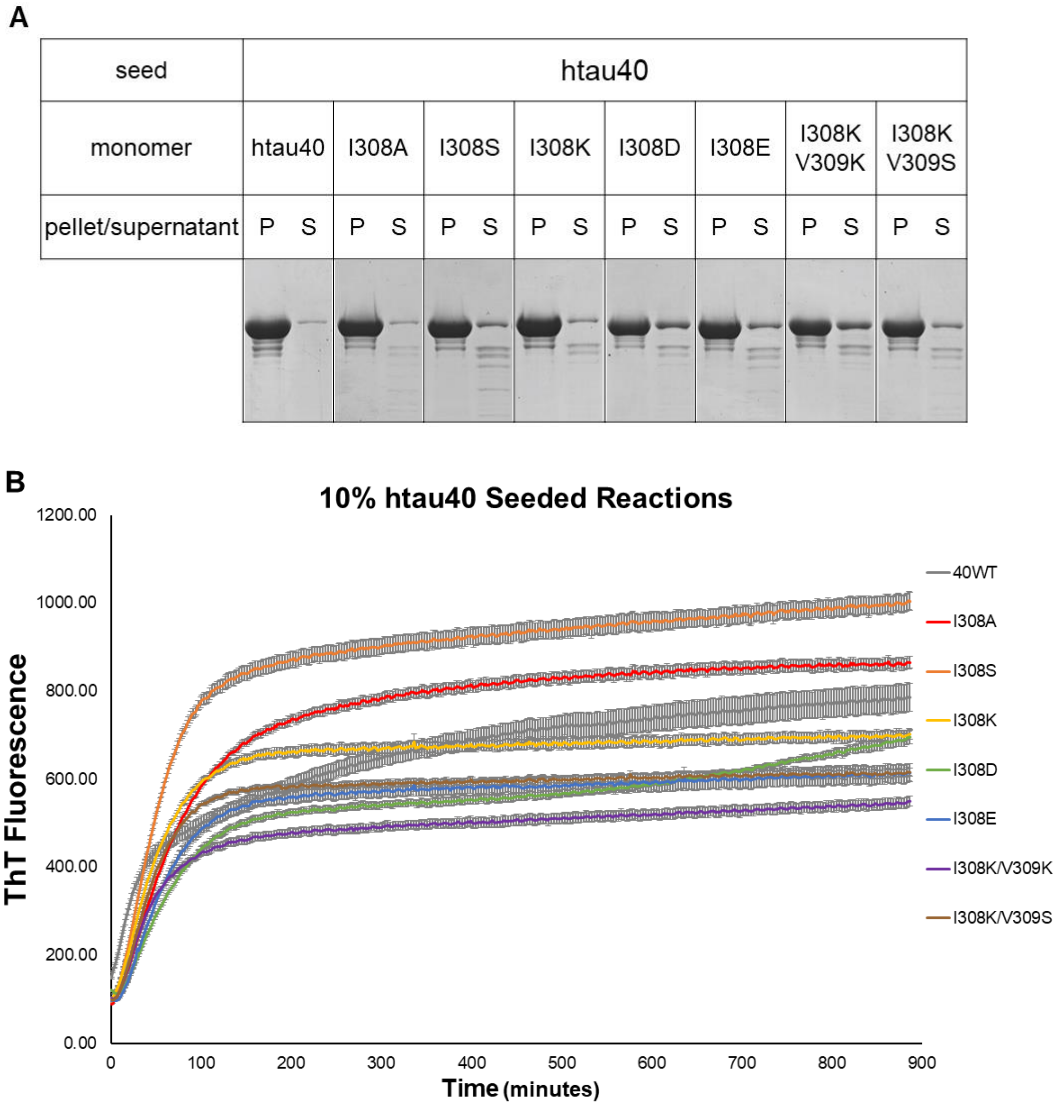

Figure 5.4 Elongation competency of mutant monomers on 10% htau40 seeds. A, SDS-PAGE assessment of 10% htau40 seeded reactions with different mutant monomers. P = pellet, S = supernatant. B, ThT fluorescence showing kinetics of growth reactions between htau40 monomer (grey trace) or mutant monomers: I308A (red trace), I308S (orange trace), I308K (yellow trace), I308D (green trace), I308E (blue trace), I308KV309K (purple trace), and I308K/V309S (brown trace) with 10% htau40 seeds. Error bars represent ± S.D. from triplicate measurements. These results show the elongation competency for these mutant monomers on 10% htau40 seeds.

5.4 Suppressed nucleation of mutant monomer during amplification

The most extended nucleation lag phase, and successful elongation of seeds in 10% molar equivalent seeded sedimentation reactions, made the I308D, I308E, I308K, and I308K/V309S mutants promising candidates to use in our amplification assay. Screening experiments provided good initial data on mutant lag phases under quiescent conditions, but how they react to the sonication events during the amplification assay needed to be tested. In order to do this, mutant monomers along with heparin, in a 1:4 ratio respectively, were subjected to the assay with various parameter changes on each trial. Following the given number of cycles for a particular trial the reactions were spun down at 128,000x g for 30 min, pellets were separated from supernatants, and assessed on SDS-PAGE with Coomassie staining as previously described. These experiments used a wide range of systematic parameter changes in an attempt to find a condition vigorous enough that amplification from a single fibril would be possible, and no spontaneous monomer nucleation would occur. Parameters in question were sonication time, incubation time, power of sonication, and total monomer concentration. Appendix B: Amplification assay trials, provides a table documenting some attempted combinations of parameter settings, and qualitative notation as to whether or not particular mutants tested spontaneously nucleated at each condition. All 13 mutants were tested, however, those identified through quiescent nucleation to spontaneously nucleate faster than the others were not tested as thoroughly. These experiments did show a wide range

of variability, but highlighted two very promising experimental parameter sets that consistently resulted in negligible nucleation of specific mutant monomers. The first was 30 min cycles consisting of 1 min sonication at 15 percent power followed by 29 min incubation with 10 µM tau monomer, 40 µM heparin, 1 mM TCEP kept at a constant 37 °C. The second promising set of assay parameters was 15 min cycles consisting of 1 min sonication at 15 percent power followed by 14 min incubation with 10 µM tau monomer, 40 µM heparin, 1 mM TCEP kept at a constant 37 °C. The same instrument was used to collect all data shown here, and its average power output for a 1 min sonication at 15 percent power was 7600 ± 400 J. However, operating at the same settings, a similar instrument setup in the lab produced higher overall power output.

In the absence of any seeds, the spontaneous nucleation of the four most promising mutants (I308D, I308E, I308K, and I308K/V309S) along with htau40 were investigated. First, using the 30 min cycle parameters for 35-65 cycles in 5 cycle increments (Figure 5.5). The results after 35 cycles show that none of the monomer in question had gone through self-nucleation and aggregated, as evidenced by protein being found exclusively in the supernatant after sedimentation and SDS-PAGE analysis. After 40 cycles htau40 monomer underwent nucleation and elongation, as protein is now found in the pellet. However, after 40 cycles the mutants in question remain in the supernatant. This indicates that in the context of our amplification assay, the self-nucleation of these mutants is suppressed with respect to htau40. This trend is also present

over 45-55 cycles, for which these mutant monomers all remain exclusively in the supernatant. The experiment consisting of 60 cycles resulted in only one mutant not self-nucleating to form aggregates, I308D. The remaining monomers, I308E, I308K and I308K/V309S along with htau40, all indicate that spontaneous nucleation and elongation occurred after 60 cycles by the presence of protein in the pellets. The results from experiments consisting of 60 and 65 cycles show the integrity of the monomer seems to be compromised as it appears to degrade. This degradation is seen as smaller fragments on the lower half of the SDS-PAGE gel not visible in Figure 5.5. Therefore, regardless of their lack of nucleation, this high number of 30 min cycles appears not ideal for use with seeded experiments.

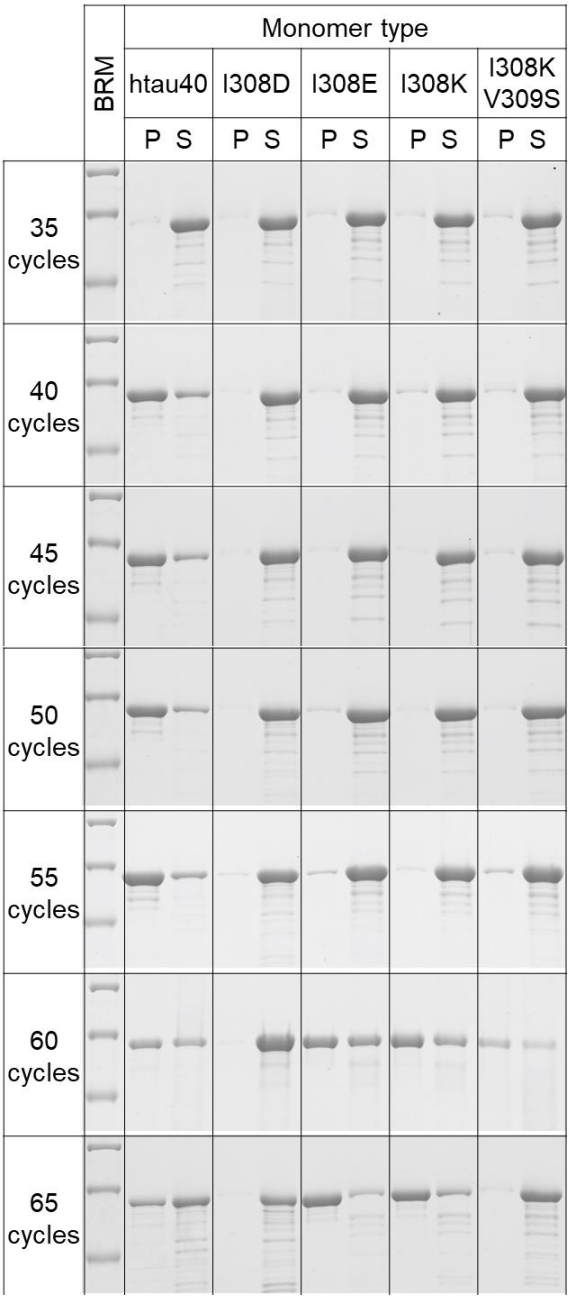

Figure 5.5 Nucleation suppression with 30 min cycles. SDS-PAGE with Coomassie staining assessment of monomer aggregation following cycles of 1 min sonication 29 min incubation for 35, 40, 45, 50, 55, 60 and 65 cycles. Monomer used, from left to right on each gel segment, htau40, I308D, I308E, I308K, and I308K/V309S. BRM = broad range marker showing three bands with molecular weights of 97, 66 and 45 kDa, P = pellet, S = supernatant. These results show that all mutant monomers have suppressed self-nucleation compared to htau40, with I308D showing the most extended lag phase.

Similar experiments were performed to examine the spontaneous nucleation of the same five monomer types using 15 min cycles repeated 96, 144, and 192 times. These 15 min cycles consisted of 1 min sonication at 15 percent power followed by 14 min incubation with 10 µM tau monomer, 40 µM heparin, 1 mM TCEP kept at a constant 37 °C. The results from these experiments (Figure 5.6) show that for the 96, 144, and 192 cycles investigated, htau40 and mutant I308E monomers have nucleated to form fibrils appearing in the pellet upon SDS-PAGE analysis. The remaining monomers in question, I308D, I308K, and I308K/V309S, show suppression of nucleation for experiments consisting of 96 and 144 cycles. However, after 192 cycles nucleation has occurred for all monomer tested. Collectively, the data from experiments using two different cycle times reveal that mutant monomers exhibit suppressed self-nucleation with respect to htau40 monomer. The results further indicate that suppression was the most pronounced for the I308D mutant.

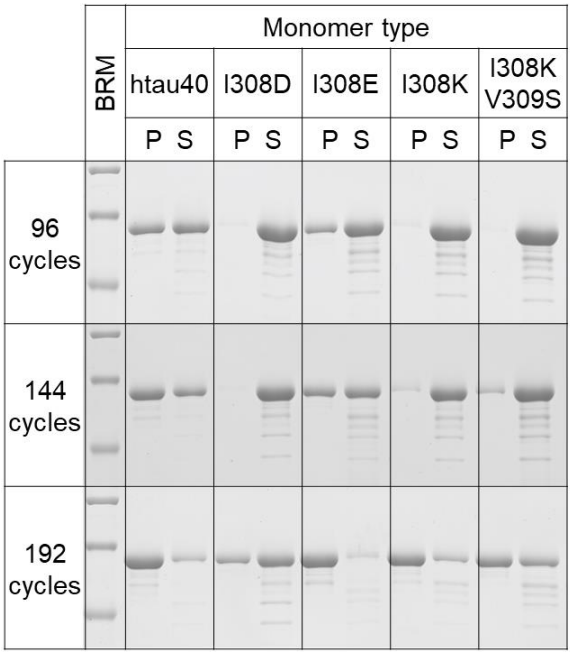

Figure 5.6 Nucleation suppression with 15 min cycles. SDS-PAGE with Coomassie staining assessment of monomer self-nucleation following cycles of 1 min sonication 14 min incubation for 96, 144, and 192 cycles. Monomer used, from left to right on each gel segment, htau40, I308D, I308E, I308K, and I308K/V309S. BRM = broad range marker showing three bands with molecular weights of 97, 66 and 45 kDa, P = pellet, S = supernatant. The results demonstrate that under the given conditions I308D mutant monomers are most resistant to self-nucleation.

5.5 Seeded amplification using I308D mutant monomer

The monomer chosen to test the ability to amplify fibrils from low concentrations of htau40 seeds was I308D, due to its suppressed nucleation during multiple rounds of 30 min and 15 min cycles. Individual reactions contained different percentages of htau40 seed, starting at 0.1% dropping in one order of magnitude increments down to 0.000001%, and a control with no seed. Percentages are with respect to the molar monomer equivalent in the reaction, 10 µM. The reactions were subjected to 50 cycles of 1 min sonication followed by 29 min of incubation. Pellet fractions for these experiments are shown in Figure

5.7. Different trials are the result of biological triplicate seed batches. The same experimental setup with decreasing seed concentration was applied to 96 cycles of 1 min sonication followed by 14 min incubation (Figure 5.8). While the results show variability in the amount of amplification from particular seed percentages, they highlight the ability of the I308D mutant monomer to elongate onto low seed concentrations. Future experiments using I308D mutant monomer are needed to optimize assay parameters to consistently amplify fibrils from even lower concentration of seeds. Promising preliminary data has been collected exploring the use of an additional protein, bovine serum albumin (BSA), that does not participate in aggregation and further suppresses tau nucleation. BSA is potentially acting to suppress tau nucleation by preventing surface nucleation, and reducing the collisions between tau monomers needed for nucleation. The use of I308D mutant monomer in conjunction with BSA is anticipated to allow for more vigorous parameters and improve detection sensitivity.

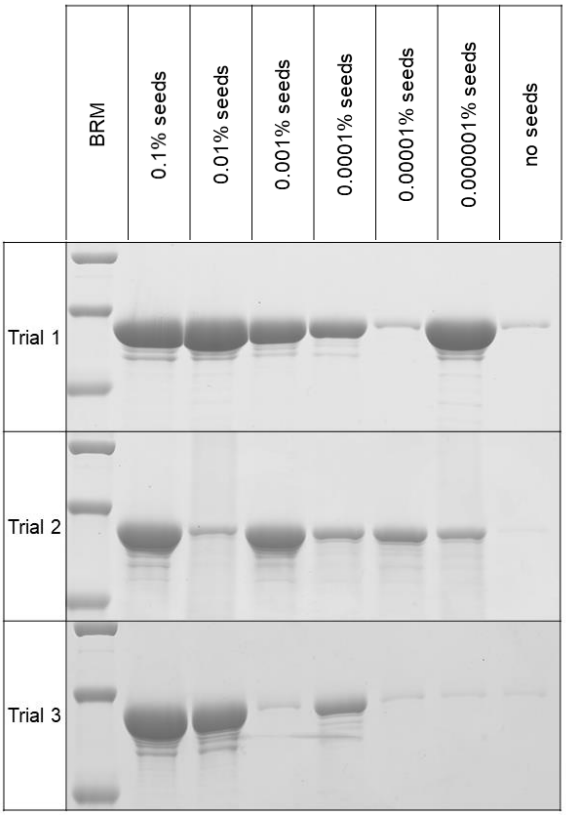

Figure 5.7 Amplifying fibrils from dilute htau40 seed concentrations with 30 min cycles. SDS-PAGE assessment showing pellet fractions from reactions between I308D monomer with decreasing htau40 seed concentration using 50 cycles of 1 min sonication followed by 29 min incubation. The seed concentrations are with respect to monomer present in the reaction (10 µM). Trials 1, 2, and 3 are the result of biological triplicate htau40 seed batches. BRM = broad range marker showing three bands with molecular weights of 97, 66 and 45 kDa. The results highlight the potential for mutant monomer to amplify fibrils from low seed concentration, and the need to further optimize assay parameters.

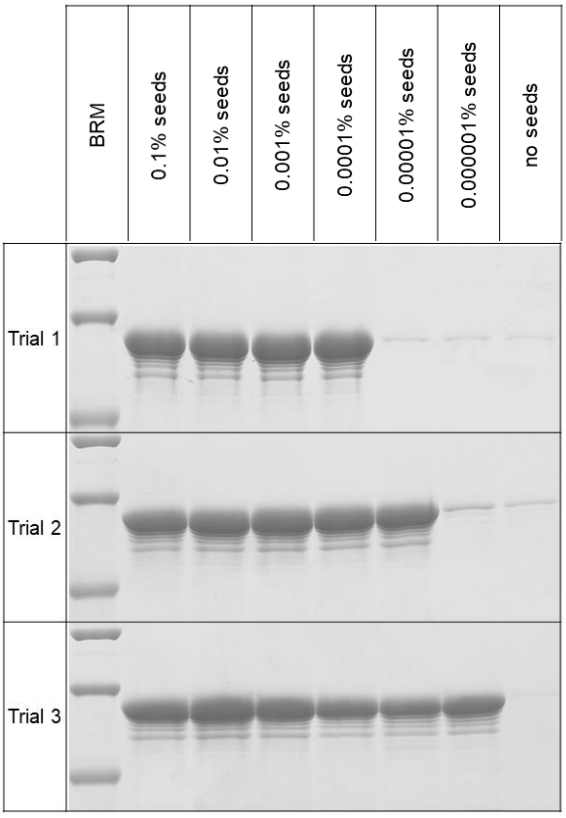

Figure 5.8 Amplifying fibrils from dilute htau40 seed concentrations with 15 min cycles. SDS-PAGE assessment showing pellet fractions from reactions between I308D monomer with decreasing htau40 seed concentration using 96 cycles of 1 min sonication followed by 14 min incubation. The seed concentrations are with respect to monomer present in the reaction (10 µM). Trials 1, 2, and 3 are the result of biological triplicate htau40 seed batches. BRM = broad range marker showing three bands with molecular weights of 97, 66 and 45 kDa. The results show variability in the assay, but highlight the potential for I308D mutant monomer to amplify fibrils from low seed concentrations.

CHAPTER SIX: DISCUSSION

6.1 Structural insights into tau fibrils reveal potential mechanism for disparate pathology

The mechanisms underlying tau fibril propagation that result in the large phenotypic diversity of tauopathies are not fully understood, but one explanation is the differential propagation of fibril conformers (147). Once grown, the spread of small fibrillar species has been shown to happen in a trans-synaptic manner. This means the conformers that form in one particular cell can spread and induce fibrillar growth in neighboring cells (148). This trans-synaptic propagation does not appear to be random, but rather the sequential appearance of pathology seems to parallel the connectivity of the neuronal network chain, as observed in some AD patients (149). Factors that have been proposed to influence the cell-to-cell transmission of certain fibrils include distinct conformational states or PTMs (150–152). Therefore, in order to halt the pathological spreading of tau, it is critical to have a better understanding of how distinct conformers arise, and how their structural features influence growth properties.

It has been shown for tau and other amyloid fibrils, such as α-synuclein and amyloid-β, that the conformation or structure of fibrils dictates their growth properties (76, 152, 153). Also, how distinct fibril conformers composed of the same protein type can exhibit different growth properties (97). Since the

elongation of small fibril species proceeds in a conformationally templated manner, and those elongated fibrils then have the potential to fragment and recruit new monomer onto their ends (93); it is even more critical to understand what factors contribute to how different conformers arise and recruit new monomer. The data presented here provides mechanistic insight to growth barriers seen with different conformers by highlighting how distinct structural features arise due to truncations, mutations, and oxidation of the htau40 isoform.

6.1.1 Characterization of htau40 fibrils

The growth properties of htau40 fibrils were characterized by seeded reactions monitoring end point fibrillar content using TEM or sedimentation with SDS-PAGE assessment, and kinetics of growth via ThT fluorescence. These experiments revealed that htau40 fibrils are able to fully recruit both htau40 (4R) and htau23 (3R) monomers. This recruitment is not driven in any way by disulfide bonding of native cysteines as these experiments were performed in a reducing environment, and identical results were obtained using seeds composed of a cysteine free version of htau40. This is a deviation from growth patterns previously observed in our lab using seeds composed of the truncated tau variant K18, which exhibit a 3R growth barrier (88). Variation in experimental conditions between full-length and K18 seeded reactions did not account for their difference in growth properties. Therefore, N- and/or C- terminal residues in htau40 appear

to greatly influence fibril conformation and growth properties. This finding set the stage for experiments with other truncated variants whose data is discussed in the next section.

The structure of htau40 fibrils was probed using two types of SDSL-EPR experiments, CW and DEER. CW experiments provided structural insight on whether or not certain residues reside in the core of htau40 fibrils. The seven positions investigated were in the fourth repeat and just outside it on the C-terminal end. These residues were chosen based on the cryo-EM structure of AD fibrils, suggesting that they point to the aqueous exterior of the fibril core (19). Spectra from all htau40 seeded fibrils suggest that all the positions investigated reside in the structured core of the htau40 fibrils. This is in agreement with the cryo-EM structure of AD fibrils which reveals that residues 306-378 make up the ordered core (19).

DEER data on htau40 fibrils revealed that they are a heterogeneous mixture of conformers. It is likely that the range of conformations stems from tau's intrinsically disordered nature, allowing for higher structural flexibility during nucleation (155). This ensemble, or cloud, of conformers is shown by the multiple peaks in the distance distributions from biological triplicate measurements of htau40 fibrils. Interestingly, while CW EPR suggests agreement for residues residing in the core of htau40 fibrils and published AD fibrils, the folding pattern of the htau40 core is likely different. As evidenced by the distances in htau40 DEER

data not matching the published AD fibril structure. However, this is not completely surprising because AD fibrils are composed of a mixture of 3R and 4R tau isoforms, whereas the fibrils investigated here are composed of only a single isoform. Additionally, other studies have highlighted how different recombinant 4R fibrils are also conformationally different from published AD fibril structure (64, 156). The different htau40 fibril structures here may be representative of fibrils in different tauopathies, or may be novel fibril types only existent *in vitro*. Selective pressures in the complex biological environment might attribute to the differences seen between *in vivo* and *in vitro* fibrils.

It is noteworthy that the published cryo-EM structures for AD and PID fibrils indicate different singular fold patterns for each disease (19, 20, 129), but it is possible that there are alternative conformers with distinctly different folds present. In clinically documented AD subtypes (128) it was shown that the amyloid fibrils associated with AD plaques, Aβ fibrils, vary in conformation between these subtypes (154). Additionally, it has been shown that multiple prion conformers exist within a single brain (157).

6.1.2 Truncations can influence tau fibril structure

Many factors may contribute to the pathology of tauopathies, truncation of tau protein is one such factor. The truncation of different proteins is a major pathological event in neurodegenerative disorders. In addition to tau, some other

proteins that exhibit this link between truncation and disease pathology include TDP-43 in association with amyotrophic lateral sclerosis (158), α-synuclein in Parkinson's disease (159), and huntingtin protein in Huntington's disease (160). The truncations to tau are not random, they are the result of specific proteolytic cleavage. Truncated variants seem to be direct participants in some disease pathology, and the presence of truncated variants has even been suggested to start a self-perpetuating cycle of tau truncation, increasing the rate of fibril formation and all the effects that go with it (161).

Some of the truncated variants investigated here correspond to known cleavage sites associated with disease truncated fragments, such as positions 421, 391 and 368 (39, 162). But as a collective group, the variants studied here were chosen to systematically test the impact of the N- and C- terminal regions on fibril growth. Variants with truncations to only the N- terminus, along with two of the variants with truncations to only the C- terminus, produce fibrils that have no 3R growth barrier. The other truncated variants that have truncations to both the N- and C- terminus, along with 1-372 variant, produce fibrils that exhibit full recruitment of 4R monomers. But these fibrils vary in the ability to recruit 3R monomers, with recruitment diminishing as the variants got shorter on the C-terminal end. These results collectively indicate that C-terminal residues play a key role in fibril conformation. The slightly diminished ability to recruit 3R tau for the 244-421 and 244-391 with respect to the variants that contain the same C-

terminal truncation but included the entire N- terminal region, suggest some synergistic role being played by the N- terminal residues. This potential N-terminal synergism is not unlikely, given its unstructured nature, it has the potential to fold back and interact with other regions of the protein (163).

Structural differences between these truncated fibrils and htau40 fibrils are likely responsible for their different recruitment properties. EPR experiments were used to investigate the structure of truncated fibrils with a 3R growth barrier. Comparing DEER data on htau40 fibrils and K18 fibrils (76) confirmed truncated monomers nucleate to form fibrils structurally distinct from full-length fibrils. CW EPR data provided more specific structural insight on K18 fibrils. Spectra from K18 seeded fibrils revealed that residues in the beginning of the fourth repeat are part of the structured K18 fibril core. However, the residues in the end of the fourth repeat and just outside it are in a region of increased structural disorder, and not part of the K18 fibril core. This is in stark contrast to the htau40 CW EPR data that revealed a high level of order for all tested positions. This contrast in structural order means this region that in htau40 fibrils is available for recruiting monomers to pack against, is not available in the K18 fibrils. The reduction in contact surface could be one explanation for the diminished 3R recruitment onto K18 seeds, along with other structural differences in other parts of these fibrils.

The C- terminal region in fibrils extracted from 4R tauopathies, PSP and CBD, are less structured in this region as well. Trypsin digestion of such fibrils

revealed fragments terminating at residue 369, while the shortest fragments from AD fibrils extended to position 385 (164). This notable similarity between regions of structural disorder in fibrils from 4R tauopathies and the K18 fibrils investigated here, along with their preferential recruitment of 4R tau, highlights this region of structural disorder as a factor contributing to their preferential recruitment (resulting in specific pathology).

A number of factors could contribute to truncated variants forming different conformers. One example is their lack of stabilization effects that full-length tau experiences through backfolding of residues that are not present in truncated variants (23). The lack of these stabilizations leaves truncated tau unhindered in its formation of other conformers during nucleation (165). The formation of structurally distinct fibrils from truncated variants could be physiologically relevant, as the activation of certain caspases responsible for the proteolytic cleavage creating truncated variants has been noted to precede aggregation (166). Also, the aggregation kinetics of truncated tau fragments are increased with respect to full-length tau (35). This is due to the removal of the terminal regions leaving a conformational ensemble of monomers with decreased interference of the aggregation prone regions. This results in a lower energetic barriers for self-association, meaning that if present, these truncated species have an advantage to initiate fibril formation over full-length tau (30). Due to growth via conformational templating on the initial seed, if a truncated variant that

has a growth barrier initiates fibril formation, that conformer could preferentially recruit full-length 4R tau and be propagated. This could ultimately result in preferential deposition of fibrils that were initiated from a truncated variant seed, but after elongation are mostly composed of full-length tau. Truncated variants are not associated with all tauopathies, but understanding how truncations can influence conformation and growth properties is useful to understand overarching propagation principles. Truncated variants that show no preferential growth, but are still structurally distinct, could be responsible for particular pathology in other disease states.

6.1.3 Mutations impact tau fibril structure

Some of the numerous mutations associated with tau protein show correlation to preferential isoform deposition in certain diseases. One potential explanation for the preferential deposition of some of these mutant fibrils is their effect on the splicing of exon 10, changing the ratio of 4R/3R tau available to participate in aggregation (24). However, since not all mutants take effect at the RNA level, other mechanisms must be responsible for their preferential deposition. To probe the potential influence certain mutations have on forming conformationally distinct fibrils with differential recruitment properties, specific mutants were investigated. I explored growth properties of fibrils with mutations to the proline at position 301 in full-length 4R tau, along with growth properties of

mutants flanking position 301. Mutations to the proline at position 301 are of particular interest because of their association with familial 4R tauopathies (167, 168), and lack of splicing alteration (135). Insight on P301S and P301L mutant fibrils is also of particular interest because multiple research models utilize these particular mutations (169).

The fibrils formed from P301 mutant monomer show recruitment of 4R monomer (>80% growth), but a robust growth barrier towards 3R monomer (<15% growth). This barrier was confirmed using sedimentation assays, ThT fluorescence, and visualized using TEM. Htau40 monomer is able to grow on P301 mutant seeds, but this growth is significantly slower than homotypic recruitment for either mutant type of seed, as shown by ThT kinetics. This suggests that while non-mutant htau40 can assume the preferred mutant conformation, this conformation is energetically less favorable to non-mutant htau40. EPR data revealed structural contrast between these P301 mutant fibrils and the htau40 fibrils. Specifically, that P301 mutants possess structural disorder in the second half of the fourth repeat and the residues immediately outside it, and are an ensemble of conformers distinct from htau40 fibrils. The structural difference of these mutant conformers is significant enough that it does not provide the contact surface necessary for 3R growth, resulting in only minimal overall recruitment. The preferential recruitment of 4R monomer displayed by these P301 mutant fibrils aligns with their pathology *in vivo,* as they are known to

be associated with 4R tauopathies (24). Since they have been shown to not shift 4R/3R expression ratios (135), one mechanism of their preferential recruitment *in vivo* could be due to the mutation promoting specific conformer formation during nucleation.

The significant 3R growth barrier observed with P301 mutant fibrils is very specific to mutating the proline at position 301. This effect is not due to the proximity of position 301 to the PHF6 motif, a region vital for initiating aggregation (136). This is evidenced by the failure of six other mutations flanking position 301 to form fibrils with a strong 3R growth barrier. These included both known disease mutants associated with 4R tauopathies (24), and synthetic point mutations in the PHF6 motif. The lack of conformational distinction as the mechanism behind the preferential deposition of the other disease mutants is unsurprising given that these particular mutations have been identified to take effect at the RNA level shifting the splicing expression 4R tau over 3R tau (170–172). Therefore, a conformational difference would be an additional mechanism for their preferential recruitment properties. The synthetic point mutations had the potential to disrupt β-sheet packing by the insertion of a charged residue into the PHF6 motif. However, they also exhibited no growth barriers. The findings highlight the vital role the proline at position 301 plays in determining fibril conformation.

Insight as to how this single proline mutation is capable of changing the overall preferred conformation of the fibril was gained from other published structures. The fibril cores from AD and PID patients have been shown to contain distinctly different folds (20). Core region sequence comparison reveals the pattern of β-strands align fairly well between these fibrils, and their two distinct fold patterns mostly arise from how the residues linking these strands together are oriented (20). There are either two or three PGGG motifs found in the core regions of these AD and PID core structures, and all are found in these linker regions. Falcon et al. used core structures to highlight the flexible nature of the PGGG motif and its ability to take on multiple conformations, such as turns, spirals, or extended arrangements (20). The data presented in the current study is in agreement with their suggestion that this motif can be a key determinant for overall core structure. A model of PID and AD fibril core structures utilizing PDB data bank accession numbers 6GX5 and 5O3L respectively are depicted in Figure 6.1, with red segments highlighting the PGGG motifs and their flexible nature. Notably, the proline mutated in the current study is part of one of the four PGGG motifs in htau40. The particular motif that contains 301 lies just outside the core region for published AD structure, but unresolved density in these cryo-EM maps suggests that this motif assumes a turn structure and will back fold to pack against β-strands in the third repeat region (19). It is possible that the growth barrier shown here with P301 mutant fibrils is the result of a different

orientation of this motif, such as an extension, as suggested in a previous study (173).

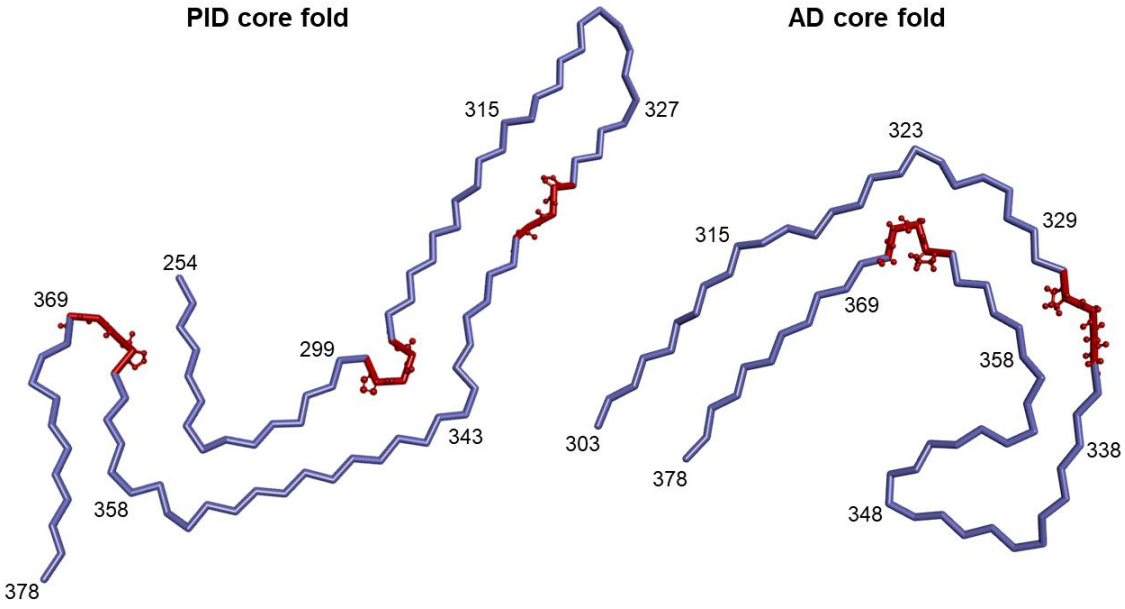

Figure 6.1 Model of PID and AD fibril core structures. Utilizing PDB accession numbers 6GX5 and 5O3L for PID and AD fibrils respectively, the PGGG motifs for each have been identified in red. These segments display a high level of flexibility and their presence in the linker regions between β-strands allows for alteration to fold pattern of the core. Given their influence on structure, mutations to these residues have the potential to shift preferred conformers resulting in differential growth properties.

Notice, the G303V mutation did not have a large structural effect despite its inclusion in one of these PGGG motifs. This switch exhibits a less drastic side chain alteration than a mutation to the proline at position 301 exhibits. The unique cyclic side chain structure and ability of proline to assume the cis or trans configuration allows for its greater influence on structure (174). It is also interesting to note that one of these PGGG motifs is found towards the end of each microtubule binding repeat. The proline in each is found at position 270,

301, 332, or 364; all of which have been identified as pathogenic mutation points. The P270 mutant fibrils are not associated with a clinical phenotype, yet they do correlate to FTD pathology (175). The P332 and P364 mutants have been associated with FTD and present with Pick body-like inclusions (176). Studies probing the growth and structural properties of these mutants would be of interest to identify if they influence 4R or 3R tau recruitment. Collectively, the mutant data presented here highlight how mutations to key structural motifs can significantly alter fibril conformation implicating a mechanism for their preferential growth properties in disease.

6.1.4 Oxidation of htau40 results in structurally distinct fibrils

Recruitment properties of htau40 fibrils composed of monomers that possess an intramolecular disulfide bond between their two native cysteines were of particular interest for a continued investigation of structural diversity in tau fibrils. Due to tau's intrinsically disordered nature, it's set of thermodynamically accessible states as a monomer is greatly increased in comparison to other natively folded proteins. This makes characterization of its monomeric state before it transitions to be part of a fibril difficult (55). However, identification of conformational states that are thermodynamically favored and have the potential to participate in fibril growth can be identified, this is helpful in understating particular growth properties (142). The interest surrounding

intramolecularly disulfide bonded htau40 was due to its potential restriction of monomer conformational states from the disulfide bond holding it in a different conformation than it would natively assume without this bond. The data presented here suggests this different preferred conformer promotes the formation of fibrils with distinct structure and growth properties from their reduced counterparts. These distinct conformers could potentially correspond to disparate pathology associated with certain diseases.

Htau40 monomers containing an intramolecular disulfide bond (htau40 oxidized) were isolated and used to form initial seed fibrils. The growth properties of these fibrils were investigated using sedimentation, ThT kinetics, and TEM. Growth in homotypic oxidized seeded reactions suggests these oxidized seeds do recruit oxidized monomers. However, these oxidized seeds exhibited a lack of recruitment of htau40 SS, htau40 AA, htau23, and htau40 crosslinked monomers. It is unlikely there is even any minor conformer present in the oxidized seed population that could recruit cysless variants, as a complete growth barrier was observed when htau40 SS monomers were offered to 50% (molar monomer equivalent) htau40 oxidized seeds. The lack of growth when offering an htau40 variant with its two native cysteines crosslinked with a bismaleimide crosslinker possessing an 8 Å spacer arm suggest the importance of specifically a disulfide bond linking the cysteines. The rationale behind using the crosslinked version of htau40 was to mimic the compact structure of the

htau40 oxidized monomer. This allowed us to test whether or not alleviating the energetic barrier to bring the monomer into a relatively compact structure would be enough to then allow for monomer addition. However, while this crosslinker does restrict the monomer conformation, it is not as compact as monomer possessing just a disulfide bond. The 8 Å spacer between maleimide groups in this linker is likely too large, and rather than mimicking the tight compact structure of oxidized monomer this crosslinked variant is rather distended in comparison. The inability of crosslinked monomer to be recruited to oxidized seeds suggests tight spatial constraint created by the disulfide bond, and perhaps it's thiol properties, are significant factors determining the recruitment of monomer to oxidized fibrils.

Additional experiments investigated the necessity of the disulfide bond in monomer elongating on htau40 oxidized fibrils. These results suggested that if the monomer has the chance to oxidize over time, it will then be able to add onto the oxidized seeds. Collectively these results from various heterotypic growth reactions reveal that the recruitment of monomer onto htau40 oxidized seeds is dependent on the capacity of the monomer to form an intramolecular disulfide bond. This in complete contrast to reactions utilizing htau40 reduced fibrils that do not possess intramolecular or intermolecular disulfide bonds. These htau40 reduced fibrils are formed in the presence of reducing agent, and their growth properties are independent from any disulfide bond influence. This is evidenced

by their full 4R and 3R tau recruitment properties showing no correlation to cysteine content. Also, these fibrils contained no higher order species, as confirmed through SDS-PAGE assessment of htau40 reduced fibrils with sample buffer lacking reducing agent showing no dimer, trimer, or higher order species (data not shown). Collectively these differential recruitment properties suggest htau40 oxidized fibrils are structurally distinct from htau40 reduced fibrils.

Due to the inability of these oxidized fibrils to recruit cysless monomer, EPR techniques to probe the structure of htau40 oxidized fibrils are not available. However, additional experiments were performed to highlight the structural differences between these oxidized and reduced fibrils. These included the comparison of denaturation profiles, digestion products, and conformational stabilities for these two fibril types. Denaturation by GdnHCl revealed that oxidized fibrils are more susceptible to denaturation than reduced fibrils, suggesting different regions of the protein are exposed implying they are conformationally distinct. Limited protease digestion resulted in different digestion products, suggesting the core structure of these fibrils are different to expose different cleavage sites. Finally, different fibril lengths were observed after applying the same sonication stress to oxidized and reduced fibrils, with reduced fibrils displaying on average a longer length than oxidized fibrils. Since a fibril's stability can be influenced by its structural features, these fragility differences suggest these fibrils are structurally distinct.

These differences, along with the different recruitment properties, collectively reveal that oxidized and reduced fibrils are structurally distinct from one another. The understanding that an intramolecular disulfide bond within 4R tau can impact fibril structure resulting in unique recruitment properties highlights another mechanism of how growth barriers can arise in certain disease states. Further investigation would need to be done to determine whether or not the distinct structural aspects of these oxidized fibrils correlate to fibrils from particular disease states with increased oxidative stress associated with them. A previous *in vitro* study, using different variations of 4R oxidized and reduced fibrils from those discussed here, also highlighted different properties between the two fibril types (57). Interestingly, following trypsin treatment they identified peptide differences. This insight, along with the data from this current study, suggests how disulfide bonds influence regions of structural order and can impact growth properties.

In addition to being structurally distinct from reduced fibrils, these oxidized fibrils also exhibit a unique characteristic of being able to be partially dissociated upon treatment with reducing agent. The observation that there is a maximum extent to this dissociation suggests these oxidized fibrils, like all other fibrils investigated via DEER analysis discussed previously, are an ensemble of conformers. It is likely that the entire population of fibrils with a similar conformation are being dissociated, while different fibril conformers remain. This

is suggested by the presence of monomeric species following treatment with reducing agent, and the assumption that fibrils do not change conformation along the long axis of the same fibril. If one monomer can be removed from the end, the whole fibril will most likely be dissociated. These fibrils that can be dissociated may not be structurally identical, yet it is likely they share common features. These include the disulfide bond being accessible to reducing agent and being the dominant structural feature of these fibrils, therefore breaking this bond results in their dissociation. The population of conformers that cannot be dissociated is likely different in that the disulfide bond is either not the only structurally significant feature (therefore breaking it does not result in dissociation), or the fibril conformation is such that the bond is not accessible to any reducing agent. This feature makes these non-dissociated fibrils of particular physiological interest. It has been previously suggested that intramolecularly disulfide bonded tau may be acted upon differently by proteolytic and degradative machineries acting to clear pathological tau from cells (34, 56). Additionally, under particular oxidative stress conditions, the typical glutathione concentration in the cytosol can be reduced (177, 178). This would allow for oxidation of tau, and previous studies have shown that under oxidizing conditions 4R tau preferably forms intra over intermolecular disulfide bonds (179). It is noteworthy that dimers created by intermolecular disulfide bonded tau have displayed a similar binding affinity for MT as monomeric non-oxidized tau (180). Yet, it is

unclear whether or not this is also true for intramolecularly disulfide bonded tau. If an intramolecular disulfide bond does decrease 4R tau's native function, oxidation is an important factor diverting them toward fibril formation.

6.2 Optimization of tau amplification assay

The increase in prevalence of tauopathies has made early detection techniques and therapeutic design the subject of numerous studies. There are currently multiple approaches to improving early detection. Radiotracers in conjunction with PET imaging (115) and detection in blood or cerebrospinal fluid samples (148, 181, 182) are some techniques currently being pursued. Tau imaging via PET tracers have recently been reported to show promising results for human testing, with potential to monitor disease progression and treatment response (116). Alternatively, the cell-to-cell transfer of small aggregates make it possible that even in early disease stages tau could be present in extracellular fluid (148, 183). However, the amount of tau fibrils would be extremely small, and an extremely sensitive assay would be needed in order to detect it (184). Immunodetection and amplification assays are two potential methods for this detection. Immunoprecipitation of full-length and truncated tau fragments is a powerful detection tool, yet the epitope specificity of the antibodies used can potentially result in some tau species not being detected (185), or fail to distinguish between normal and pathological tau (113). Amplification techniques

could be used as a precursor or in conjunction with immunodetection techniques, or the PET imaging strategy, to develop the best approach to early detection.

The previously developed PMCA assay for prion amplification (118) has been successfully modified in our lab to amplify small concentrations of tau fibrils (119). However, improving the sensitivity of this assay was desired. One way to improve assay sensitivity is to suppress monomer self-nucleation. Previous studies have shown a hexapeptide motif at the beginning of the third repeat to have high inclination to form the β-structure, and that point mutations in this region decreased aggregation propensity (136). That knowledge led us to investigate the effect that specific point mutations within the hexapeptide motif (PHF6) have on spontaneous nucleation. The data presented here show an extended lag phase, and elongation competency with high seed concentrations for monomer with mutations to I308, and monomer with double mutations to I308 and V309. The I308 mutants, and one double I308/V309S mutant were used in our amplification assay. Again, these mutant monomers showed suppressed self-nucleation for multiple parameters tested. Reactions with I308D monomer and decreasing concentrations of recombinant htau40 seeds were also subjected to the amplification assay protocol. The seeded reactions utilizing I308D monomer do show amplification from low seed concentration. However, to enhance the robustness and sensitivity of this assay, additional experiments need to be performed. The data presented here is significant as it highlights how specific

mutations can differentially affect nucleation and elongation competency. Also, the suppressed nucleation of mutant monomer importantly suggests the sensitivity of this assay has the potential to be enhanced.

Multiple factors can contribute to the variability seen with the amplification assay. Previous studies and this current study suggest that fibril nucleation, for multiple monomer types, results in a population of conformers (21, 64, 76). These conformers could have different responses to selective pressures, some with a higher probability of nucleation, resulting in the inconsistent amount of monomer self-nucleation. The ensemble-like nature of free monomer cannot be avoided; however, other points of variability in seeded reactions could be addressed. This would involve teasing apart the experimental parameters to identify how systematic changes to each parameter affect experimental results. For instance, to account for growth rate and fragility of fibrils, the time of incubation and sonication, along with the power of sonication must be considered. The trends exhibited by each parameter change need to be characterized such that different settings can be chosen and confidently applied universally to samples, or ideal settings applied to particular samples.

Along with characterization of how individual parameters effect amplification, future work could involve double mutations in the PHF motifs between residues 306-311 and 275-270. Mutations to both these regions could potentially diminish spontaneous nucleation even more as these two motifs have

been suggested to cross-talk during aggregation (173). Also, given the sensitivity of this assay, experimental technique during reaction preparation needs to be considered. Experimental technique that minimizes the agitation during mixing and transfer, yet still prepares homogenous reactions is desired. A protocol that optimizes this preparation could alleviate variability. A parameter that can also contribute to variability of this assay is intrinsic power variation from the sonicator horn. This has also been noted by other groups utilizing sonicator horns for PMCA experiments as well (186).

Although optimization is still needed, the studies here provide a significant step toward enhancing the sensitivity of this amplification by identifying mutants with suppressed self-nucleation. Once optimized, this assay could be used in conjunction with immunodetection techniques, or inform the optimization of other detection assays. Given the potential to detect tau fibrils in blood samples, once optimized, this assay could act as a routine precursor check before any more invasive detection or treatment techniques are pursued.

REFERENCES

1. Lee, V. M.-Y., Goedert, M., and Trojanowski, J. Q. (2001) Neurodegenerative Tauopathies. *Annu. Rev. Neurosci.* **24**, 1121–1159
2. Uversky, V. N., and Fink, A. L. (2006) Protein Misfolding, Aggregation, and Conformational Diseases. *Protein Rev.* **4**, 1–419
3. McKee, A. C., Cantu, R. C., Nowinski, C. J., Hedley-Whyte, T., and Gavett, B. E. (2009) Chronic Traumatic Encephalopathy in Athletes: Progressive Tauopathy After Repetitive Head Injury. *J. Neuropathol. Exp. Neurol.* **68**, 709–753
4. Tolnay, M., and Probst, A. (2003) Review Article The Neuropathological Spectrum of Neurodegenerative Tauopathies. **55**, 299–305
5. Association, A. (2018) 2018 Alzheimer's Disease Facts and Figures. *ebook*. **14**, 367–429
6. Hebert, L. E., Weuve, J., Scherr, P. A., and Evans, D. A. (2013) Alzheimer disease in the United States (2010–2050) estimated using the 2010 census. *Neurology*. **80**, 1778 LP-1783
7. Shirao, T. (1995) The roles of microfilament-associated proteins, drebrins, in brain morphogenesis: A review. *J. Biochem.* **117**, 231–236
8. Weingarten, M. D., Lockwood, A. H., Hwo, S. Y., and Kirschner, M. W. (1975) A protein factor essential for microtubule assembly. *Proc. Natl. Acad. Sci. U. S. A.* **72**, 1858–62
9. Drubin, D. G., and Kirscher, M. W. (1986) Tau protein in living cells. *J Cell Biol*. **103**, 2739–2746
10. Crowther, R. A., and Goedert, M. (2000) Abnormal tau-containing filaments in neurodegenerative diseases. *J. Struct. Biol.* **130**, 271–279
11. Goedert, M., Wischik, C. M., Crowther, R. A., Walker, J. E., and Klug, A. (1988) Cloning and sequencing of the cDNA encoding a core protein of the paired helical filament of Alzheimer disease: identification as the microtubule-associated protein tau. *Proc. Natl. Acad. Sci. U. S. A.* **85**, 4051–5
12. Kosik, K. S., Orecchio, L. D., Binder, L., Trojanowski, J. Q., Lee, V. M. Y., and Lee, G. (1988) Epitopes that span the tau molecule are shared with paired helical filaments. *Neuron*. **1**, 817–825
13. Andreadis, A., Brown, W. M., and Kosik, K. S. (1992) Structure and Novel Exons of the Human τ Gene. *Biochemistry*. **31**, 10626–10633
14. Andreadis, A., Broderick, J. A., and Kosik, K. S. (1995) Relative exon affinities and suboptimal splice site signals lead to non-equivalence of two cassette exons. *Nucleic Acids Res.* **23**, 3585–3593
15. Goedert, M., and Ross, J. (1990) Expression of separate isoforms of human tau protein: correlation with the tau pattern in brain and effects on tubulin polymerization. *EMBO J.* **9**, 4225

16. Buée, L., Bussière, T., Buée-Scherrer, V., Delacourte, a, and Hof, P. R. (2000) Tau protein isoforms, phosphorylation and role in neurodegenerative disorders. *Brain Res. Brain Res. Rev.* **33**, 95–130
17. Gustke, N., Trinczek, B., Biernat, J., Mandelkow, E. M., and Mandelkow, E. (1994) Domains of τ Protein and Interactions with Microtubules. *Biochemistry*. **33**, 9511–9522
18. Von Bergen, M., Barghorn, S., Biernat, J., Mandelkow, E. M., and Mandelkow, E. (2005) Tau aggregation is driven by a transition from random coil to beta sheet structure. *Biochim. Biophys. Acta - Mol. Basis Dis.* **1739**, 158–166
19. Fitzpatrick, A. W. P., Falcon, B., He, S., Murzin, A. G., Murshudov, G., Garringer, H. J., Crowther, R. A., Ghetti, B., Goedert, M., and Scheres, S. H. W. (2017) Cryo-EM structures of tau filaments from Alzheimer's disease. *Nature*. **547**, 185–190
20. Falcon, B., Zhang, W., Murzin, A. G., Murshudov, G., Garringer, H. J., Vidal, R., Crowther, R. A., Ghetti, B., Scheres, S., and Goedert, M. (2018) Structures of filaments from Pick's disease reveal a novel tau protein fold. *Nature*. **561**, 137–140
21. Weismiller, H. A., Murphy, R., Wei, G., Ma, B., Nussinov, R., and Margittai, M. (2018) Structural disorder in four-repeat Tau fibrils reveals a new mechanism for barriers to cross-seeding of Tau isoforms. *J. Biol. Chem.* **293**, 17336–17348
22. Wegmann, S., Medalsy, I. D., Mandelkow, E., and Müller, D. J. (2013) The fuzzy coat of pathological human Tau fibrils is a two-layered polyelectrolyte brush. *Proc. Natl. Acad. Sci. U. S. A.* **110**, E313-21
23. Bibow, S., Mukrasch, M. D., Chinnathambi, S., Biernat, J., Griesinger, C., Mandelkow, E., and Zweckstetter, M. (2011) The dynamic structure of filamentous Tau. *Angew. Chemie - Int. Ed.* **50**, 11520–11524
24. Goedert, M. (2005) Tau gene mutations and their effects. *Mov. Disord.* **20**, S45–S52
25. Martin, L., Latypova, X., and Terro, F. (2011) Post-translational modifications of tau protein: implications for Alzheimer's disease. *Neurochem. Int.* **58**, 458–71
26. Gong, C.-X., Liu, F., Grundke-Iqbal, I., and Iqbal, K. (2005) Post-translational modifications of tau protein in Alzheimer's disease. *J. Neural Transm.* **112**, 813–38
27. Spillantini, M. G., and Goedert, M. (2013) Tau pathology and neurodegeneration. *Lancet Neurol.* **12**, 609–22
28. Kopeikina, K. J., Hyman, B. T., and Spires-Jones, T. L. (2013) Soluble forms of tau are toxic in Alzheimer ' s disease. *Transl. Neurosci.* **3**, 223–233
29. Quinn, J. P., Corbett, N. J., Kellett, K. A. B., and Hooper, N. M. (2018) Tau

Proteolysis in the Pathogenesis of Tauopathies: Neurotoxic Fragments and Novel Biomarkers. *J. Alzheimer's Dis.* **63**, 1–21
30. Novak, P., Cehlar, O., Skrabana, R., and Novak, M. (2018) Tau Conformation as a Target for Disease-Modifying Therapy: The Role of Truncation. *J. Alzheimers. Dis.* **64**, S535–S546
31. Vechterova, L., Kontsekova, E., Zilka, N., Ferencik, M., Ravid, R., and Novak, M. (2003) DCII: A novel monoclonal antibody revealing Alzheimer's disease-specific tau epitope. *Neuroreport*. **14**, 87–91
32. Novak, M., Kabat, J., and Wischik, C. M. (1993) Molecular characterization of the minimal protease resistant tau unit of the Alzheimer's disease paired helical filament. *EMBO J.* **12**, 365–370
33. Jicha, G. A., Berenfeld, B., and Davies, P. (1999) Sequence requirements for formation of conformational variants of tau similar to those found in Alzheimer's disease. *J. Neurosci. Res.* **55**, 713–723
34. Chesser, A. S., Pritchard, S. M., and Johnson, G. V. W. (2013) Tau clearance mechanisms and their possible role in the pathogenesis of Alzheimer disease. *Front. Neurol.* **4**, 1–12
35. Gamblin, T. C., Chen, F., Zambrano, A., Abraha, A., Lagalwar, S., Guillozet, A. L., Lu, M., Fu, Y., Garcia-Sierra, F., LaPointe, N., Miller, R., Berry, R. W., Binder, L. I., and Cryns, V. L. (2003) Caspase cleavage of tau: linking amyloid and neurofibrillary tangles in Alzheimer's disease. *Proc. Natl. Acad. Sci. U. S. A.* **100**, 10032–10037
36. Zhao, Y., Tseng, I. C., Heyser, C. J., Rockenstein, E., Mante, M., Adame, A., Zheng, Q., Huang, T., Wang, X., Arslan, P. E., Chakrabarty, P., Wu, C., Bu, G., Mobley, W. C., Zhang, Y. wu, St. George-Hyslop, P., Masliah, E., Fraser, P., and Xu, H. (2015) Appoptosin-Mediated Caspase Cleavage of Tau Contributes to Progressive Supranuclear Palsy Pathogenesis. *Neuron*. **87**, 963–975
37. Rissman, R. a., Poon, W. W., Blurton-Jones, M., Oddo, S., Torp, R., Vitek, M. P., LaFerla, F. M., Rohn, T. T., and Cotman, C. W. (2004) Caspase-cleavage of tau is an early event in Alzheimer disease tangle pathology. *J. Clin. Invest.* **114**, 121–130
38. Park, S.-Y., and Ferreira, A. (2005) The Generation of a 17 kDa Neurotoxic Fragment: An Alternative Mechanism by which Tau Mediates -Amyloid-Induced Neurodegeneration. *J. Neurosci.* **25**, 5365–5375
39. Zhang, Z., Song, M., Liu, X., Kang, S. S., Kwon, I.-S., Duong, D. M., Seyfried, N. T., Hu, W. T., Liu, Z., Wang, J.-Z., Cheng, L., Sun, Y. E., Yu, S. P., Levey, A. I., and Ye, K. (2014) Cleavage of tau by asparagine endopeptidase mediates the neurofibrillary pathology in Alzheimer's disease. *Nat. Med.* **20**, 1254
40. Kenessey, A., Nacharaju, P., Ko, L.-W., and Yen, S.-H. (1997) Degradation of Tau by Lysosomal Enzyme Cathepsin D: Implication for Alzheimer

Neurofibrillary Degeneration. *J. Neurochem. Lippincott—Raven Publ. Philadelphia J. Neurochem*. **69**, 2026–2038
41. Sengupta, S., Horowitz, P. M., Karsten, S. L., Jackson, G. R., Geschwind, D. H., Fu, Y., Berry, R. W., and Binder, L. I. (2006) Degradation of tau protein by puromycin-sensitive aminopeptidase in vitro. *Biochemistry*. **45**, 15111–15119
42. Arai, T., Guo, J. P., and McGeer, P. L. (2005) Proteolysis of non-phosphorylated and phosphorylated tau by thrombin. *J. Biol. Chem.* **280**, 5145–5153
43. Henriksen, K., Wang, Y., Sørensen, M. G., Barascuk, N., Suhy, J., Pedersen, J. T., Duffin, K. L., Dean, R. A., Pajak, M., Christiansen, C., Zheng, Q., and Karsdal, M. A. (2013) An Enzyme-Generated Fragment of Tau Measured in Serum Shows an Inverse Correlation to Cognitive Function. *PLoS One*. **8**, e64990
44. Goedert, M., and Jakes, R. (2005) Mutations causing neurodegenerative tauopathies. **1739**, 240–250
45. Cente, M., Filipcik, P., Pevalova, M., and Novak, M. (2006) Expression of a truncated tau protein induces oxidative stress in a rodent model of tauopathy. *Eur. J. Neurosci.* **24**, 1085–1090
46. Sarsour, E. H., Kumar, M. G., Chaudhuri, L., Kalen, A. L., and Goswami, P. C. (2009) Redox Control of the Cell Cycle in Health and Disease. *Antioxid. Redox Signal.* **11**, 2985–3011
47. Selva Rivas-Arancibia, C. G.-R., Nancy Gomez-Crisostomo, E. F.-G., and Dulce Flores Briseño, L. N. and E. R.-M. (2011) *Oxidative Stress and Neurodegenerative Disease*, 10.5772/28857
48. Lynch, T., Cherny, R. A., and Bush, A. I. (2000) Oxidative processes in Alzheimer's disease: The role of Aβ-metal interactions. *Exp. Gerontol.* **35**, 445–451
49. Huang, X., Moir, R. D., Tanzi, R. E., Bush, A. I., and Rogers, J. T. (2004) Redox-active metals, oxidative stress, and Alzheimer's disease pathology. *Ann. N. Y. Acad. Sci.* **1012**, 153–163
50. Savelieff, M. G., Lee, S., Liu, Y., and Lim, M. H. (2013) Untangling amyloid-beta, tau, and metals in Alzheimer's disease. *ACS Chem. Biol.* **8**, 856–865
51. Cuajungco, M. P., Fagét, K. Y., Huang, X., Tanzi, R. E., and Bush, A. I. (2006) Metal Chelation as a Potential Therapy for Alzheimer's Disease. *Ann. N. Y. Acad. Sci.* **920**, 292–304
52. Zatta, P., Drago, D., Bolognin, S., and Sensi, S. L. (2009) Alzheimer's disease, metal ions and metal homeostatic therapy. *Trends Pharmacol. Sci.* **30**, 346–355
53. Crouch, P. J., White, A. R., and Bush, A. I. (2007) The modulation of metal bio-availability as a therapeutic strategy for the treatment of Alzheimer's disease. *FEBS J.* **274**, 3775–3783

54. Friedhoff, P., Schneider, A., Mandelkow, E. M., and Mandelkow, E. (1998) Rapid assembly of Alzheimer-like paired helical filaments from microtubule-associated protein tau monitored by fluorescence in solution. *Biochemistry*. **37**, 10223–10230
55. Barghorn, S., and Mandelkow, E. (2002) Toward a unified scheme for the aggregation of tau into Alzheimer paired helical filaments. *Biochemistry*. **41**, 14885–14896
56. Schweers, O., Biernat, J., and Mandelkow, E. (1995) Oxidation of cysteine-322 in the repeat domain of microtubule-associated protein tau controls the in vitro assembly of paired helical filaments. **92**, 8463–8467
57. Furukawa, Y., Kaneko, K., and Nukina, N. (2011) Tau protein assembles into isoform- and disulfide-dependent polymorphic fibrils with distinct structural properties. *J. Biol. Chem.* **286**, 27236–27246
58. Kuret, J., Chirita, C. N., Congdon, E. E., Kannanayakal, T., Li, G., Necula, M., Yin, H., and Zhong, Q. (2005) Pathways of tau fibrillization. *Biochim. Biophys. Acta - Mol. Basis Dis.* **1739**, 167–178
59. Bhattacharya, K., Rank, K. B., Evans, D. B., and Sharma, S. K. (2001) Role of cysteine-291 and cysteine-322 in the polymerization of human tau into Alzheimer-like filaments. *Biochem. Biophys. Res. Commun.* **285**, 20–26
60. Wang, Y., and Mandelkow, E. (2016) Tau in physiology and pathology. *Nat. Rev. Neurosci.* **17**, 5–21
61. van Herpen, E. (2004) *Tau on the Map: the role of mutations in FTDP-17*. Ph.D. thesis, 10.1017/S1431927608085371
62. Goedert, M., and Spillantini, M. G. (2000) Tau mutations in frontotemporal dementia FTDP-17 and their relevance for Alzheimer's disease. *Biochim. Biophys. Acta - Mol. Basis Dis.* **1502**, 110–121
63. Goedert, M., Jakes, R., and Crowther, R. A. (1999) Effects of frontotemporal dementia FTDP-17 mutations on heparin-induced assembly of tau filaments. *FEBS Lett.* **450**, 306–311
64. Meyer, V., Dinkel, P. D., Luo, Y., Yu, X., Wei, G., Zheng, J., Eaton, G. R., Ma, B., Nussinov, R., Eaton, S. S., and Margittai, M. (2014) Single Mutations in Tau Modulate the Populations of Fibril Conformers through Seed Selection. *Angew. Chemie*. **126**, 1616–1619
65. Lee, V. M.-Y., Goedert, M., and Trojanowski, J. Q. (2001) Neurodegenerative Tauopathies. *Annu. Rev. Neurosci.* **24**, 1121–1159
66. Narhi, L. O., Schmit, J., Bechtold-Peters, K., and Sharma, D. (2012) Classification of protein aggregates. *J. Pharm. Sci.* **101**, 493–498
67. Fowler, D. M., Koulov, A. V., Alory-Jost, C., Marks, M. S., Balch, W. E., and Kelly, J. W. (2006) Functional amyloid formation within mammalian tissue. *PLoS Biol.* **4**, 0100–0107
68. Pepys, M. B. (2001) Pathogenesis, diagnosis and treatment of systemic

amyloidosis. *Philos. Trans. R. Soc. London. Ser. B Biol. Sci.* **356**, 203 LP-211
69. Makin, O. S., and Serpell, L. C. (2005) Structures for amyloid fibrils. *FEBS J.* **272**, 5950–5961
70. Missmahl, H. P., and Hartwig, M. (1953) Polarization optical investigations on the amyloid substance. *Virchow's Arch. Pathol. Anat. Physiol. Clin. Med.* **324**, 489–508
71. Cohen, A. S., and Calkins, E. (1959) Electron Microscopic Observations on a fibrous component in amyloid of diverse origins. *Nature*. **183**, 1202–1203
72. Sunde, M., Serpell, L. C., Bartlam, M., Fraser, P. E., Pepys, M. B., and Blake, C. C. F. (1997) Common core structure of amyloid fibrils by synchrotron X-ray diffraction. *J. Mol. Biol.* **273**, 729–739
73. Takeda, T., and Klimov, D. K. (2009) Side Chain Interactions Can Impede Amyloid Fibril Growth: Replica Exchange Simulations of Aß Peptide Mutant. *J. Phys. Chem. B*. **113**, 11848–11857
74. Trovato, A., Chiti, F., Maritan, A., and Seno, F. (2006) Insight into the structure of amyloid fibrils from the analysis of globular proteins. *PLoS Comput. Biol.* **2**, 1608–1618
75. Margittai, M., and Langen, R. (2008) Fibrils with parallel in-register structure constitute a major class of amyloid fibrils: molecular insights from electron paramagnetic resonance spectroscopy. *Q. Rev. Biophys.* **41**, 265–297
76. Meyer, V., Holden, M. R., Weismiller, H. A., Eaton, G. R., Eaton, S. S., and Margittai, M. (2016) Fracture and Growth Are Competing Forces Determining the Fate of Conformers in Tau Fibril Populations. *J. Biol. Chem.* **291**, jbc.M116.715557
77. Johansson, J. (2005) Amyloid fibrils. *FEBS J.* **272**, 5941
78. Frieden, C. (2007) Protein aggregation processes : In search of the mechanism. *Protein Sci.* **16**, 2334–2344
79. Knowles, T. P. J., Waudby, C. A., Devlin, G. L., Cohen, S. I. A., Welland, M. E., and Dobson, C. M. (2009) An Analytical Solution to the Kinetics. *Science (80-.).* **326**, 1533–1537
80. Cohen, S. I. a, Vendruscolo, M., Dobson, C. M., and Knowles, T. P. J. (2012) From macroscopic measurements to microscopic mechanisms of protein aggregation. *J. Mol. Biol.* **421**, 160–71
81. Ramachandran, G., and Udgaonkar, J. B. (2013) Mechanistic studies unravel the complexity inherent in tau aggregation leading to Alzheimer's disease and the tauopathies. *Biochemistry*. **52**, 4107–26
82. Jarrett, J. T., and Lansbury, P. T. (1992) Amyloid fibril formation requires a chemically discriminating nucleation event: studies of an amyloidogenic sequence from the bacterial protein OsmB. *Biochemistry*. **31**, 12345–52
83. Hamada, D., and Dobson, C. M. (2002) A kinetic study of β-lactoglobulin

amyloid fibril formation promoted by urea. *Protein Sci.* **11**, 2417–2426
84. Wang, S. S., Hung, Y.-T., Wang, P., and Wu, J. W. (2007) The formation of amyloid fibril-like hen egg-white lysozyme species induced by temperature and urea concentration-dependent denaturation. *Korean J. Chem. Eng.* **24**, 787–795
85. Schmit, J. D., Ghosh, K., and Dill, K. (2011) What drives amyloid molecules to assemble into oligomers and fibrils? *Biophys. J.* **100**, 450–8
86. Dinkel, P. D., Holden, M. R., Matin, N., and Margittai, M. (2015) RNA Binds to Tau Fibrils and Sustains Template-Assisted Growth. *Biochemistry*. **54**, 4731–4740
87. King, M. E., Gamblin, T. C., Kuret, J., and Binder, L. I. (2000) Differential assembly of human tau isoforms in the presence of arachidonic acid. *J. Neurochem.* **74**, 1749–1757
88. Dinkel, P. D., Siddiqua, A., Huynh, H., Shah, M., and Margittai, M. (2011) Variations in filament conformation dictate seeding barrier between three- and four-repeat tau. *Biochemistry*. **50**, 4330–4336
89. Siddiqua, A., and Margittai, M. (2010) Three- and four-repeat tau coassemble into heterogeneous filaments: An implication for Alzheimer disease. *J. Biol. Chem.* **285**, 37920–37926
90. Zhang, J., and Muthukumar, M. (2009) Simulations of nucleation and elongation of amyloid fibrils. *J. Chem. Phys.* **130**, 035102
91. Buell, A. K., Galvagnion, C., Gaspar, R., Sparr, E., Vendruscolo, M., Knowles, T. P. J., Linse, S., and Dobson, C. M. (2014) Solution conditions determine the relative importance of nucleation and growth processes in α-synuclein aggregation. *Proc. Natl. Acad. Sci. U. S. A.* **111**, 7671–7676
92. Cohen, S. I. a, Linse, S., Luheshi, L. M., Hellstrand, E., White, D. a, Rajah, L., Otzen, D. E., Vendruscolo, M., Dobson, C. M., and Knowles, T. P. J. (2013) Proliferation of amyloid-β42 aggregates occurs through a secondary nucleation mechanism. *Proc. Natl. Acad. Sci. U. S. A.* **110**, 9758–63
93. Margittai, M., and Langen, R. (2004) Template-assisted filament growth by parallel stacking of tau. *Proc. Natl. Acad. Sci. U. S. A.* **101**, 10278–10283
94. Weissmann, C., Enari, M., Klohn, P.-C., Rossi, D., and Flechsig, E. (2002) Transmission of prions. *Proc. Natl. Acad. Sci.* **99**, 16378–16383
95. Collinge, J., and Clarke, A. R. (2007) A general model of prion strains and their pathogenicity. *Science*. **318**, 930–936
96. Tanaka, M., Collins, S. R., Toyama, B. H., and Weissman, J. S. (2006) The physical basis of how prion conformations determine strain phenotypes. *Nature*. **442**, 585–589
97. Kaufman, S. K., Sanders, D. W., Thomas, T. L., Ruchinskas, A. J., Vaquer-Alicea, J., Sharma, A. M., Miller, T. M., and Diamond, M. I. (2016) Tau Prion Strains Dictate Patterns of Cell Pathology, Progression Rate, and Regional Vulnerability In Vivo. *Neuron*. **92**, 796–812

98. Sanders, D. W., Kaufman, S. K., DeVos, S. L., Sharma, A. M., Mirbaha, H., Li, A., Barker, S. J., Foley, A. C., Thorpe, J. R., Serpell, L. C., Miller, T. M., Grinberg, L. T., Seeley, W. W., and Diamond, M. I. (2014) Distinct Tau Prion Strains Propagate in Cells and Mice and Define Different Tauopathies. *Neuron*. **82**, 1271–1288
99. Guo, J. L., Narasimhan, S., Changolkar, L., He, Z., Stieber, A., Zhang, B., Gathagan, R. J., Iba, M., McBride, J. D., Trojanowski, J. Q., and Lee, V. M. Y. (2016) Unique pathological tau conformers from Alzheimer's brains transmit tau pathology in nontransgenic mice. *J. Exp. Med.* **213**, 2635–2654
100. Narasimhan, S., Guo, J. L., Changolkar, L., Stieber, A., McBride, J. D., Silva, L. V., He, Z., Zhang, B., Gathagan, R. J., Trojanowski, J. Q., and Lee, V. M. Y. (2017) Pathological tau strains from human brains recapitulate the diversity of tauopathies in non-transgenic mouse brain. *J. Neurosci.* **37**, 1230–17
101. Braak, H., Alafuzoff, I., Arzberger, T., Kretzschmar, H., and Tredici, K. (2006) Staging of Alzheimer disease-associated neurofibrillary pathology using paraffin sections and immunocytochemistry. *Acta Neuropathol.* **112**, 389–404
102. Probst, A., Langui, D., and Ulrich, J. Alzheimer's Disease: A Description of the Structural Lesions. *Brain Pathol.* **1**, 229–239
103. Tolnay, M., and Probst, A. (1999) Tau protein pathology in Alzheimer's disease and related disorders. *Neuropathol. Appl. Neurobiol.* **25**, 171–187
104. Goedert, M., Spillantini, M. G., Cairns, N. J., and Crowther, R. A. (1992) Tau proteins of alzheimer paired helical filaments: Abnormal phosphorylation of all six brain isoforms. *Neuron*. **8**, 159–168
105. Bronner, I. F., Ter Meulen, B. C., Azmani, a., Severijnen, L. a., Willemsen, R., Kamphorst, W., Ravid, R., Heutink, P., and Van Swieten, J. C. (2005) Hereditary Pick's disease with the G272V tau mutation shows predominant three-repeat tau pathology. *Brain*. **128**, 2645–2653
106. McKhann, G. M., Albert, M. S., Grossman, M., Miller, B., Dickson, D., and TRojanowski, J. (2001) Clinical and Pathological Diagnosis of Frontotemporal Dementia. *Arch. Neurol.* **58**, 1803
107. Komori, T. (1999) Tau-positive glial inclusions in progressive supranuclear palsy, corticobasal degeneration and Pick's disease. *Brain Pathol.* **9**, 663–679
108. Togo, T., Sahara, N., Yen, S.-H., Cookson, N., Lees, A., and Dickson, D. (2002) Argyrophilic Grain Disease Is a Sporadic 4-Repeat Tauopathy. *J. Neuropathol. Exp. Neurol.* **61**, 547–556
109. Tolnay, M., Sergeant, N., Ghestem, A., Chalbot, S., de Vos, R. A., Jansen Steur, E. N., Probst, A., and Delacourte, A. (2002) Argyrophilic grain disease and Alzheimer's disease are distinguished by their different

distribution of tau protein isoforms. *Acta Neuropathol.* **104**, 425–434
110. Goedert, M., Masuda-Suzukake, M., and Falcon, B. (2017) Like prions: The propagation of aggregated tau and α-synuclein in neurodegeneration. *Brain*. **140**, 266–278
111. Rauch, J. N., Olson, S. H., and Gestwicki, J. E. (2016) Interactions between Microtubule-Associated Protein Tau (MAPT) and Small Molecules. *Cold Spring Harb. Perspect. Med.* **10**, 1–14
112. Binder, L. I., Frankfurter, A., and Rebhun, L. I. (1985) The distribution of tau in the mammalian central nervous central nervous. *J. Cell Biol.* **101**, 1371–1378
113. Combs, B., Hamel, C., and Kanaan, N. M. (2016) Pathological conformations involving the amino terminus of tau occur early in Alzheimer's disease and are differentially detected by monoclonal antibodies. *Neurobiol. Dis.* **94**, 18–31
114. Carmel, G., Mager, E. M., Lester, I., Kuret, J., and Binder, L. I. (1996) The Structural Basis of Monoclonal Antibody Alz50's Selectivity for Alzheimer's Disease Pathology The Structural Basis of Monoclonal Antibody Alz50 ' s Selectivity for Alzheimer ' s Disease Pathology *. *J. Biol. Chem.* **271**, 32789–32795
115. Saint-Aubert, L., Lemoine, L., Chiotis, K., Leuzy, A., Rodriguez-Vieitez, E., and Nordberg, A. (2017) Tau PET imaging: present and future directions. *Mol. Neurodegener.* **12**, 1–21
116. Wong, D. F., Comley, R., Kuwabara, H., Rosenberg, P. B., Resnick, S. M., Ostrowitzki, S., Vozzi, C., Boess, F., Oh, E., Lyketsos, C. G., Honer, M., Gobbi, L., Klein, G., George, N., Gapasin, L., Kitzmiller, K., Roberts, J., Sevigny, J., Nandi, A., Brasic, J. R., Mishra, C., Thambisetty, M., Moghekar, A., Mathur, A., Albert, M., Dannals, R. F., and Borroni, E. (2018) Characterization of 3 Novel Tau Radiopharmaceuticals, 11C-RO-963, 11C-RO-643, and 18F-RO-948, in Healthy Controls and in Alzheimer Subjects. *J. Nucl. Med.* **59**, 1869–1876
117. Ren, Y., and Sahara, N. (2013) Characteristics of tau oligomers. *Front. Neurol.* **4**, 1–6
118. Saborio, G. P., Permanne, B., and Soto, C. (2001) Sensitive detection of pathological prion protein by cyclic amplification of protein misfolding. *Nature*. **411**, 810–813
119. Meyer, V., Dinkel, P. D., Hager, E. R., and Margittai, M. (2014) Amplification of Tau Fibrils from Minute Quantities of Seeds. *Biochem. Soc. Trans.* **53**, 5804–5809
120. Atarashi, R., Sano, K., Satoh, K., and Nishida, N. (2011) Real-time quaking-induced conversion: A highly sensitive assay for prion detection. *Prion*. **5**, 150–153
121. Saijo, E., Ghetti, B., Zanusso, G., Oblak, A., Furman, J. L., Diamond, M. I.,

Kraus, A., and Caughey, B. (2017) Ultrasensitive and selective detection of 3-repeat tau seeding activity in Pick disease brain and cerebrospinal fluid. *Acta Neuropathol.* **133**, 751–765
122. Tanaka, M., Chien, P., Naber, N., Cooke, R., and Weissman, J. S. (2004) Conformational variations in an infectious protein determine prion strain differences. *Nature*. **428**, 323
123. Verges, K. J., Smith, M. H., Toyama, B. H., and Weissman, J. S. (2011) Strain conformation, primary structure and the propagation of the yeast prion [PSI+]. *Nat. Struct. Mol. Biol.* **18**, 493–500
124. Goldfarb, D., and Stoll, S. (2018) *EPR spectroscopy : fundamentals and methods*
125. Margittai, M., and Langen, R. (2006) Side chain-dependent stacking modulates tau filament structure. *J. Biol. Chem.* **281**, 37820–37827
126. Radli, M., Verdonschot, R. E., Ferrari, L., and Rüdiger, S. G. D. (2017) Successful aggregation of Tau protein labelled on its native cysteines. *bioRxiv Biochem.* https://doi.org/10.1101/211904
127. Sillen, A., Wieruszeski, J. M., Leroy, A., Younes, A. Ben, Landrieu, I., and Lippens, G. (2005) High-resolution magic angle spinning NMR of the neuronal tau protein integrated in Alzheimer's-like paired helical fragments. *J. Am. Chem. Soc.* **127**, 10138–10139
128. Andronesi, O. C., Biernat, J., Seidel, K., Griesinger, C., Mandelkow, E., Baldus, M., Bergen, M. Von, Biernat, J., Seidel, K., Griesinger, C., Mandelkow, E., and Baldus, M. (2008) Characterization of Alzheimer ' s-like Paired Helical Filaments from the Core Domain of Tau Protein Using Solid-State NMR Spectroscopy. *J. Am. Chem. Soc.* **130**, 5922–5928
129. Falcon, B., Zhang, W., Schweighauser, M., Murzin, A. G., Vidal, R., Garringer, J., Ghetti, B., Scheres, S. H. W., and Goedert, M. (2018) Tau filaments from multiple cases of sporadic and inherited Alzheimer 's disease adopt a common fold. *Acta Neuropathol.* **136**, 669–708
130. Yu, X., Luo, Y., Dinkel, P., Zheng, J., Wei, G., Margittai, M., Nussinov, R., and Ma, B. (2012) Cross-seeding and conformational selection between three- and four-repeat human Tau proteins. *J. Biol. Chem.* **287**, 14950–14959
131. Siddiqua, A., Luo, Y., Meyer, V., Swanson, M. a., Yu, X., Wei, G., Zheng, J., Eaton, G. R., Ma, B., Nussinov, R., Eaton, S. S., and Margittai, M. (2012) Conformational basis for asymmetric seeding barrier in filaments of three- and four-repeat tau. *J. Am. Chem. Soc.* **134**, 10271–10278
132. Altenbach, C., Flitsch, S. L., Khorana, H. G., and Hubbell, W. L. (1989) Structural Studies on Transmembrane Proteins. 2. Spin Labeling of Bacteriorhodopsin Mutants at Unique Cysteines. *Biochemistry*. **28**, 7806–7812
133. Schweers, O., Schönbrunn-Hanebeck, E., Marx, A., and Mandelkow, E.

(1994) Structural studies of tau protein and Alzheimer paired helical filaments show no evidence for β-structure. *J. Biol. Chem.* **269**, 24290–24297
134. Jeschke, G., Chechik, V., Ionita, P., Godt, A., Zimmermann, H., Banham, J., Timmel, C. R., Hilger, D., and Jung, H. (2006) DeerAnalysis2006- a comprehensive software package for analyzing pulsed ELDOR data. *Appl. Magn. Reson.* **30**, 473–498
135. Froelich, S., Houlden, H., Pickering-brown, S., Chakraverty, S., Isaacs, A., Grover, A., Hackett, J., Adamson, J., Lincoln, S., Dickson, D., Davies, P., Petersen, R. C., Stevens, M., Graaff, E. De, Wauters, E., Baren, J. Van, Hillebrand, M., Joosse, M., Morris, J. C., Reed, L. A., Trojanowski, J., Basun, H., Snowden, J., Craufurd, D., Neary, D., and Owen, F. (1998) Association of missense and 59-splice-site mutations in tau with the inherited dementia FTDP-17. *Lett. to Nat.* **393**, 702–705
136. von Bergen, M., Friedhoff, P., Biernat, J., Heberle, J., Mandelkow, E. M., and Mandelkow, E. (2000) Assembly of tau protein into Alzheimer paired helical filaments depends on a local sequence motif ((306)VQIVYK(311)) forming beta structure. *Proc. Natl. Acad. Sci. U. S. A.* **97**, 5129–34
137. Jeschke, G. (2012) DEER distance measurements on proteins. *Annu. Rev. Phys. Chem.* **63**, 419–46
138. Borbat, P. P., and Freed, J. H. (2000) Chapter 9 Double-Quantum ESR and Distance Measurements. **19**, 383–459
139. Rivas-arancibia, S., Guevara-guzma, R., Lo, Y., Zanardo-gomes, M., Angoa-pe, M., and Raisman-vozari, R. (2010) Oxidative Stress Caused by Ozone Exposure Induces Loss of Brain Repair in the Hippocampus of Adult Rats. **113**, 187–197
140. Ataya, T. A. W., Himohama, S. H. U. N. S., and Hiba, S. H. C. (2001) Oxidative Damage Is the Earliest Event in Alzheimer Disease. **60**, 759–767
141. Cleveland, D. W., Hwo, S. Y., and Kirschner, M. W. (1977) Physical and chemical properties of purified tau factor and the role of tau in microtubule assembly. *J. Mol. Biol.* **116**, 227–247
142. Walker, S., Ullman, O., and Stultz, C. M. (2012) Using intramolecular disulfide bonds in tau protein to deduce structural features of aggregation-resistant conformations. *J. Biol. Chem.* **287**, 9591–9600
143. Zhou, Z., Fan, J. B., Zhu, H. L., Shewmaker, F., Yan, X., Chen, X., Chen, J., Xiao, G. F., Guo, L., and Liang, Y. (2009) Crowded cell-like environment accelerates the nucleation step of amyloidogenic protein misfolding. *J. Biol. Chem.* **284**, 30148–30158
144. England, J. L., and Haran, G. (2011) Role of Solvation Effects in Protein Denaturation: From Thermodynamics to Single Molecules and Back. *Annu. Rev. Phys. Chem.* **62**, 257–277
145. Morihara, K., and Tsuzuki, H. (1975) Specificity of proteinase k from

titirachium album limber for synthetic peptides. *Agric. Biol. Chem.* **39**, 1489–1492
146. Kim, A. C., Lim, S., and Kim, Y. K. (2018) Metal Ion Effects on Aβ and Tau Aggregation. *Int. J. Mol. Sci.* **19**, 1–15
147. Sanders, D. W., Kaufman, S. K., DeVos, S. L., Sharma, A. M., Mirbaha, H., Li, A., Barker, S. J., Foley, A. C., Thorpe, J. R., and Diamond, M. I. (2014) Distinct Tau Prion Strains Propagate in Cells and Mice and Define Different Tauopathies. *Neruon*. **82**, 1271–1288
148. Kfoury, N., Holmes, B. B., Jiang, H., Holtzman, D. M., and Diamond, M. I. (2012) Trans-cellular propagation of Tau aggregation by fibrillar species. *J. Biol. Chem.* **287**, 19440–19451
149. Braak, H., and Tredici, K. Del (2018) Spreading of tau pathology in sporadic Alzheimer's disease along cortico-cortical top-down connections. *Cereb. Cortex*. **28**, 3372–3384
150. Katsinelos, T., Zeitler, M., Dimou, E., Karakatsani, A., Müller, H. M., Nachman, E., Steringer, J. P., Ruiz de Almodovar, C., Nickel, W., and Jahn, T. R. (2018) Unconventional Secretion Mediates the Trans-cellular Spreading of Tau. *Cell Rep.* **23**, 2039–2055
151. Breydo, L. (2013) Strain phenomenon in protein aggregation: Interplay between sequence and conformation. *Intrinsically Disord. proteins*. **1**, e27130–e27130
152. García-Sierra, F., Ghoshal, N., Quinn, B., Berry, R. W., and Binder, L. I. (2003) Conformational changes and truncation of tau protein during tangle evolution in Alzheimer's disease. *J. Alzheimers. Dis.* **5**, 65–77
153. Guo, J. L., Covell, D. J., Daniels, J. P., Iba, M., Stieber, A., Zhang, B., Riddle, D. M., Kwong, L. K., Xu, Y., Trojanowski, J. Q., and Lee, V. M. Y. (2013) Distinct a-synuclein strains differentially promote tau inclusions in neurons. *Cell*. **154**, 103–117
154. Qiang, W., Yau, W. M., Lu, J. X., Collinge, J., and Tycko, R. (2017) Structural variation in amyloid-β fibrils from Alzheimer's disease clinical subtypes. *Nature*. **541**, 217–221
155. Habchi, J., Tompa, P., Longhi, S., and Uversky, V. N. (2014) Introducing protein intrinsic disorder. *Chem. Rev.* **114**, 6561–6588
156. Fichou, Y., Vigers, M., Goring, A. K., Eschmann, N. A., and Han, S. (2018) Heparin-induced tau filaments are structurally heterogeneous and differ from Alzheimer's disease filaments. *Chem. Commun.* **54**, 4573–4576
157. Puoti, G., Giaccone, G., Rossi, G., Canciani, B., Bugiani, O., and Tagliavini, F. (1999) Sporadic Creutzfeldt-Jakob disease: Co-occurrence of different types of PrPSc in the same brain. *Neurology*. **53**, 2173
158. Arai, T., Hasegawa, M., Nonoka, T., Kametani, F., Yamashita, M., Hosokawa, M., Niizato, K., Tsuchiya, K., Kobayashi, Z., Ikeda, K., Yoshida, M., Onaya, M., Fujishiro, H., and Akiyama, H. (2010) Phosphorylated and

cleaved TDP-43 in ALS, FTLD and other neurodegenerative disorders and in cellular models of TDP-43 proteinopathy. *Neuropathology*. **30**, 170–181
159. Levin, J., Giese, A., Boetzel, K., Israel, L., Högen, T., Nübling, G., Kretzschmar, H., and Lorenzl, S. (2009) Increased α-synuclein aggregation following limited cleavage by certain matrix metalloproteinases. *Exp. Neurol.* **215**, 201–208
160. Graham, R. K., Deng, Y., Slow, E. J., Haigh, B., Bissada, N., Lu, G., Pearson, J., Shehadeh, J., Bertram, L., Murphy, Z., Warby, S. C., Doty, C. N., Roy, S., Wellington, C. L., Leavitt, B. R., Raymond, L. A., Nicholson, D. W., and Hayden, M. R. (2006) Cleavage at the Caspase-6 Site Is Required for Neuronal Dysfunction and Degeneration Due to Mutant Huntingtin. *Cell*. **125**, 1179–1191
161. Zilka, N., Kovacech, B., Barath, P., Kontsekova, E., and Novák, M. (2012) The self-perpetuating tau truncation circle. *Biochem. Soc. Trans.* **40**, 681–686
162. Zilka, N., Filipcik, P., Koson, P., Fialova, L., Skrabana, R., Zilkova, M., Rolkova, G., Kontsekova, E., and Novak, M. (2006) Truncated tau from sporadic Alzheimer's disease suffices to drive neurofibrillary degeneration in vivo. *FEBS Lett.* **580**, 3582–3588
163. Jeganathan, S., Von Bergen, M., Brutlach, H., Steinhoff, H. J., and Mandelkow, E. (2006) Global hairpin folding of tau in solution. *Biochemistry*. **45**, 2283–2293
164. Taniguchi-Watanabe, S., Arai, T., Kametani, F., Nonaka, T., Masuda-Suzukake, M., Tarutani, A., Murayama, S., Saito, Y., Arima, K., Yoshida, M., Akiyama, H., Robinson, A., Mann, D. M. A., Iwatsubo, T., and Hasegawa, M. (2016) Biochemical classification of tauopathies by immunoblot, protein sequence and mass spectrometric analyses of sarkosyl-insoluble and trypsin-resistant tau. *Acta Neuropathol.* **131**, 267–280
165. Carmel, G., Mager, E. M., Binder, L. I., and Kuret, J. (1996) The structural basis of monoclonal antibody Alz50's selectivity for Alzheimer's disease pathology. *J. Biol. Chem.* **271**, 32789–32795
166. De Calignon, A., Fox, L. M., Pitstick, R., Carlson, G. A., Bacskai, B. J., Spires-Jones, T. L., and Hyman, B. T. (2010) Caspase activation precedes and leads to tangles. *Nature*. **464**, 1201–1204
167. Dumanchin, C., Camuzat, A., Campion, D., Verpillat, P., Hannequin, D., Dubois, B., Saugier-Veber, P., Martin, C., Penet, C., Charbonnier, F., Agid, Y., Frebourg, T., and Brice, A. (1998) Segregation of a missense mutation in the microtubule-associated protein tau gene with familial frontotemporal dementia and parkinsonism. *Hum. Mol. Genet.* **7**, 1825–1829
168. Lossos, A., Reches, A., Gal, A., Newman, J. P., Soffer, D., Gomori, J. M., Boher, M., Ekstein, D., Biran, I., Meiner, Z., Abramsky, O., and

Rosenmann, H. (2003) Frontotemporal dementia and parkinsonism with the P301S tau gene mutation in a Jewish family. *J. Neurol.* **250**, 733–740
169. Mutations MAPT *Alzforum*. [online] https://www.alzforum.org/mutations/mapt (Accessed December 30, 2018)
170. Grover, A., Deurel, M., Yen, S. H., and Hutton, M. (2002) Effects on splicing and protein function of three mutations in codon N296 of tau in vitro. *Neurosci. Lett.* **323**, 33–36
171. Lyon, C. B., Ros, R., Thobois, S., Streichenberger, N., Kopp, N., Sánchez, M. P., Pérez, M., Hoenicka, J., Avila, J., Honnorat, J., and de Yébenes, J. G. (2005) A new mutation of the tau gene, G303V, in early-onset familial progressive supranuclear palsy. *Arch. Neurol.* **62**, 1444–1450
172. Iijima, M., Tabira, T., Poorkaj, P., Schellenberg, G. D., Trojanowski, J. Q., Lee, V. M. Y., Schmidt, M. L., Takahashi, K., Nabika, T., Matsumoto, T., Yamashita, Y., Yoshioka, S., and Ishino, H. (1999) A distinct familial presenile dementia with a novel missense mutation in the tau gene. *Neuroreport*. **10**, 497–501
173. Von Bergen, M., Barghorn, S., Li, L., Marx, A., Biernat, J., Mandelkow, E. M., and Mandelkow, E. (2001) Mutations of Tau Protein in Frontotemporal Dementia Promote Aggregation of Paired Helical Filaments by Enhancing Local β-Structure. *J. Biol. Chem.* **276**, 48165–48174
174. MacArthur, M. W., and Thornton, J. M. (1991) Influence of proline residues on protein conformation. *J. Mol. Biol.* **218**, 397–412
175. Rizzu, P., Van Swieten, J. C., Joosse, M., Hasegawa, M., Stevens, M., Tibben, A., Niermeijer, M. F., Hillebrand, M., Ravid, R., Oostra, B. A., Goedert, M., van Duijn, C. M., and Heutink, P. (1999) High Prevalence of Mutations in the Microtubule-Associated Protein Tau in a Population Study of Frontotemporal Dementia in the Netherlands. *Am. J. Hum. Genet.* **64**, 414–421
176. Rossi, G., Bastone, A., Piccoli, E., Mazzoleni, G., Morbin, M., Uggetti, A., Giaccone, G., Sperber, S., Beeg, M., Salmona, M., and Tagliavini, F. (2012) New mutations in MAPT gene causing frontotemporal lobar degeneration: Biochemical and structural characterization. *Neurobiol. Aging*. **33**, 834.e1-834.e6
177. Wüllner, U., Seyfried, J., Groscurth, P., Beinroth, S., Winter, S., Gleichmann, M., Heneka, M., Löschmann, P. A., Schulz, J. B., Weller, M., and Klockgether, T. (1999) Glutathione depletion and neuronal cell death: The role of reactive oxygen intermediates and mitochondrial function. *Brain Res.* **826**, 53–62
178. Forman, H. J., Zhang, H., and Rinna, A. (2009) Glutathione: Overview of its protective roles, measurement, and biosynthesis. *Mol. Aspects Med.* **30**, 1–12
179. Barghorn, S., and Mandelkow, E. (2002) Toward a unified scheme for the

aggregation of tau into Alzheimer paired helical filaments. *Biochemistry*. **41**, 14885–14896
180. Di Noto, L., DeTure, M. A., and Purich, D. L. (1999) Disulfide-cross-linked Tau and MAP2 homodimers readily promote microtubule assembly. *Mol. Cell Biol. Res. Commun.* **2**, 71–76
181. Sigurdsson, E. M. (2016) Tau immunotherapy. *Neurodegener. Dis.* **16**, 34–38
182. Meredith, J. E., Sankaranarayanan, S., Guss, V., Lanzetti, A. J., Berisha, F., Neely, R. J., Slemmon, J. R., Portelius, E., Zetterberg, H., Blennow, K., Soares, H., Ahlijanian, M., and Albright, C. F. (2013) Characterization of Novel CSF Tau and ptau Biomarkers for Alzheimer's Disease. *PLoS One*. **8**, 1–14
183. Wu, J. W., Herman, M., Liu, L., Simoes, S., Acker, C. M., Figueroa, H., Steinberg, J. I., Margittai, M., Kayed, R., Zurzolo, C., Di Paolo, G., and Duff, K. E. (2013) Small misfolded tau species are internalized via bulk endocytosis and anterogradely and retrogradely transported in neurons. *J. Biol. Chem.* **288**, 1856–1870
184. Walker, L. C., Diamond, M. I., Duff, K. E., and Hyman, B. T. (2013) Mechanisms of protein seeding in neurodegenerative diseases. *JAMA Neurol.* **70**, 304–310
185. Binder, L. I., Guillozet-Bongaarts, A. L., Garcia-Sierra, F., and Berry, R. W. (2005) Tau, tangles, and Alzheimer's disease. *Biochim. Biophys. Acta - Mol. Basis Dis.* **1739**, 216–223
186. Deleault, N. R., Harris, B. T., Rees, J. R., and Supattapone, S. (2007) Formation of native prions from minimal components in vitro. *Proc. Natl. Acad. Sci.* **104**, 9741–9746

APPENDIX A: TAU PURIFICATION

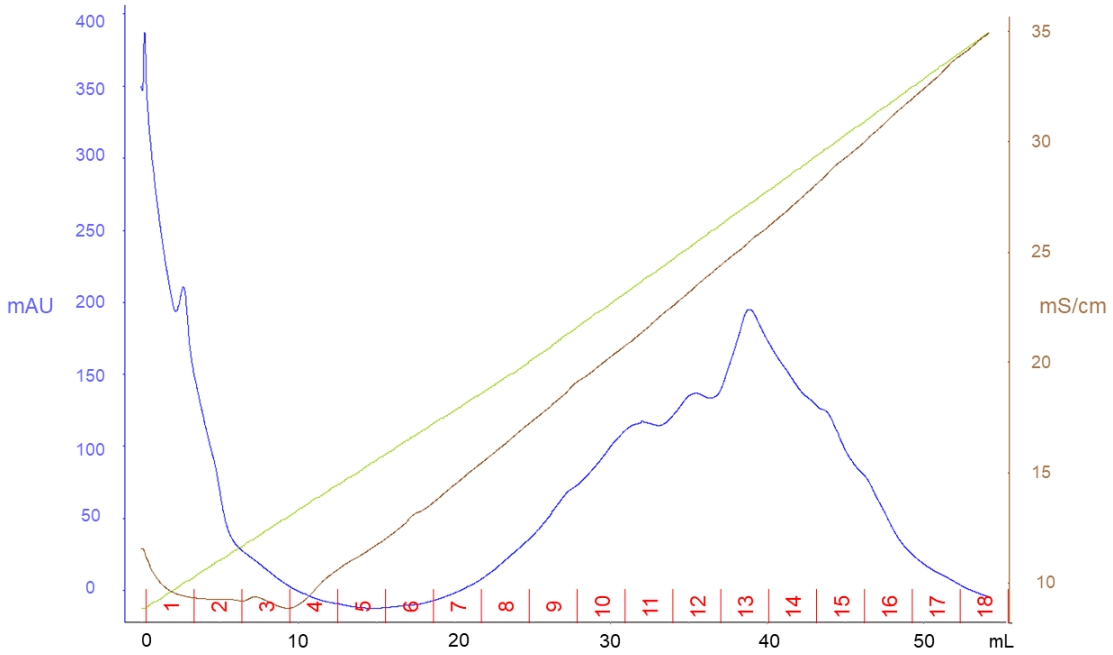

Representative trace from cation exchange chromatography. Chromatograph for a sample of htau40 showing utilizing a Mono S 10/100 GL cation exchange column monitoring absorbance at 280 nm (blue trace). Linear gradient of 1000 mM NaCL starting at 0% and ending the run at approximately 35%, mixing with a 50mM NaCl buffer (light green trace). Conductivity trace (brown trace) showing increase parallel to linear gradient of high salt buffer causing tau to elute off the column between approximately 25-30 mS/cm. Elution volume was collected in 3 mL fractions and assessed via SDS-PAGE before proceeding to gel filtration.

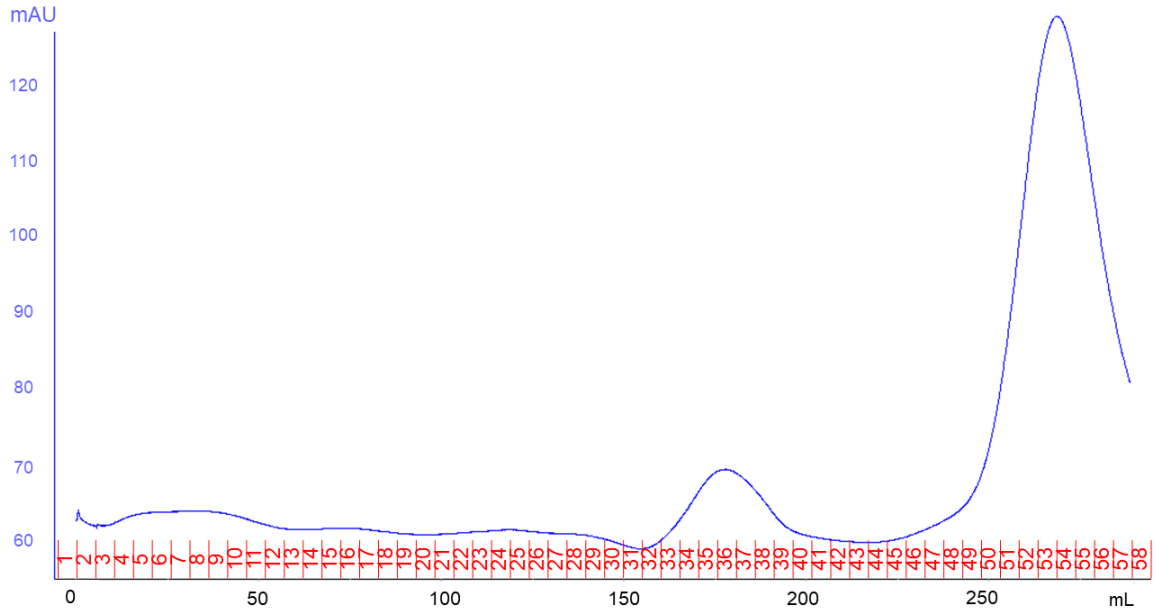

Representative trace from gel filtration chromatography. Chromatograph for an htatu40 sample run over a column with Superdex 200 media. Absorbance measured at 280 nm (blue trace). Elution volume collected in 5 mL fractions. Based on its size the peak starting around fraction 49 is htau40, fractions containing this peak were run on SDS-PAGE to be assessed before precipitation.

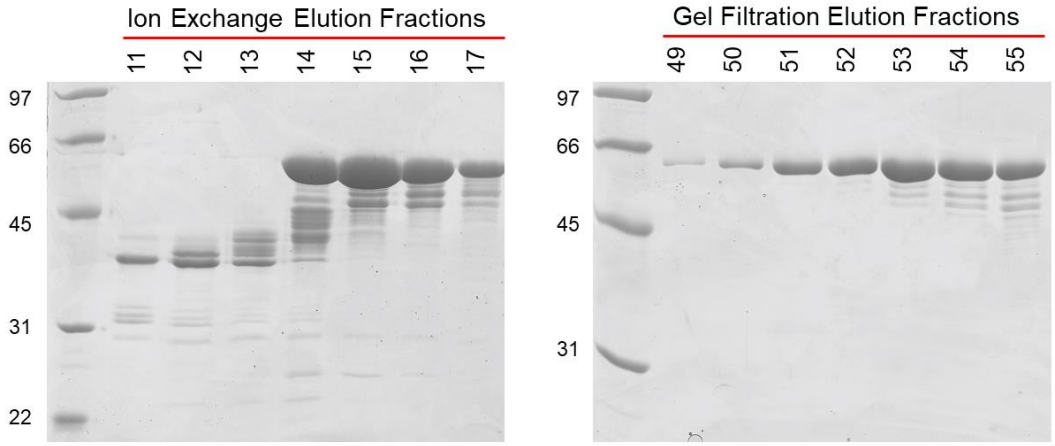

Representative purification gels from ion exchange chromatography and gel filtration chromatography. A, SDS-PAGE assessment of fractions 11-17 from an ion exchange sample of htau40, fractions 14-17 were pooled and subjected to gel filtration. B, SDS-PAGE assessment of fractions from a gel filtration sample of htau40, fractions 51-55 were pooled and let precipitate overnight in a 1:1 ratio with methanol along with 2 mM DTT.

APPENDIX B: AMPLIFICATION ASSAY TRIALS

ID	# cycles	sonciation time	incubation time	power amplitude	µM tau monmer	µM heparin	TCEP (mM)	Temperature
1	45	1 min	29 min	15	10	40	1	37°C
2	60	1min	29 min	15	10	40	1	37°C
3	60	5sec	30 min	5	5	20	1	37°C
4	70	5sec	30 min	5	5	20	1	37°C
5	80	5sec	30 min	5	5	20	1	37°C
6	50	5sec	30 min	5	10	40	1	37°C
7	50	5sec	30 min	10	5	20	1	37°C
8	50	10sec	30 min	10	5	20	1	37°C
9	52	1 min	29 min	15	10	40	1	37°C
10	60	1 min	29 min	15	10	40	1	37°C
11	70	1 min	29 min	15	10	40	1	37°C
12	96	1min	14 min	15	10	40	1	37°C
13	144	1 min	9 min	15	10	40	1	37°C
14	144	1min	14 min	15	10	40	1	37°C

Table 1. Combinations of amplification assay parameters tested. Top horizontal row indicates the parameter in question. Left most column indicates an arbitrarily assigned ID to each combination of parameters, ID's are used in table 2 for results of particular monomers for different parameter combinations.

ID	htau40	V306A	V306K	V306S	I308D	I308E	I308A	I308K	I308S	V309A	V309K	V309S	I308K V309K	I308K V309S
1	Y	N	N	Y	N	N	N	N	Y	Y	Y	Y	Y	N
1	Y				N	N		Y						
1	N				N	N		N						
1	Y	N	N	Y	N	N	N	N	Y	Y	Y	Y	Y	N
1	Y	Y	Y	N	N	N		N						N
1	Y				N	N		N						
2	Y				N	N		N						
3	N		N					N			N			
4	N		Y					N			N			
6	Y							N		Y	Y	N		
7	Y		Y	Y				N		Y	N	N		
8	N			Y				N		Y		N		
9	Y				N	N		N						
10	N				N	N		N						
11	N				N	N		N						
12	Y				N	N		N						
13	N				N	N		N						
12	N				N	N		N						
14	Y					N								

Table 2. Qualitative results for different amplification assay parameters with different mutants. Top horizontal row indicates the type monomer used. The left most column identifies the ID for the specific assay parameters detailed in Table 1. For each particular monomer/parameter combination Y indicates spontaneous nucleation occurred and N indicates spontaneous nucleation did not occur. Y or N determinations were made based on SDS-PAGE assessment of pellet and supernatant fractions following experiments.

APPENDIX C: TAU VARIANTS

Sequence of htau40

```
          10         20         30         40         50         60
MAEPRQEFEV MEDHAGTYGL GDRKDQGGYT MHQDQEGDTD AGLKESPLQTPTEDGSEEPG

          70         80         90        100        110        120
SETSDAKSTP TAEDVTAPLV DEGAPGKQAA AQPHTEIPEG TTAEEAGIGD TPSLEDEAAG

         130        140        150        160        170        180
HVTQARMVSK SKDGTGSDDK KAKGADGKTK IATPRGAAPP GQKGQANATR IPAKTPPAPK

         190        200        210        220        230        240
TPPSSGEPPK SGDRSGYSSP GSPGTPGSRS RTPSLPTPPT REPKKVAVVR TPPKSPSSAK

         250        260        270        280        290        300
SRLQTAPVPM PDLKNVKSKI GSTENLKHQP GGGKVQIINK KLDLSNVQSK CGSKDNIKHV

         310        320        330        340        350        360
PGGGSVQIVY KPVDLSKVTS KCGSLGNIHH KPGGGQVEVK SEKLDFKDRV QSKIGSLDNI

         370        380        390        400        410        420
THVPGGGNKK IETHKLTFRE NAKAKTDHGA EIVYKSPVVS GDTSPRHLSN VSSTGSIDMV

         430        440
DSPQLATLAD EVSASLAKQG L
```

Sequence of htau23

```
          10         20         30         40         50         60
MAEPRQEFEV MEDHAGTYGL GDRKDQGGYT MHQDQEGDTD AGLKAEEAGI GDTPSLEDEA

          70         80         90        100        110        120
AGHVTQARMV SKSKDGTGSD DKKAKGADGK TKIATPRGAA PPGQKGQANA TRIPAKTPPA

         130        140        150        160        170        180
PKTPPSSGEP PKSGDRSGYS SPGSPGTPGS RSRTPSLPTP PTREPKKVAV VRTPPKSPSS

         190        200        210        220        230        240
AKSRLQTAPV PMPDLKNVKS KIGSTENLKH QPGGGKVQIV YKPVDLSKVT SKCGSLGNIH

         250        260        270        280        290        300
HKPGGGQVEV KSEKLDFKDR VQSKIGSLDN ITHVPGGGNK KIETHKLTFR ENAKAKTDHG

         310        320        330        340        350
AEIVYKSPVV SGDTSPRHLS NVSSTGSIDM VDSPQLATLA DEVSASLAKQ GL
```

Variant	Average molecular weight (kDa)
1-441, htau40	45850
1-352, htau23	36760
151-441	30649
244-441	21119
1-421	43869
1-391	40738
1-372	38602
244-421	18950
244-391	15819
244-384	15080
244-378	14411
244-372, K18	13682
244-368	13184

APPENDIX D: RECIPES

Extraction Buffer: 500 mM NaCl 20 mM PIPES 5 mM EDTA	Cation Exchange Buffer: A 50 mM NaCl 20 mM PIPES 0.5 mM EDTA * 0.45 µm filtered	Cation Exchange Buffer: B 1000 mM NaCl 20 mM PIPES 0.5 mM EDTA * 0.45 µm filtered
Size Exclusion Buffer: 100 mM NaCl 20 mM TRIS 1 mM EDTA * 0.45 µm filtered	Assembly Buffer: pH 7.4 100 mM NaCl 10 mM HEPES 0.1 mM NaN_3 * 0.45 µm filtered	10 X SDS Running Buffer: 190 mM Glycine 25 mM TRIS 0.1 % SDS
NZY Broth: (autoclaved) 10 g/L N-Z Amine 5 g/L yeast extract 5 g/L NaCl *immediately before use add: 12.5 mM $MgCl_2$ 12.5 mM $MgSO_4$ 10 mM glucose	Kanamycin Culture Plates: 20 g/L LB broth 10 g/L LB agar *once autoclaved cool to 55 °C add 50 mg/L kanamycin	Coomassie Stain: (0.5 L) 200 mL Methanol 50 mL Acetic Acid 250 mL DI water 1 g Coomassie *mix well then filter
Destain: (2 L) 100 mL Methanol 250 mL Acetic Acid 1650 mL DI water	Separating Gel Buffer: 1.5 M TRIS 14 mM SDS *pH to 8.8 with HCl	Stacking Gel Buffer: 0.5 M TRIS 14 mM SDS *pH to 6.8 with HCl
Stacking Gel: 61% water 13% Bisacrylamide 25% stacking gel buffer 1% SDS (10% solution) *right before use add: 0.6% APS (10% solution) 0.06% Temed	Separating Gel: **(12%)** 35% water 38% Bisacrylamide 25% separating gel buffer 1% SDS (10% solution) *right before use add: 0.6% APS (10% solution) 0.06% Temed	Separating Gel: **(15%)** 23% water 50% Bisacrylamide 25% separating gel buffer 1% SDS (10% solution) *right before use add: 0.6% APS (10% solution) 0.06% Temed
SDS Sample Buffer: 62.6 mM TRIS *pH to 6.8 with HCl 4% SDS 10% sucrose 5% βME *completely mix then add 6 mM Bromophenol Blue		

APPENDIX E: MATERIALS AND INSTRURMENTS

Material/ instrument	Manufacturer	Product/ CAT #	general usage	important specifications
DNA primers	Integrated DNA Technologies		making point mutations	melting point <65 °C
QuikChange II	Agilent Technologies	200524-5	site-directed mutagenesis kits	polymerase: PFU ultra
PCR certified water	Teknova	W3340	primer and DNA dilutions, PCR reactions	ACS reagent grade
MJ Mini Personal Thermal Cycler	BIO RAD	PTC-1148	PCR cycles	
QuikChange XL1- Blue supercompetent cells	Agilent Technologies	200518-41	transforming PCR product	optimized for DNA amplification
BL21 (DE3) cells	Agilent Technologies	200131	transforming pure DNA	optimized for expression
Polypropylene round-bottom tubes	Falcon	352059	transformation	shape and polymer optimized for heat shock step
N-Z amine	Sigma	N4517	NZY mixture for transformation	
Yeast	Difco	0127-17-9	NZY mixture for transformation	
Magnesium Sulfate heptahydrate	Fluka	63138	NZY mixture for transformation	
Magnesium Chloride	Sigma	M-8266	NZY mixture for transformation	
Glucose	Sigma	G8270	NZY mixture for transformation	

Kanamycin	Gold Biotechnology	K-120-25	antibiotic included in all bacterial growth	pET28b plasmid used is Kanamycin resistant
Luria-Bertani broth (Miller)	Difco BC	214-906	bacterial growth media	powder, Miller's modification 10 g/L NaCl
LB Agar Miller	Fisher Bioreagents	BP-1425-500	bacterial growth media for culture plates	
culture plates	Fisher Scientific	FB0875713	hold solidified LB agar on which bacterial colonies grow	100 mm x 15 mm sterile polystyrene
Plasmid MIDI kit	Qiagen	12145	DNA purification	appropriate volume scale for extracting DNA from a 50 mL starter culture
Isopropanol	Fisher Scientific	A415-4	DNA precipitation	molecular biology grade
UV/Vis spectrometer	Varian	Cary 100Bio	any measurements in the UV/Vis wavelength range	
MaxQ4000 Incubator	Thermo Scientific	SHKE4000-7	shaking at 200 rpm for bacterial growth	always set to 37 °C, can hold the weight of 6 L of expression+ glass flasks
Incubator	Barnstead Lab-Line	150	bacterial growth on culture plates	always set to 37 °C, only used for culture plates no tau reactions
Isotemp Incubator	Fisher Scientific		all seeded reactions, seed fibril formation and any 37 °C incubation that was not a culture plate	always set to 37 °C, internal plug so stir plate can be inside incubator for seed fibril formation

Refrigerated circulation bath	Neslab	RTE4	heat shock for transformation	sensitive enough to accurately hold at 42.5 °C for transformation heat shock
water bath	Precision		heat expression homogenate at 80 °C for 20 min	capable of getting to 80 °C and holding >12 50 mL conical tubes
Sorvall LYNX 6000 centrifuge	Thermo Scientific	75006590	any centrifugation in 50 mL tubes or 1 L Nalgene bottles	interchangeable rotors, temperature control, robust because it gets a lot of usage
Isopropyl β-D-1-thiogalactopyranoside (IPTG)	Gold Biotechnology	12481C100	induce protein expression since tau gene is under the control of the lac operator	0.5 mM working concentration
Sodium Chloride	J.T. Baker	4058-06	used in making buffering solutions	ultrapure
piperazine-N,N'-bis(2-ethanesulfonic acid) (PIPES)	Research Products International	5625-37-6	used in making buffering solutions	high purity, pH 6.5
ethylenediaminetetraacetic acid (EDTA)	Fisher Scientific	S311-3	used in making buffering solutions	
β-mercaptoethanol (βME)	Fisher Bioreagents	BP176-100	added to expression homogenate and ingredient in sample buffer	
Sonifier	Fisher Scientific	Model 40:0.15:4C	sonication steps during purification protocol	equipped with a Branson 6-mm tip
ammonium sulfate	MP Biomedicals	808237	salting out tau protein	gentle salting out results in better yields

dithiothreitol (DTT)	Gold Biotechnology	DTT100	reducing agent during purification	protease free, must be prepared fresh daily
syringe filter	Acrodisc	PN-AP4558	sample filtration prior to ion exchange chromatography	GxF/GHP, pore size 0.45 µm
Akta FPLC	GE Healthcare		purification	robust, dual pump system
Cation exchange column	GE Healthcare	17-5169-01	purification	mono S 10/100 GL
150 mL superloop complete	GE Healthcare	18-1023-85	purification	pressure limit 2 Mpa
Protogel	National Diagnostics	EC-890	making 12% and 15% gels	30% (w/v) Acrylamide: 0.8% (w/v) Bis-Acrylamide
trizma base (TRIS)	Sigma	T1503	ingredient in gels and size exclusion buffer	crystalline
sodium dodecyl sulfate (SDS)	J.T. Baker	4095-02	ingredient in gels and gel running buffer	ultrapure
ammonium persulfate (APS)	Fisher Scientific	A682-500	ingredient in making gels	
temed	BIO RAD	161-0801	ingredient in making gels	
glycine	Fisher Bioreagents	BP381-5	ingredient in gel running buffer	white crystals or crystalline powder
sucrose	MP Biomedicals	821713	ingredient in sample buffer	ultrapure
bromophenol blue	Sigma-Aldrich	114391	ingredient in sample buffer	powder form
Coomassie Brilliant Blue	Thermo Scientific	20278	ingredient in stain	

Methanol	Fisher Chemical	A456-4	ingredient in stain, destain, and used for protein precipitation	precipitate proteins larger than 200 amino acids
Acetone	Fisher Chemical	A929-4	protein precipitation	precipitate proteins smaller than 200 amino acids
acetic acid	Fisher Chemical	A490-212	ingredient in stain and destain	
Akta Purifier	GE Healthcare		gel filtration chromatography	dual pump system, very robust
10 mL superloop complete	GE Healthcare	56301597	purification	
XK 26/100 chromatography column	GE Healthcare	28988951	size exclusion chromatography	large size so 10 mL samples can be sent over it
Superdex 200	GE Healthcare	17-1043-01	size exclusion chromatography	for proteins >200 amino acids
Superdex 75	GE Healthcare	17-1044-01	size exclusion chromatography	for proteins <200 amino acids
guanidine hydrochloride (GdnHCl)	Thermo Scientific	24115	dissolving protein pellets for monomerization and guan melt experiments	liquid, 8 M, ultra pure
guanidine hydrochloride (GdnHCl)	Fisher Biochemicals	BP178-1	cleaning PD10 columns and stir bars	crystals, make 6-8 M stock
PD10 desalting columns	GE Healthcare	17-0851-01	monomerization	clean before and after each use, ~20 uses per column
4-(2-hydroxyethyl)-1-piperazineethanesulfonic acid (HEPES)	J.T. Baker	41153-05	Assembly buffer	pH 7.4

sodium azide	Fisher Scientific	26628-228	Assembly buffer	granular
Nylon Membrane Filter	Whatman (GE Healthcare)	7404-004	vacuum filtration filter	0.45 μm
bicinchoninic acid protein Assay kit	Pierce, Thermo Fisher Scientific	23225	protein concentration determination	make a standard curve each time do not use extinction coefficient
tris(2-carboxyethyl)phosphine (TCEP)	Gold Biotechnology	TCEP25	reducing agent once protein is pure	high purity
Heparin	Celsus	EN-02912	necessary for all tau aggregation experiments	low molecular weight ~4400 kDa
Teflon-coated micro stir bar	Big Science Inc	SBM-0502-MIC	initial fibril formation	PTFE 5 x 2 mm micro
Microcentrifuge tubes	MultiMax	3466	initial fibril formation	2 mL, flat bottom so stir bar can freely rotate
microcentrifuge tubes	Beckman Coulter	357448	any ultracentrifugation	polypropylene, 1.5 mL
L7-55 ultracentrifuge	Beckman		any ultracentrifugation	
ultracentrifuge rotor	Fiberlite	F45L-24x1.5	any ultracentrifugation	ran at 128,000 x g, but max is ~211,000 x g
Sonifier	Fisher Scientific	Model 100	breaking initial fibrils to create seeds	equipped with a 2-mm tip, at power setting 2 output of 4 ± 1 w(RMS)
Thioflavin T (ThT)	Sigma	T3516	monitoring reaction kinetics	syringe filtered
FLUOstar Omega plate reader	BGM Labtech		monitoring reaction kinetics	excitation/emission filters 440/480 nm

Optical Btm Plt Polymer/Base plate	Nunc, Thermo Scientific	265301	monitoring reaction kinetics	96 wells, N/Treated N/SterPS
100-1250 µL pipet tips	VWR	89079-470	pipetting	autoclaved before use
1-200 µL pipet tips	VWR	89079-446	pipetting	autoclaved before use
0.1-10 µL pipet tips	VWR	89079-464	pipetting	autoclaved before use
specialty gel loading tips	Fisherbrand	02-707-181	loading gels and supernatant removal	autoclaved before use
Formvar/ Carbon 200 mesh copper grids	Electron Microscopy Sciences	FCF-200-Cu	visualizing aggregates via TEM	
uranyl acetate	Electron Microscopy Sciences	22400	staining aggregates for TEM	2%, 0.2 µm syringe filtered
T12 Biotwin Electron transmission microscope	FEI Tecnai		electron microscopy	owned by University of Colorado, Boulder, using high tension of 100 KV and a Gatan CCD camera
[1-oxyl-2,2,5,5-tetramethyl-Δ3-pyrroline-3-methyl]methanethiosulfonate (MTSL)	Toronto Research Chemicals	875000	EPR spectroscopy	powder taken up in DMSO to 40 mg/mL for usage
[1-acetyl-2,2,5,5-tetramethyl-Δ3-pyrroline-3-methyl]methanethiosulfonate	Toronto Research Chemicals		spin dilution for EPR samples	non-paramagnetic analog of MTSL, also taken up in DMSO to 40 mg/mL
EMX Plus spectrometer	Bruker		CW EPR measurements	operating at X-band, room temp
ER 4119HS resonator	Bruker		CW EPR measurements	

capillary tubes	Vitrotubes	CV6084	CW EPR samples	0.6 ID x 0.84 OD
quartz Q-band tubes	VITROCOM		DEER samples	SFS round cell 1.1 mm ID
ELEXSYS E580 spectrometer	Bruker		DEER measurements	
ER 5107D2 dielectric resonator	Bruker		DEER measurements	
580-400U ELDOR unit	Bruker	E5803006	DEER measurements	second microwave source
10 W amplifier	Bruker	HA8019	DEER measurements	increase sensitivity
Oxford CF935 cryostat	Mercury iTC	ITC503	DEER measurements	maintain 80 K using liquid nitrogen
hydrogen peroxide	Sigma-Aldrich	216763	Oxidation of htau40	30% (w/w) in H_2O
Dialysis tubing	Spectra/Por	132676	dialysis	flat width 10 mm, molecular weight cutoff 12-14 kDa
centrifugal filter units	Amicon Ultra	UFC501024	spin concentration	molecular weight cutoff 10 kDa
Superdex 200 10/300 GL	GE Healthcare	28990944	size exclusion chromatography for oxidation experiments	bed volume ~24 mL
anaerobic chamber and glove box	Coy Lab Products		anaerobic experiments	
Coy Anaerobic Monitor (CAM-12 detector)	Coy Lab Products		anaerobic experiments	Oxygen content was kept between 10-20 parts per million

proteinase K (PK)	Promega	V30213	limited protease digestion	
phenylmethylsulfonyl fluoride (PMSF)	Sigma	P-7626	stop proteolysis	
Mini-PROTEAN TGX stain-free gels	Bio-Rad	456-8095	visualize protease digestion products	4-20% precast gradient gel
bis(maleimido)ethane (BMOE)	Thermo Scientific	22323	crosslinking cysteines in htau40	power, taken up in DMSO to 20 mM
nontreated black bottom 96 microwell plates	Thermo Scientific	237105	amplification assay	
clear polyolefin sealing tape	Thermo Scientific	232702	sealing plates for amplification assay	DNase-RNase- free
ultrasonic processor	Qsonica	Q700	amplification assay	coupled with a microplate horn filled with 700 mL filtered water
temperature control unit	Qsonica	model 10-180-GI-PI-08S	amplification assay	maintain constant 37 °C